Title
Light Harvesting and Its Regulation in Photosynthetic Grana Membranes

Author
Amarnath, Kapil

Publication Date
2013

Peer reviewed|Thesis/dissertation

Light harvesting and its regulation in photosynthetic grana membranes

by

Kapil Amarnath

A dissertation submitted in partial satisfaction of the

requirements for the degree of

Doctor of Philosophy

in

Chemistry

in the

Graduate Division

of the

University of California, Berkeley

Committee in charge:

Professor Graham R. Fleming, Chair

Professor David E. Wemmer

Professor Krishna K. Niyogi

Spring 2013

Light harvesting and its regulation in photosynthetic grana membranes

Abstract

Light harvesting and its regulation in photosynthetic grana membranes

by

Kapil Amarnath

Doctor of Philosophy in Chemistry

University of California, Berkeley

Professor Graham R. Fleming, Chair

Photosystem II (PSII) initiates photosynthesis in plants by absorbing and converting light energy from the sun into chemical energy, a process called light harvesting. PSII is composed of proteins bound to pigment cofactors that can be grouped into antenna proteins, which absorb light and transfer excitation energy to other pigment-protein complexes, and reaction centers, which can convert excitation energy into chemical energy via a charge separation reaction. In plants, the proteins associated with PSII are located in the grana membrane, which is densely packed with photosystem II and major light harvesting complexes (LHCII). PSII reversibly binds with LHCII to form PSII supercomplexes. PSII supercomplexes and LHCIIs form a large, variably fluid array of pigment-protein complexes that gives rise to an energy transfer network that operates like a "smart" solar cell. In dim sunlight, the grana membrane harvests light with 90% efficiency. In response to light of fluctuating intensity and wavelength, the antenna proteins of PSII can regulate light harvesting. Understanding the design principles of light harvesting in grana membranes in different light conditions would be useful as a blueprint for designing robust solar cells.

This thesis presents measurements and models for understanding light harvesting in variable light conditions. We have developed the fluorescence lifetime snapshot technique to monitor changes in the energy transfer network of the grana membrane of green algae and plant leaves in response to changes in incident light. Using this technique, we suggest that there are two mechanisms for green algae to acclimate to changes in light intensity. To fully leverage the snapshot data, a structure-based model of energy transfer for the grana membrane is required. We constructed a detailed model of energy transfer and trapping in PSII supercomplexes and show how to use this model to construct an energy transfer model for the grana membrane. Together, the snapshot technique and membrane model will aid in the elucidation of the principles of light harvesting and its regulation in grana membranes.

To my parents

Contents

List of Figures

List of Tables

Acknowledgments

I would like to first thank my adviser, Graham Fleming, for giving me the opportunity to work in his group and his wisdom in the ways of scientific research. In the summer of 2008, I was having difficulty finding a group that would be a good fit for my newfound interests in biophysics, and Graham took a chance by accepting me into his group without knowing much about me. Throughout my five years in the group, Graham has given me tidbits of advice whose value I realized only well after they were uttered. Kris Niyogi has been virtually a co-adviser to me and has always opened his door for discussions. His wide-ranging knowledge of photosynthesis was useful for interpreting results, and his reasonable, measured approach to doing research has provided a model for me as I continue in science. Phill Geissler's first semester class on statistical mechanics was the first physical chemistry class that I had liked to that point, and I relished doing the problem sets and going to his lectures. I took every class that I could from Phill, and I eventually even got to teach for him. He is an amazing teacher. I would like to thank David Wemmer for asking excellent questions on my qualifying exam and providing useful comments on my thesis. Lastly, I would like to thank Charles Harris and Michelle Chang for their help and support when serving on my qualifying exam committee.

I enjoyed Graham's very hands-off approach to advising but could not have made progress without the help of many Fleming group members. I was first mentored by Tae Ahn. Tae got me to ask questions about NPQ and suggested the idea of the fluorescence lifetime snapshot measurement. Also, for help early on and in studying for my qualifying exam, Naomi Ginsberg, Yuan-Chung Cheng, and Gabriela Schlau-Cohen were invaluable. In my second year in the Fleming group I began working on the snapshot apparatus and was aided immensely by an undergraduate, Sam Park. Sam brought a lot of useful electronics knowledge and enthusiasm to the project. I struggled with where to go after building the apparatus in my 4th year. During this time I worked closely with Thuy Truong from the Niyogi group on trying to use sample variation to answer questions, but it proved difficult. Towards the end of this year, I realized the importance of energy transfer models for understanding NPQ and the fluorescence lifetime snapshot data. After the summer, I talked to Doran Bennett, who knew much more about energy transfer than I did, about working to construct a detailed energy transfer model of photosystem II. I have enjoyed working with him ever since. While the modeling was ongoing, I was helped by Julia Zaks to take data on algae. More generally, she has been a useful sounding board for my ideas throughout my PhD. I enjoyed working alongside Julia and Emily Jane Sylak-Glassman on extending the snapshot method to measuring leaves. I would like to thank Matt Brooks and Graham Peers from the Niyogi lab for helpful discussions. I am grateful also for the kindness and camaraderie from both Fleming and Niyogi groups. Lastly, I would like to thank the administrative assistants Tiff Dressen, Nancy Turley, Jonathan Weld, Marilyn Kobayashi, and Lynn Keithlin for their help.

I would like to thank the people who have kept me sane throughout my PhD. I met several lifelong friends in my first year of graduate school when I lived at the International House: Simon Schieder, Garvesh Raskutti, Joseph Williams, and Sina Akhavan. Simon kept me positive at the end of my first year. Garvesh was a great roommate, workout buddy,

and conversational companion throughout. Joseph and Sina were always there to chat freely about all aspects of life. Harriet Provine was a big part of my life in my first 4 years of graduate school, and we remain very good friends. She loved me even when I was tired and cranky about graduate school. My roommates the last couple of years - Stephen Thurman, Max Gee, and Peter Epstein - were great to talk to and affected the way I thought about my life. Lastly, to Jothi Auntie, JG Mama, Minnie, Nevin, Raj, Steph, and Chloè - thank you for the love and support (and food) that family can especially offer.

Finally, I thank my parents, who, as I think about them, fill me up with love. The older I get, the more I want to see them and hug them. They have always been worried only that I be happy and healthy and tried to make sure that was the case throughout my PhD even though they were in faraway Tennessee. They initiated me into science, and I hope to make them proud in the years to come.

Chapter 1

Introduction

1.1 Overview

The grana membrane of eukaryotic photosynthetic organisms is a "smart" solar cell. The grana membrane consists of an array of pigment-protein complexes associated with photosystem II that absorb light from the sun and convert it into chemical energy with ∼90% quantum efficiency in dim sunlight. This light-harvesting apparatus acclimates to changes in sunlight intensity and wavelength and can repair itself. Learning the principles by which light harvesting is efficient and robust could be useful for optimizing plants for making fuel and food and for designing artificial photosynthetic devices. Light-harvesting functionality is determined by the precise arrangement of pigment and proteins in the membrane. In cases where the arrangement is not fully known, as is the case in the grana membrane, an interplay of measurements and models of light harvesting are required. Light harvesting happens on the picosecond (10^{-12} s) timescale but the changes in the light-harvesting apparatus in response to changes in sunlight occur on the second to hour timescale. We[1] have developed a new technique, fluorescence lifetime snapshots, for measuring light harvesting on both of those timescales. We have constructed a detailed model for light harvesting in grana membranes for leveraging the snapshot data and determining the principles for efficient energy collection.

In this Chapter, I will introduce photosynthesis, light harvesting, and nonphotochemical quenching, a general term for the acclimation of light harvesting to changing light conditions. I will describe the experimental techniques used for understanding light harvesting. I will then focus on the questions regarding light harvesting and its regulation in response to fluctuations in light intensities, energy-dependent quenching, and outline the remainder of the thesis.

[1]When referring to the work performed, I will use the royal "we," since the work presented here was collaborative. When referring to the dissertation, I will use the personal "I."

1.2 Photosynthesis

1.2.1 Introduction

Photosynthesis is the biological process by which energy from the sun is used to make sugar to spur growth and fuel all life on earth. Many species - bacteria, algae, and plants - can perform photosynthesis. While the protein components of photosynthesis in these organisms vary, the general principle of operation is the same. Energy from sunlight is used to drive the oxidation of an electron donor whose electrons are used to reduce carbon dioxide and make sugar. The overall equation of oxygenic photosynthesis is

$$6\,CO_2 + 6\,H_2O + h\nu \rightarrow C_6H_{12}O_6 + 6\,O_2 \tag{1.1}$$

The reduction of carbon dioxide and the oxidation of water are physically separate processes that each define the two major components of photosynthesis. The so-called "light reactions" absorb and convert photo-energy into reducing equivalents in the form of nicotinamide adenine dinucleotide phosphate (NADPH) and energy in the form of adenosine triphosphate (ATP), using the electrons from water. The "carbon reactions" use the NADPH and ATP from the light reactions to power metabolic reactions that reduce carbon dioxide into glucose.

Photosynthesis in eukaryotic organisms occurs in the organelle called the chloroplast, whose dimensions are each on the order of a few microns. Inside the chloroplast are a network of membranes called the thylakoid membranes (for images, see the review by Nevo et al. [95]). The thylakoid membranes are composed of stacked membranous discs called the grana membranes which are connected by tubes called the stroma lamellae. The width of the grana discs is $\sim$400 nm. The volume enclosed by the thylakoids is called the lumen, and the volume outside of the thylakoids in the chloroplast is called the stroma. The carbon reactions occur in the stroma. The proteins complexes involved in the light reactions are located in the thylakoid membrane.

A schematic of the light reactions is shown in Figure 1.1. The protein complexes involved in the light reactions are photosystem II (PSII), cytochrome b_6f (Cyt b_6f), photosystem I (PSI), and ATP synthase. Light is captured by the photosystems and converted into a highly reducing electron and oxidizing cation via a charge separation reaction. These reactions drive linear electron flow (red arrows) from PSII to the plastoquinone (PQ) pool, through Cyt b_6f and PSI. At PSI, a ferredoxin:$NADP^+$ oxidoreductase reductase reduces $NADP^+$ to NADPH. The oxidation and reduction reactions of the PQ pool result in the transfer of protons from the stroma to the lumen (blue arrows). To replenish the loss of electrons due to charge separation, PSI is reduced by electrons from the electron carrier plastocyanin (PC), and PSII oxidizes water. After electrons go through the linear electron chain, a proton gradient builds up across the membrane. The gradient drives the formation of ATP via ATP synthase. ATP and NADPH are used in the carbon reactions, which reduce carbon dioxide to glucose. PSII is in the grana membranes, while Cyt b_6f, PSI, and ATP synthase are primarily in the stroma lamellae [41].

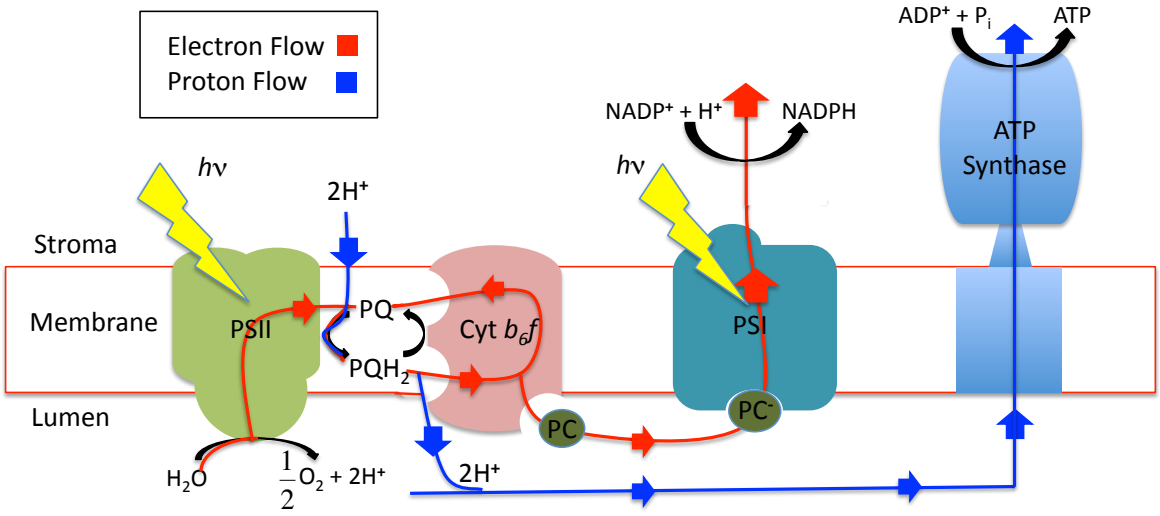

Figure 1.1: A schematic of the light reactions. The absorption of light ($h\nu$) is indicated by the lightning bolt graphics. Proton movement is indicated by the blue lines and arrows, and electron movement is indicated by the red lines and arrows. Abbreviations are elaborated in the main text.

Light harvesting, the step in which light is absorbed and converted into chemical energy, is indicated in Figure 1.1 by the lightning bolts and electron flows through PSII and PSI. The photosystems are multiprotein complexes consisting of antenna proteins that absorb and transfer photo-energy and reaction centers, where excitation energy is converted into a charge separated state. The need for antenna proteins arises from the fact that sunlight is typically quite dilute and because having an entire photosynthetic machinery (Figure 1.1) for each chlorophyll would be energetically costly for the plant [20]. However, sunlight intensities fluctuate and can be intense enough to fully reduce the plastoquinone pool. Under these conditions, the PSII reaction centers can generate singlet oxygen ($^1O_2$) species that can damage reaction centers and other essential components of the photosynthetic apparatus [10, 84]. The threat of damage makes it essential for PSII to be efficient at light harvesting in low light conditions but also photoprotective in high light conditions.

1.2.2 Light harvesting in photosystem II

Light harvesting in PSII occurs in the grana membrane, which is shown schematically in Figure 1.2. The grana membrane is 70-80% protein and thus is quite densely packed with proteins. It is primarily composed of PSII supercomplexes, which are shown as rods, and major light-harvesting complexes (LHCII), shown as circles. LHCII is an antenna protein. The PSII supercomplex is a two-fold symmetric dimer of proteins and is the smallest assembly of proteins that can perform light harvesting and charge separation in plants. PSII consists of a reaction center (RC) surrounded by antenna proteins.

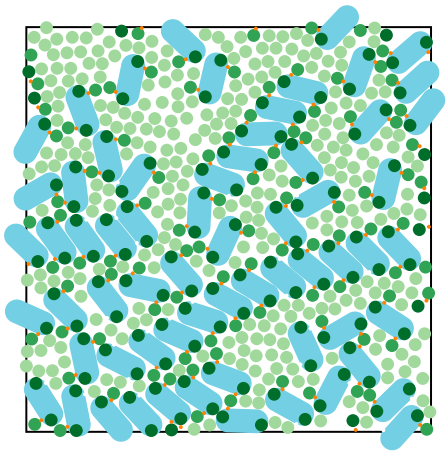

Figure 1.2: A schematic of a portion of the grana membrane. The view is of the face of the membrane. The PSII supercomplexes are shown as rods and the LHCII antenna proteins are shown as circles. Figure courtesy of Anna Schneider.

All of these proteins bind light absorbing pigments called chlorophylls, carotenoids, and pheophytins. An example of a pigment-protein complex, LHCII, is shown in the left of Figure 1.3. The protein serves as a scaffold that holds the pigment cofactors in defined distances and orientations from each other. Light is absorbed by the light-harvesting pigments chlorophyll *a* (Chl-a), chlorophyll *b* (Chl-b), and carotenoids (Figure 1.3, right). Chl-a absorption has two peaks at 420 nm (Soret band) and 680 nm (Q_y band). Chl-b's Soret band is slightly lower in energy, while its Q_y band is higher in energy. Carotenoid absorption peaks around 500 nm. Together, the three pigments cover most of the visible spectrum. The chlorophylls are primarily involved in the absorption of light and transfer of excitation energy to the reaction center, where a small group of chlorophylls and pheophytins (chlorophylls lacking a central Mg^{2+}) trap the excitation by performing a rapid charge transfer reaction.

Excitation energy transfer must beat the "fluorescence lifetime clock" to efficiently convert absorbed light energy into charge separation in the reaction center [47]. When chlorophyll is excited to its singlet excited state, it has three intrinsic pathways by which it can decay back to the ground state. It can decay by fluorescence, which involves the spontaneous emission of a photon of energy, by internal conversion, which is vibrational relaxation back to the ground state, and by intersystem crossing to its triplet state, followed by a slow relaxation back to the ground state [140]. The timescale for the decay of the excited state to the ground state is the fluorescence lifetime. The fluorescence lifetime for chlorophyll is the reciprocal of the sum of the rates of fluorescence and intersystem crossing, since the rate constant for internal conversion for chlorophyll is much slower than that for the other

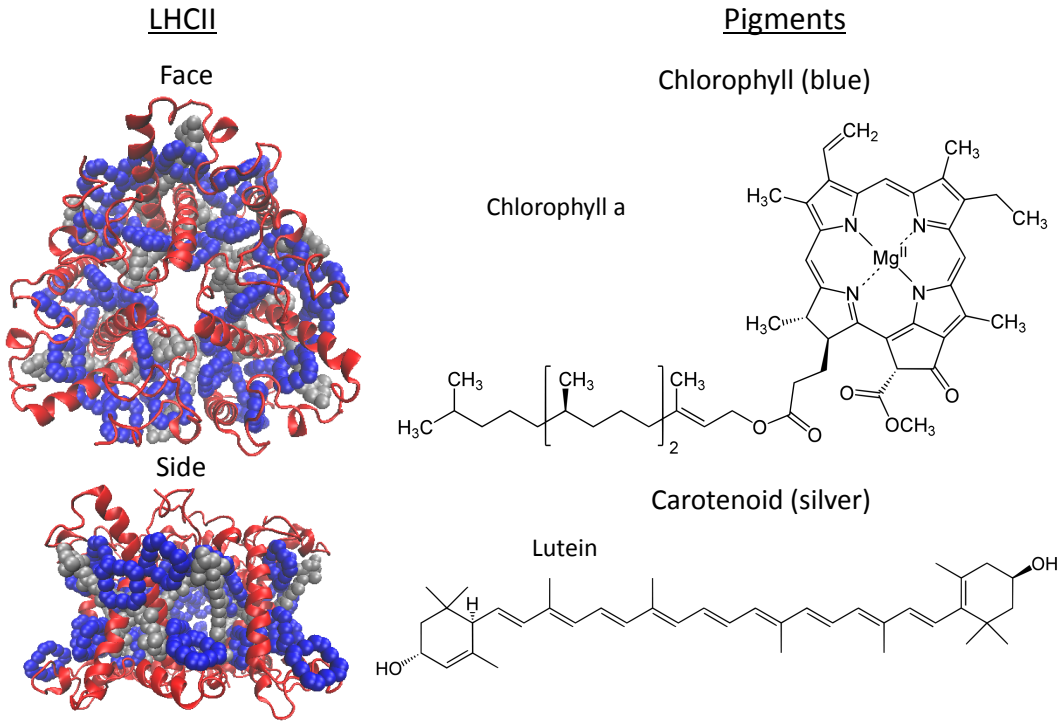

Figure 1.3: Left, The structure of the LHCII antenna. LHCII is a trimer and each monomer is bound to 14 chlorophylls and 3 carotenoids. The protein backbone is shown as a ribbon in red, while blue spheres outline the chlorin group (the conjugated ring) of the chlorophyll and silver spheres are the atoms of carotenoids. Top, LHCII looking face down as in Figure 1.2. Bottom, LHCII looking from the side as in Figure 1.1. Right, examples of pigments that bind to LHCII. Top, the pigment chlorophyll *a*. The chlorophyll chlorin group is the light absorbing moiety, while the phytyl chain (the linear carbon chain) is necessary for binding to the protein. Bottom, the carotenoid pigment lutein. Both pigment images were freely licensed from wikipedia.org.

processes [24]. The fluorescence lifetime for chlorophyll embedded in proteins is ∼4 ns [145]. Energy transfer to the reaction center must be significantly faster than 4 ns to avoid loss by fluorescence and intersystem crossing.

Because the excited states of chlorophylls are quantized, the dynamics of energy transfer must be described using the Schrödinger equation. A quantum system displays net population transfer only if the Hamiltonian is time-dependent [137]. If the time-dependent perturbation of the Hamiltonian is taken to first order, the resulting expression for the dynamics is Fermi's golden rule, which is given by

$$w_{l\to k} = \frac{2\pi}{\hbar} \left|\langle k|V_{kl}|l\rangle\right|^2 \delta(E_k - E_l), \tag{1.2}$$

where $w_{l\to k}$ is the rate from a state l to state k, V_{kl} is the perturbative coupling between the two states and $\delta(E_k - E_l)$ enforces energy conservation.

In one picture of energy transfer in PSII, the states are excitons and the perturbative coupling is due to fluctuations in the site basis. Excitons are linear combinations of states from the site (or pigment) basis that are the eigenvectors of the electronic-coupling Hamiltonian. When this coupling is too strong to be considered perturbative, one can use the exciton basis as a useful basis for Equation 1.2.2 to describe energy transfer. Perturbative coupling arises between excitons from fluctuations in the site basis due to vibrations in the pigment-protein complex. In this description, the coupling between two excitons is proportional to their overlap in the site basis (D. I. G. Bennett, personal communication). The electronic structure of the pigments in PSII is such that the rates of energy transfer computed using this model are significantly faster than the fluorescence lifetime, and excitation energy can be efficiently transferred to the reaction center. More precisely, the electronic couplings in PSII span a wide range and the above model is not sufficient to describe energy transfer, as will be seen in Chapter 5.

In the reaction center, the excitation on the central group of 6 pigments - 4 Chl-a and 2 pheophytin - triggers an electron transfer that occurs on the ps timescale. The mechanism of this reaction is still under debate [122]. The electron is quickly transferred to the plastoquinone pool, thus "separating charge," before charge recombination can occur. The reducing potential of the electron is used to power the electron transfer chain shown in Figure 1.1.

1.2.3 Nonphotochemical quenching

In low light (<300 μmol photons m^{-2} s^{-1}), light harvesting proceeds as described in the previous section. During the day, however, sunlight can typically reach 1800 μmol photons m^{-2} s^{-1}, which is 11 photons $Å^{-2}$ s^{-1}. Because the absorption cross-section of chlorophyll is approximately 1 $Å^2$ per molecule and each reaction center has roughly 250 chlorophylls, there are 2500 excitations per second per reaction center. If we assume that it takes ∼1 ms for the highly energy electron to be transferred to the PQ pool, then the RC can take 1000 excitations per second. The remaining 1500 excitations are excess light.

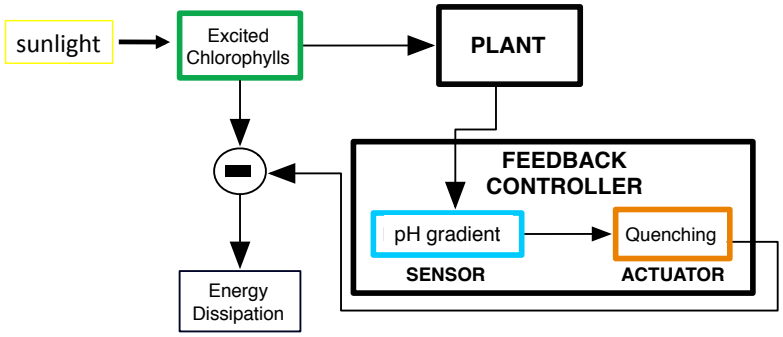

Figure 1.4: Schematic of the feedback loop of nonphotochemical quenching. The excitation energy is input for the plant, the series of light reactions. Outputs from these light reactions, such as the pH gradient, are used as sensors of changing light conditions. The sensor triggers the actuator, which are quenchers that dissipate excess energy, relieve excitation energy pressure on the plant, and prevent damage.

The excess excitation energy from these 'surplus' photon absorptions can relax to the Chl triplet state. These triplets can react with ground state triplet oxygen to generate singlet oxygen ($^1O_2$) that can cause photo-oxidative damage to the reaction center proteins [74]. In light-harvesting complexes, Chl triplets can be quenched by neighboring carotenoids, whose triplet state energy is too low to generate $^1O_2$. If a carotenoid was present in the RC, it would block water oxidation because the potential difference for electron transfer from a carotenoid typically found in photosynthesis [20] to $P680^+$ (∼0.5 V [48]) is more favorable than that for electron transfer from water to $P680^+$ (∼0.2 V [139]). This process would 'short circuit' the electron transfer chain connecting P680 to the water splitting complex. For this reason, damage is localized to the D1 protein of the reaction center, as the primary electron donor (P680) cannot be protected by carotenoid quenching of Chl triplets. To prevent damage, avoid the energetic cost of repair [120], and increase plant fitness [72], PSII contains feedback mechanisms, collectively called nonphotochemical quenching (NPQ), in which excitations can be harmlessly dissipated as heat (Figure 1.4).

Oxygen evolving photosynthetic organisms, such as cyanobacteria, algae, and plants, all have NPQ responses [102]. The mechanisms of NPQ in plants and green algae are generally broken down into energy-dependent quenching (qE), state transitions (qT), inhibition quenching (qI) [93], and zeaxanthin-dependent quenching (qZ) [96]. The classification of different contributors to quenching is somewhat controversial. Mechanisms are sometimes grouped by the timescales of activation and relaxation [43]. The response times of qE are seconds to minutes, of qZ are 15-30 minutes, of qT are tens of minutes, and of qI are hours. Alternatively, the different types of quenching are sometimes grouped by their molecular trigger(s) (Figure 1.4). qE and qZ are trigged by pH gradient [25, 96], qT by reduction of the plastoquinone pool [87], and qI by PSII damage [93]. Despite being subcategorized into qE, qZ, qT, and qI, there are relationships between the various components in NPQ. For

instance, both qE and qZ involve zeaxanthin, but unlike qE, qZ is not reversible within seconds to minutes [96]. Because the processes that give rise to NPQ are not fully understood, it is not clear whether different kinetic components of NPQ involve different photophysical sites and mechanisms or different triggers.

In each mechanism of NPQ, the light-harvesting apparatus quenches excitation in response to changes in sunlight [49, 62, 83]. While there has been significant work on all of the NPQ components, the mechanisms of all of them remain controversial. This thesis will focus on qE, though the methods presented could also be used to study any of the other components of NPQ.

1.3 Interplay between modeling and experiment is required for understanding light harvesting

To understand light harvesting is to know how the structure and arrangement of pigments in the light-harvesting proteins give rise to light-harvesting functionality. There are two components that are required for describing the dynamics of light harvesting in dim light - energy transfer through antenna complexes and electron transfer in the reaction center. Energy transfer dynamics are determined by the Hamiltonian of a pigment-protein complex, which includes the electronic excited states and their couplings of the pigments, the vibrational modes of the complex, and the interaction between the electronic excited states and the vibrational modes. The crystal structure of the complex contributes to the off-diagonal terms of the electronic Hamiltonian and can, using intensive molecular dynamics simulations, give information about the diagonal terms of the electronic Hamiltonian [1]. Obtaining numbers for the remaining terms requires ultrafast experiments that probe energy transfer (Section 1.4.1). Such measurements are used to inform and construct detailed models of energy transfer. In large assemblies such as PSII supercomplexes and grana membranes, the structure and arrangement of pigments, until recently, has been unknown. Thus, measurements of fluorescence lifetime and fluorescence yield have been used in combination with simple models to gain an understanding of light harvesting in these larger assemblies (Sections 1.4.2 and 1.4.3). Measurements of light harvesting are essential for determining the aspects of energy transfer that cannot be derived the crystal structures of the pigment-protein complexes.

1.4 Measuring light harvesting

1.4.1 Ultrafast spectroscopy

The fast rates of energy transfer require experimental methods with which to probe them. The development of laser systems that can readily achieve mode-locking using Ti:Sapphire as the gain medium has enabled the use of ultrafast ($\sim$100 fs) laser pulses to understand light harvesting. The primary technique that has been used is transient absorption spectroscopy

[16]. In TA measurements, two pulsed beams, a pump and a probe, are applied to the sample with a fixed time delay between them. Energy transfer dynamics can be observed by, for example, the excited state absorption of chlorophyll pigments of lower energy than those initially excited. Recently, the development of two-dimensional electronic spectroscopy has enabled the visualization of energy transfer in pigment-protein complexes such as LHCII [51]. These techniques have been useful for mapping the energy transfer dynamics of pigment-protein complexes onto their molecular structure. However, neither technique is useful for measuring the dynamics of spectrally crowded samples such as PSII supercomplexes or grana membranes.

1.4.2 Time-resolved fluorescence

Chlorophyll fluorescence lifetimes are typically measured to understand light harvesting in protein assemblies such as the PSII supercomplex and the grana membrane. Fluorescence lifetimes can be measured by a variety of techniques [73], but the most common is time correlated single photon counting (TCSPC) (Figure 1.5). In TCSPC, a short pulse of light is used to excite the sample. A beamsplitter before the sample diverts some of the laser power to a photodiode, whose resulting current triggers the TCSPC board electronics to start a timer at the same time that the laser excites the sample. Reflected light from the lasers and emitted fluorescence from the sample go through the collection optics. A monochromator selects the fluorescence. When a fluorescence photon hits the detector, it stops the timer that was initiated when the pulse excited the sample. The laser power is set such that it is very unlikely that there will be more than one fluorescence photon per laser pulse. The TCSPC board bins that fluorescence time. The process is repeated for millions of pulses to build up a fluorescence decay.

Because the laser pulse has width in time and the TCSPC electronics are not infinitely fast, the data $I(t)$ represents a convolution of the fluorescence decay $F(t)$ with the instrument response function $IRF(t)$,

$$I(t) = \int_{-\infty}^{t} IRF(t')F(t-t')dt, \tag{1.3}$$

$F(t)$ is assumed to have some form with free parameters, such as a sum of exponentials, so that it can be extracted from the data by performing an iterative forward convolution fit. $F(t)$ provides information on the decay of the excited state population of the sample. When the sample is a pigment in solution, $F(t)$ is likely one exponential and the time constant of the exponential has the simple interpretation of being the excited state lifetime of the pigment. $F(t)$ for pigment-protein complexes and membranes is more complex, and its physical description will be discussed at length in Chapter 4.

While TCSPC can be used to measure energy transfer in large protein assemblies, it typically takes tens of minutes to acquire enough counts to obtain a statistically reasonable fit. This problem has precluded TCSPC from being used to measure the light harvesting as it acclimates to changes in sunlight intensity and wavelength.

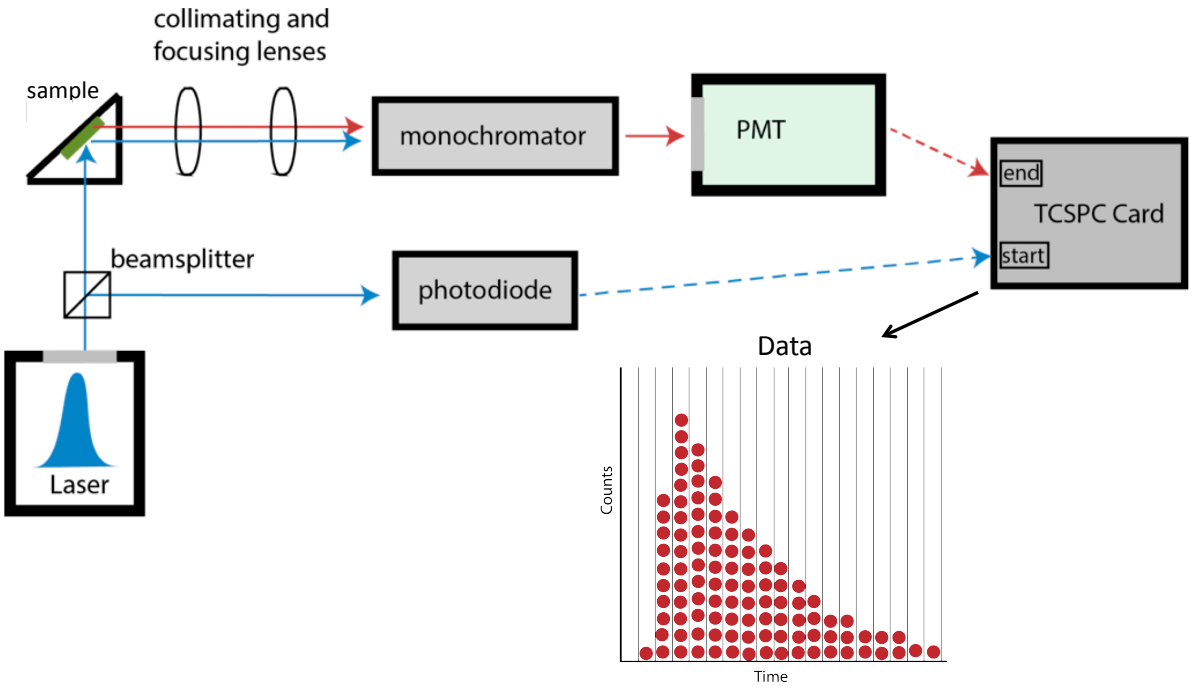

Figure 1.5: A schematic of time correlated single photon counting (TCSPC). A pulse of laser light (blue) is used to excite a flat, solid sample. The sample can also be a solution in the cuvette. In that case, the laser will excite the sample at a 90° angle to the fluorescence collection. At the same time, the TCSPC card begins a timer (start). A detected photon of fluorescence (red) stops the timer and the time the photon was emitted is binned. The process is repeated many times to build a histogram (Data). Figure courtesy of Emily Jane Sylak-Glassman.

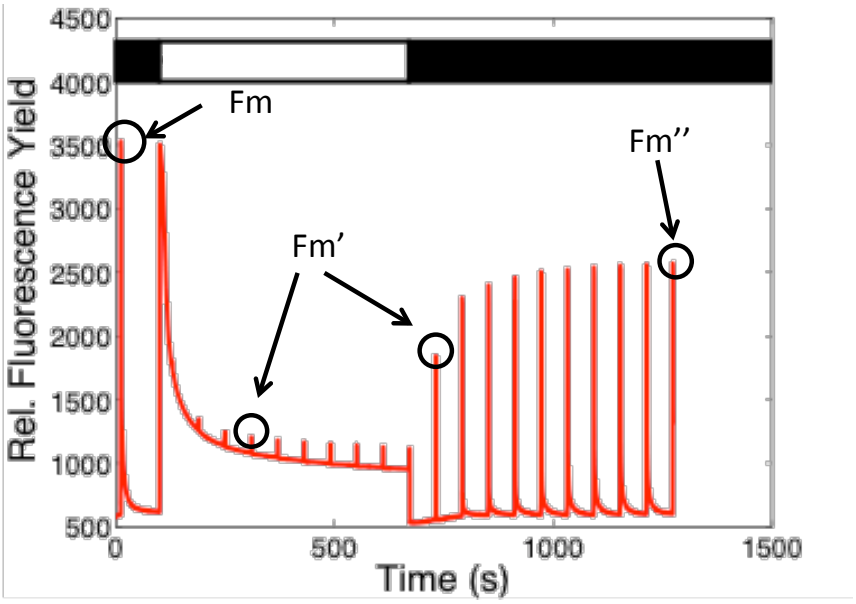

Figure 1.6: A PAM trace of a leaf from wild-type *A. thaliana* is shown, in red. The bar at the top of the figure indicates periods of darkness (black) and actinic light illumination at an intensity of 680 μmol photons m^{-2} s^{-1} (white). The saturating pulses occurred wherever there is a spike in fluorescence. The trace was averaged over 6 different leaves. The F_m peak and the F_m'' peaks are indicated. The F_m' peaks are all the peaks in fluorescence that are not F_m and F_m'', and only two of them are pointed out for clarity.

1.4.3 Pulsed amplitude modulated (PAM) fluorimetry

PAM fluorimetry is a widely used tool for measuring changes in the chlorophyll fluorescence yield as plants acclimate to changing light conditions [133]. PAM fluorimeters only detect fluorescence resulting from a low intensity (< 0.1 μmol photons m^{-2} s^{-1}) modulated measuring light that minimally affects the photochemistry or NPQ in the plant. As a result, PAM can measure the relative fluorescence yield of a leaf or alga as it acclimates to changing light conditions. It is easy to use and can be used for the rapid characterization of plants in the field and algae in the ocean.

Typical PAM fluorimeter measurements of qE consist of a dark-acclimated sample exposed to actinic light (light that results in productive photosynthesis) until qE reaches a steady state (approximately 10 minutes), followed by a period of dark re-acclimation until qE turns off (Figure 1.6). To distinguish the effects of photochemical quenching and non-photochemical quenching, short (< 1 s) pulses of high intensity (up to 20,000 μmol photons m^{-2} s^{-1}) actinic light are periodically used to close PSII reaction centers (peaks in Figure 1.6). Reaction centers are considered to be open when the primary plastoquinone electron acceptor in the reaction center, Q_A, is oxidized and is considered closed when Q_A is reduced [3, 140].

Many parameters about light harvesting, such as the approximate yield of productive charge separation during light acclimation, can be calculated from the PAM trace [3, 8, 28]. To characterize the NPQ response of a plant, it is useful to compare the fluorescence yield when the PSII RCs are closed before and during light acclimation. F_m is proportional to the maximum fluorescence yield measured during a saturating pulse of actinic light applied to dark-acclimated leaves. F'_m is the maximum fluorescence yield following exposure to light, also measured during saturating pulses. A parameter called NPQ can be calculated with these parameters.

$$\text{NPQ} = \frac{F_m - F'_m}{F'_m} \tag{1.4}$$

The NPQ parameter is useful for measuring the dynamics of changes in light harvesting. It is also used to compare relative amounts of quenching between various mutants and light conditions, because it increases as quenching turns on and decreases as quenching turns off. To separate qE from qT, qZ, and qI, F''_m, the maximum fluorescence yield after qE has relaxed, is often measured [3].

PAM traces also allow researchers to quickly assay the qE response with different mutants, light conditions, and chemical treatments. These measurements are often correlated with other biochemical measurements that quantify parameters such as the protein or pigment content to investigate the relationship between these components and qE. However, essential information about energy transfer is missing in the fluorescence yield, which is proportional to the integral of the fluorescence decay. Two different fluorescence decays can give rise to identical fluorescence yields.

1.5 Energy-dependent quenching (qE)

1.5.1 Components

qE in all eukaryotic photosynthetic organisms is dependent on the formation of the pH gradient [25, 94, 152], which serves as the sensor for high light. The molecules that the pH gradient affects for turning on qE have primarily been discovered via genetic studies. There appear to be two mechanisms of qE, one that developed before and one that developed after plants moved to land. While both mechanisms are pH-dependent and quench fluorescence in response to light, their molecular components and mechanistic details appear to be different. Interestingly, *Physcomitrella patens*, a moss that was one of the first photosynthetic organisms to make the transition to land, appears to have both mechanisms of qE [4].

The mechanism of qE in plants has primarily been studied using the model weed, *Arabidopsis thaliana*. The *npq4* mutant of *A. thaliana* lacks the PsbS protein and shows no qE in PAM traces [76]. The *npq4-E122Q* and *npq4-E226Q* mutants, each of which has one lumen-exposed glutamate residue mutated such that it cannot be protonated, have qE levels that are midway between that of wild-type and *npq4*. This result showed that PsbS is pH-sensitive and likely undergoes some conformational change when the lumen pH is low [78]. The *npq1*

mutant in *A. thaliana* showed the importance of the conversion of the carotenoid violaxanthin to zeaxanthin by the enzyme violaxanthin de-epoxidase (VDE) [99]. VDE is located in the lumen, activated by a low lumen pH, and exchanges violaxanthin with zeaxanthin in the light-harvesting complexes on a minutes timescale [63]. In addition, the light-harvesting complexes appear to be required for qE [53].

The mechanism in algae has primarily been studied using the model green alga, *Chlamydomonas reinhardtii*. Zeaxanthin was shown to be required for 30% of the qE response [97]. Lutein appears to be necessary for the remainder of qE [98]. The *npq4* mutant in *C. reinhardtii* lacks the LHCSR3 protein and showed no qE response [115]. LHCSR3 appears to be required for sensing the pH gradient and may be a site of quenching, as it binds pigments [22, 115].

In both plants and algae, qE involves the quenching of excitation energy after the pH gradient develops. How the components described above work in concert with the pigment-protein complexes of the light-harvesting apparatus of PSII to induce quenching continue to be outstanding questions.

1.5.2 Mechanistic picture

The array of LHCIIs and PSII supercomplexes in the grana membrane (Figure 1.2) gives rise to an energy transfer network in which the pigments in the light harvesting proteins absorb light and transfer the resulting excitation energy to RCs, where it is converted into chemical energy. In order to turn on chlorophyll quenching, this energy transfer network must change in response to the protonation of the pH-sensitive proteins (e.g., LHCSR3, PsbS, VDE).

We represent the energy transfer network of the grana membrane using a simple grid in Figure 1.7. We use this picture to illustrate the changes in the energy transfer network that may occur when qE turns on. It is a simplification and reduction of the complete network, which contains ∼10,000 chlorophylls and whose description has not yet been conclusively determined [35]. The nodes (circles) represent groups of chlorophylls at which excitation energy can be localized and are either antenna or RCs. The dark-acclimated membrane without qE is shown on the left. Excitation energy can be absorbed at any of nodes and transferred on the picosecond (10^{-12} s) timescale along the lattice grid lines until it reaches a reaction center (grey nodes) [145]. Once it reaches a reaction center, the excitation energy can be converted into chemical energy. The ΔpH triggers a series of changes in the membrane (Figure 1.7, right) that alter the energy transfer network on a timescale of tens of seconds to minutes. Some antennae (white nodes) gain a photophysical pathway or mechanism with a rate of relaxation to the ground state that is fast relative to fluorescence and intersystem crossing. Efficient quenching of chlorophyll excitations could prevent the excitation from reaching a reaction center that is susceptible to damage. To alter the properties of the pigments such that they become quenching sites may require a rearrangement of the proteins in the membrane, which is indicated by the changes in the connectivity of the network.

While this general picture of quenching is agreed upon, nearly all of the details remain

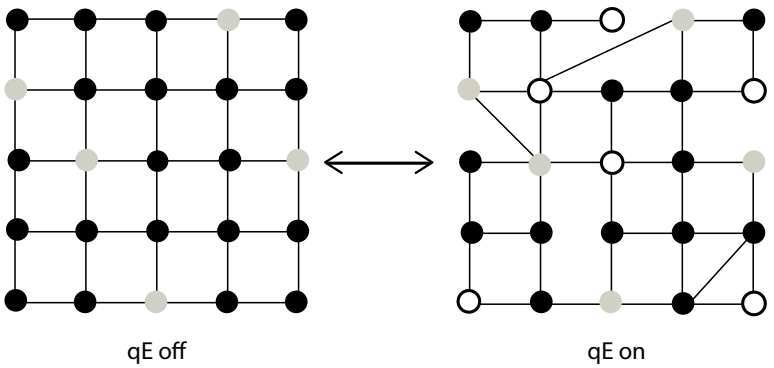

Figure 1.7: The figure shows a schematic of the chlorophyll connectivity of a small portion of the grana membrane when qE is off (left) and when qE is on (right). The black circles represent non-quenching chlorophyll, such as those in LHCII. The grey circles represent PSII reaction centers, and the white circles represent qE quenching sites. At both of these types of sites, there is a rate for removing excitation from the grid. The grid lines display the connectivity for energy transfer between different groups of chlorophyll.

controversial in both plants and algae mainly because of the difficulty in experimentally accessing the information in Figure 1.7. Observing qE requires an intact grana membrane that can generate a pH gradient. However, the grana membrane is complicated and heterogeneous, and its structure is difficult to characterize. Thus, qE has often been studied on proteins isolated from their native membrane environment [126]. The proteins can then be exposed to different, controlled conditions, and the spectroscopic techniques in Sections 1.4.1 and 1.4.2 can be used to extensively characterize the energetic structure. The problem with this approach is that it is quite possible (likely, even) that a protein normally in a crowded membrane environment such as that of the grana (Figure 1.2), once isolated, will behave differently than it would *in vivo*. Another difficulty is in the wide range of timescales that must be monitored simultaneously to capture the changes in Figure 1.7. Characterizing the energy transfer dynamics and connectivity requires methods with picosecond resolution, while the changes in the membrane grid take place on the seconds to minutes timescale.

The lack of knowledge about energy transfer in the membrane and the difficulty in measurement have resulted in a number of theories for the mechanism of qE [126]. Most hypotheses on the mechanism have been based on measurements of certain aspects of the mechanism, such as the nature of the pH trigger [66, 135], the changes in the membrane that occur during qE [64], the site of qE [58], and the photophysical mechanism of qE [2, 6, 55, 71, 92, 125]. It is partly because of this fragmented approach that the mechanism of qE remains unclear.

1.6 Measurements and structure-based models of energy transfer in grana membranes to understand light harvesting in variable light conditions

Understanding light harvesting in variable light conditions requires methods that measure the many timescales involved in light harvesting and its regulation in intact, living systems such as whole leaves and live algae. The methods currently available for measuring qE typically measure either slow biochemical/structural changes (sec to min timescale, which can be characterized using PAM fluorimetry) or the fast dynamics in the light-harvesting antenna (fs to ns timescale, by measuring fluorescence lifetimes or transient absorption) in dark or light-acclimated samples. Understanding how the triggers/components of qE act in concert to activate quenching requires a technique that bridges both slow and fast timescales. The photophysical mechanisms and sites involved in qE are intimately tied to the biochemical and biophysical changes that occur to activate these mechanisms.

To fill this gap in techniques for measuring qE, we have developed a technique for measuring the changing fluorescence lifetime as qE turns on in plants and algae, which we call "fluorescence lifetime snapshots" (Figure 1.8). It is a two-dimensional technique with one time axis being the fluorescence decay time, and the second the adaptation/relaxation timescale. To access the information about the energy transfer grid underlying this data, we have developed a detailed model of energy transfer in grana membranes. This strategy of using fluorescence lifetime snapshots and energy transfer models to leverage the information in those snapshots is a general one that can be used to study any of the mechanisms of NPQ. Moreover, it can be applied to using other ultrafast spectroscopic techniques for studying the photophysical mechanisms of NPQ.

The development of the fluorescence lifetime snapshot technique on live cells of green algae in Chapter 2 and leaves of plants in Chapter 3. The need for an accurate model of energy transfer in grana membranes to interpret the snapshot data is described in Chapter 4. The development of the membrane model is described in Chapters 5 and 6. Chapter 6 concludes with an outlook on how the two developments from this thesis - the snapshot technique and the detailed energy transfer for the grana membrane - can be used to understand the light harvesting and its regulation in fluctuating light conditions.

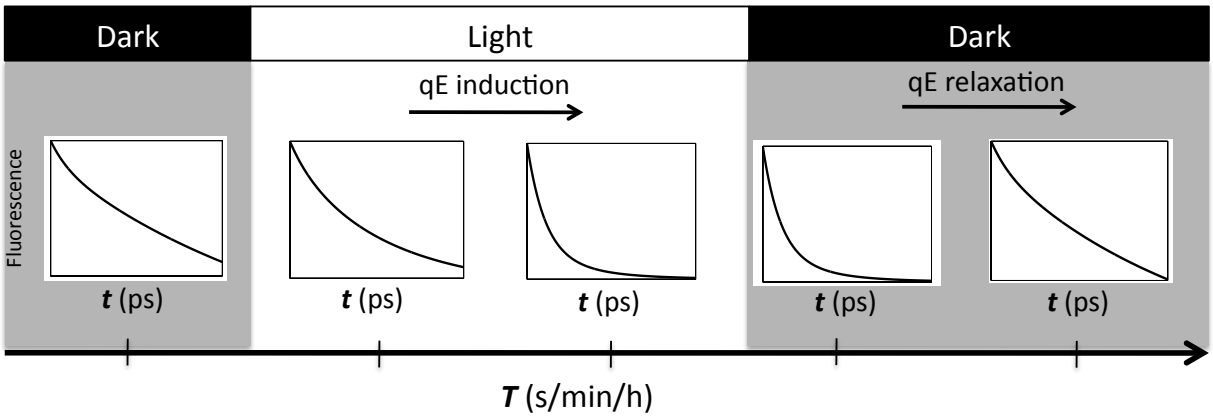

Figure 1.8: Schematic of the "fluorescence lifetime snapshots" measurement. The measurement tracks changes on both the T timescale (sec to hours) as well as in the t timescale (ps to ns). qE triggering and the thylakoid membrane rearrangement occurs on the T timescale. Quenching of chlorophyll fluorescence occurs on the t timescale and contains information about the energy transfer network of the grana membrane.

Chapter 2

Fluorescence lifetime 'snapshots' reveal two qE mechanisms in live cells of *Chlamydomonas reinhardtii*

2.1 Experimental setup and strategy

A particular difficulty in performing fluorescence lifetime experiments on intact photosynthetic samples undergoing qE is that it takes several minutes to accumulate enough counts to obtain fits that have sufficiently small confidence intervals. Gilmore and coworkers were able to chemically pause thylakoids undergoing qE using dithiothreitol (DTT), 3-(3,4-dichlorophenyl)-1,1-dimethylurea (DCMU), and methyl viologen [49]. Johnson and Ruban added glutaraldehyde, which irreversibly cross-links proteins and chemically "freezes" the sample, to plant chloroplasts that had induced qE [65]. While both of these strategies were allowed measurement of a fluorescence lifetime for light-acclimated thylakoids or chloroplasts, they cannot be used to measure fluorescence lifetimes during acclimation, as they require stopping the acclimation of qE before measurement.

The measurement of the fluorescence lifetimes of intact algae or leaves is complicated by the fact that turning on qE using strong light sources instead of chemical inhibitors will induce high levels of background fluorescence or saturate the sensitive detectors typically used for TCSPC. To address this problem, Holzwarth and coworkers developed a method using a rotating cuvette by which the fluorescence lifetime could be measured while qE was kept on [58, 85]. This setup, however, required data acquisition times of ∼45 min, which is longer than the time for qE induction and relaxation.

To measure fluorescence lifetime snapshots, we built a shutter apparatus to allow light acclimation to occur without damage to the detector (Figure 2.1) [5]. The apparatus is a conventional single photon counting (SPC) setup with the addition of an actinic light source and three shutters which can be open or closed in front of the excitation, actinic, and detection beams. The apparatus was built such that actinic light could be applied to the sample, with short periods in which the sample would interact with the laser to measure the

time-resolved fluorescence while the PSII reaction centers remained saturated (Figure 2.3*A*). To record an adequate number of fluorescence counts for the shortest increments in the adaptation trajectory, the experiment could also be performed using the pulsed laser as both an actinic and a measuring light source (Figure 2.3*B*). The repetition rate of the laser (75.7 MHz) and the pulse energy at the sample (5 pJ) were chosen to keep PSII reaction centers closed and maximize fluorescence collection while avoiding singlet-singlet and singlet-triplet annihilation conditions. We used the apparatus to study the qE mechanism of *C. reinhardtii*.

2.2 Materials and methods

2.2.1 Growth and sample preparation of *C. reinhardtii*

Cells of the 4A$^-$ strain were grown in low light (40 μmol photons m^{-2} s^{-1}) with a reduced carbon source (tris-acetate phosphate (TAP) medium) for 1 to 2 days until exponential growth was reached. Approximately 1×10^5 cells from this culture were used to inoculate 50 mL of minimal (high salt (HS)) media. The HS culture was grown in high light (400–440 μmol photons m^{-2} s^{-1}) in air, with ambient CO_2 as the only carbon source. Cultures that were in the late-logarithmic growth phase, between 3 and 5x10^6 cells mL^{-1}, were used for experiments. Before performing fluorescence measurements on the samples, the cells were dark incubated for 30-50 min. The sample was prepared in a 1 cm pathlength cuvette. The cuvette contained algae diluted to a concentration of 0.5 OD at 410 nm with 500 μL of 0.1% agarose to suspend the algae and water to 1.5 mL.

2.2.2 PAM fluorescence measurements

The maximum efficiency of PS II (F_v/F_m) was measured as described in Peers et al. [115] and was $\sim$0.6 for all measurements. The measurement shown in Figure 2.2 was done as described in Section 2.3.1.

2.2.3 Fluorescence lifetime apparatus

Time-resolved fluorescence measurements were acquired using a time-correlated single photon counting (TCSPC) apparatus. A commercial mode-locked oscillator (Mira 900F, Coherent) pumped by a diode-pumped, frequency-doubled Nd:YVO4 laser (Verdi V-10, Coherent) generated $\sim$150 fs pulses with a repetition rate of 76 MHz and was tuned to 820 nm with a full width at half-maximum (fwhm) of 12 nm. This output was frequency doubled to 410 nm using a 1-mm-thick beta barium borate (BBO) crystal. The pulse energy at the sample was 10 pJ. Fluorescence emission was sent through a polarizer set at the magic angle. The fluorescence was then sent through a spectrograph (Newport 77400-M) and detected with a microchannel plate photomultiplier tube (MC-PMT) (Becker-Hickl PML-16C). The MC-PMT could discriminate the fluorescence photons into 16 channels, separated 12

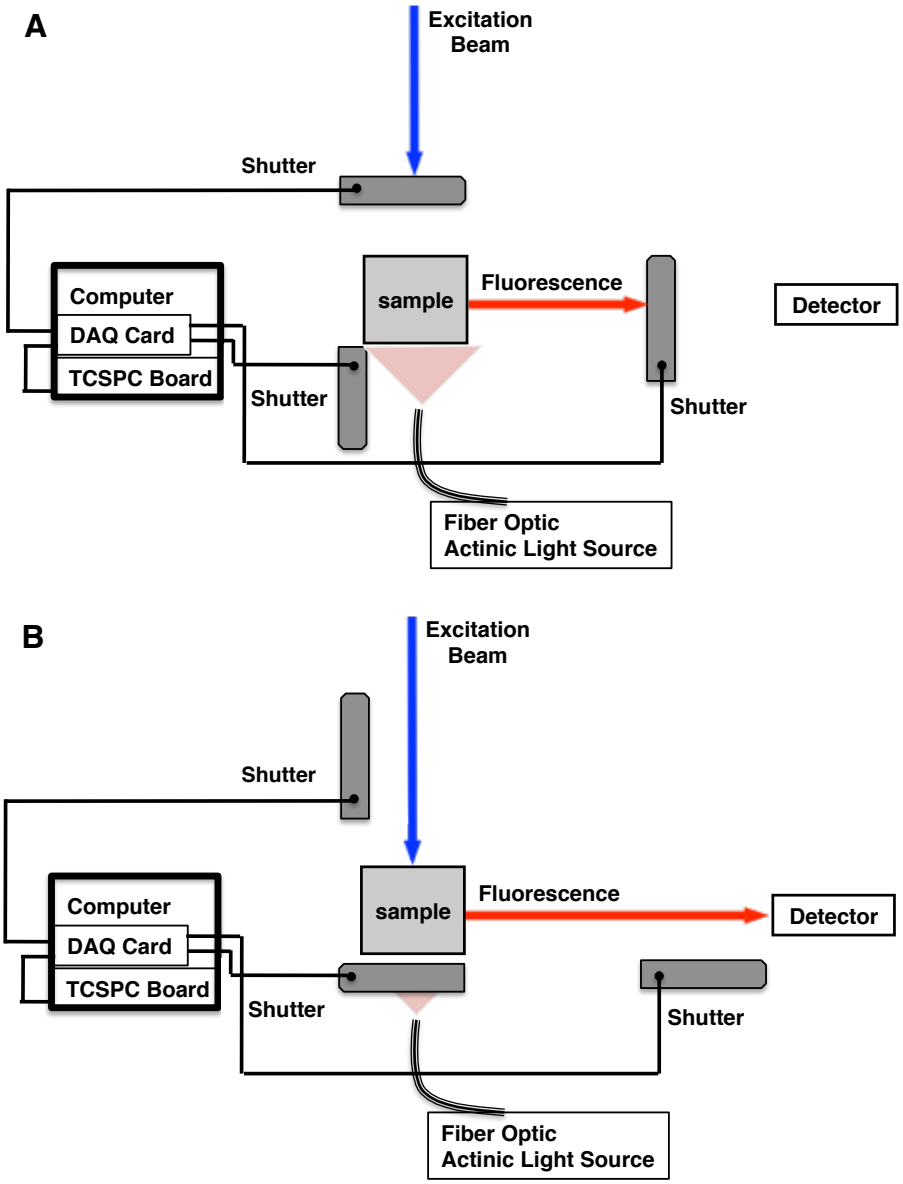

Figure 2.1: The shutter apparatus for measuring fluorescence lifetime snapshots. The sample can interact with the laser and/or a white actinic light source, both of whose access to the sample is gated by a controllable shutter. The path of fluorescence photons to the detector is also gated by a shutter. Light acclimation occurred when the configuration was in A. Data was collected only when the apparatus was in configuration B.

nm apart from each other. Each channel contained the fluorescence decay for photons at that wavelength, ±1 nm. The MC-PMT was controlled using the DCC-100 detector control (Becker-Hickl), with the gain set to 90%. The photons were collected into 3.6 ps wide bins using a Becker-Hickl SPC-630 counting board. The full width half maximum of the instrumental response function was 150 ps.

2.2.4 Shutter apparatus

The shutter apparatus built for measuring the adaptation of *C. reinhardtii* cells to different light conditions is shown in Figure 2.1. The sample can interact with the laser and/or a white actinic light source (Schott KL1500 LCD), both of whose access to the sample is gated by a controllable shutter. The path of fluorescence photons to the detector is also gated by a shutter. The shutters were constructed using a rotary solenoid (LEDEX, Part No. 810-282-330) which was connected to a 12-V power supply (Circuit Specialists, Inc., 3645A). To control the shutters, a 5-V square wave was sent from the computer through a data acquisition card (National Instruments, PCI-6229) to three relays (Potter & Brumfield, JWS-117-1). A 5-V square wave from the computer triggers the TCPSC board to start a measurement and collect photons [12].

2.2.5 Measurement of qE induction and relaxation

Actinic light measurement

The sample remained in the dark until time $T = 0$, when the shutter in front of the actinic light (1000 μmol photons m^{-2} s^{-1}) was opened. To measure a fluorescence decay, the actinic shutter was closed, and 0.1 s later the laser shutter and detector shutters were opened and the SPC board was triggered for 0.2 s. 0.1 s later the actinic light shutter was reopened. Fluorescence decays were collected at times T =1, 2, 5, 10, 15, and 19.5 s. At a time T_{relax}, the laser and detector shutters were opened again for 0.4 s, and the SPC board was triggered 0.1 s later for 0.3 s. Fluorescence decays were measured for T_{relax} = 1, 2, 10, 18, 30, and 60 s. The experiment was done 18 times on a single culture with each T_{relax} measured 3 times, and the results were averaged for better signal to noise. The experiment allowed us to obtain fluorescence decays at the selected times using actinic light as a high light source.

Laser Light Measurement

As depicted in Figure 2.3, the laser was used to induce changes in the sample. The laser illuminated the sample for 20 s, and time-resolved fluorescence decays were collected for 80 ms every 200 ms. After 20 s of laser exposure, the laser shutter was closed for a relaxation time. The measurement sequence was repeated for 12 aliquots from the same culture, and the fluorescence decay at each collection time was averaged over all aliquots. After the relaxation time ended, the laser shutter was opened for 1.6 s, during which 8 fluorescence

decays were collected every 200 ms. The relaxation times used were 1, 2, 5, 7, 10, 14, 18, 22, 26, 30, 45, and 60 s. Of the 8 fluorescence decays collected in the 1.6 seconds of the relaxation measurement, the second to the fifth fluorescence traces were summed to give the relaxation trace. Because more counts were collected in the measurement of relaxation than in measurement of the induction, each relaxation lifetime came from the average of two aliquots. Fluorescence decays were generated by adding counts at each collection time over all aliquots and over channels 6 (644 nm) to 12 (716 nm).

Role of the Laser in Both Measurements

The laser has two roles in the measurements depicted in Figure 2.3. It is used to measure the fluorescence lifetimes of the chlorophylls as in a conventional TCSPC experiment as well as serve as a photosystem II (PSII)-saturating high light source (similar to the role of the blue light in recent papers from Holzwarth and coworkers [58, 85]. To ensure that the laser does in fact close all PSII reaction centers, we estimated the laser fluence on the sample. The laser produces 2.2 x 10^7 photons at 410 nm per pulse with a beam area of 1.28 mm^2. In the focal volume of the sample, the total concentration of chlorophylls is ∼0.2 OD, and we assume there are 250 chlorophylls per reaction center. There are 6.6 x 10^{10} reaction centers in the focal volume. For a sample that has an OD of 0.2, 36% of incident photons will be absorbed by the PSII antenna. Assuming that all photons absorbed by the chlorophylls are trapped by RCs, 3.4 x 10^{-2}% of RCs are closed after one pulse. If the reaction center could not reoxidize Q_A^-, all RCs would be closed in ∼40 μs. The reaction center, however, transfers electrons from Q_A^- to Q_B on a ∼200 μs timescale [20]. Therefore, under these high light conditions, the saturation of the reaction centers in the focal volume depends on the time for plastoquinone pool to become reduced, which, in our measurement, was ∼0.3 s. The fluorescence lifetime of the sample was much shorter than the time between pulses, 13.2 ns, ensuring that excitations did not remain in the antenna from pulse to pulse. This combined with the low (5 pJ) pulse energy meant that there was negligible singlet-singlet and singlet-triplet annihilation during the measurement [145].

2.2.6 "DCMU-treated," "light acclimated," and "nigericin-treated" measurements

For the "DCMU-treated" measurement, DCMU was added to a final concentration of 500 μM to dark-acclimated *C. reinhardtii* cells. After a 1 min incubation time, fluorescence counts were collected for 5 s every 5 s for 200 s. The fluorescence decays collected during each 5 s interval did not change in fluorescence lifetime and thus were averaged together.

For the "light-acclimated" and "nigericin-treated" measurements, the sample remained in the dark until time $T = 0$, when the shutter in front of the actinic light (600 μmol photons m^{-2} s^{-1}) was opened. After 150 s, the actinic light shutter was closed and 0.1 s later the laser and the detector shutters opened for 7 s, during which fluorescence counts were collected. After this period, the laser and detector shutters were closed and 0.1 s later the

actinic light shutter was opened for 5 s. This sequence of 7 s and 5 s was repeated 7 times. The fluorescence decays collected during each 7 s interval did not change in fluorescence lifetime and thus were averaged together. This measurement was the "light acclimated" measurement. After the last 7 s and 5 s sequence, nigericin was added to the sample to a final concentration of 100 μM. After 45 s, the actinic light shutter was closed and the laser and the detector shutters opened for 5 s, during which fluorescence counts were collected. After this period, the actinic light shutter was opened, and 0.1 s later the laser and detector shutters were closed for 5 s. After this period, the laser and detector shutters were closed, and 0.1 s later the actinic light shutter was opened. This sequence of 5 s and 5 s was repeated 20 times. The fluorescence decays collected during each 5 s interval did not change in fluorescence lifetime and thus were averaged together. This measurement was the "nigericin" measurement.

2.2.7 Data fitting

Fluorescence decays were fit to Eq. 2.2 using the method of least squares using Fluofit (Picoquant). The kinetics for induction of amplitudes of the fast components were fit to Eq. 2.3 using the curve fitting software on MATLAB (Mathworks). Bootstrapping was performed using Fluofit. The amplitude-weighted lifetime $\langle\tau\rangle$ was calculated using Equation 2.1.

$$\langle\tau\rangle = \sum_i A_i\tau_i \tag{2.1}$$

A brief explanation of bootstrapping is as follows. Imagine there are N data points in a fluorescence decay. Bootstrapping involves the random selection with replacement of N data points from the fluorescence decay, followed by a fitting of this sampled data. This process of sampling from the data points in a fluorescence decay was repeated 500 times and the amplitudes and lifetimes from each fit were recorded. The 68% confidence intervals indicate the range of recorded amplitudes or lifetimes between which 68% of the bootstrapping fits fall.

2.3 Experimental results

2.3.1 PAM fluorescence trace of *C. reinhardtii*

Figure 2.2 shows a PAM fluorescence trace for wild-type *C. reinhardtii* grown photoautotrophically in high light (400 μmol photons m^{-2} s^{-1}) until the late log phase of growth, and dark acclimated for 20 minutes before measurement. Actinic light was applied at $T = 0$ s, where T is the time axis along which light adaptation occurs. During the first ~0.3 s of actinic light illumination (inset), the fluorescence yield increased as the plastoquinone pool became fully reduced, and photosystem II reaction centers became saturated [127]. Due to the induction of NPQ quenching pathways, the fluorescence yield rapidly decreased for 0.3 s $< T <$ 2.5 s, decreased much less for 2.5 s $< T <$ 10 s, and plateaued by $T = 20$ s at a

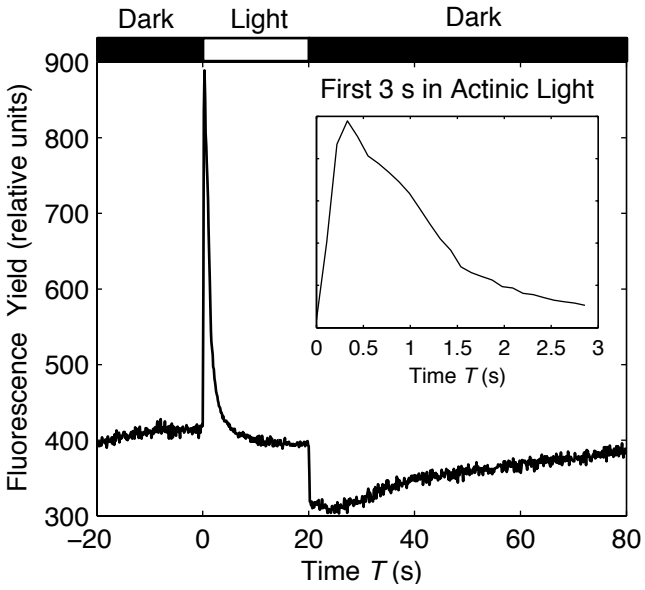

Figure 2.2: PAM fluorescence trace of wild-type *C. reinhardtii*. The actinic light intensity during the light induction period between $T = 0$ s and $T = 20$ s was 1000 μmol photons m^{-2} s^{-1}. The inset shows the fluorescence yield during the first 3 s after the actinic light is applied. The time resolution was 0.11 s.

yield slightly lower than that before actinic light was applied. The actinic light was turned off after $T = 20$ s, and the fluorescence yield dropped below what it was before the actinic light was turned on. This occurs because oxidation of the plastoquinone pool opened PSII reaction centers while NPQ quenching sites were still turned on. NPQ turned off rapidly as the algae acclimated to the darkness over the next 60 s, suggesting that the NPQ observed here is qE.

The PAM measurement allowed us to qualitatively describe the dynamics as algae acclimated to light. However, it is possible that different qE processes contributed to the changes in fluorescence yield in this organism and that the amplitudes and fluorescence lifetimes of these processes were averaged out. To determine the lifetimes and amplitudes of qE quenching processes, we measured fluorescence decays of *C. reinhardtii* at different points on the T axis as the algae induced qE in high light for 20 s and as the algae turned off qE in an ensuing 60 s of darkness.

2.3.2 Measurement of time-resolved fluorescence decays during light acclimation

We intended to use the shutter apparatus to periodically measure the fluorescence lifetime during light acclimation similar to PAM measurement, where the laser would serve as both a saturating and measuring light. This measurement, which we call the actinic light

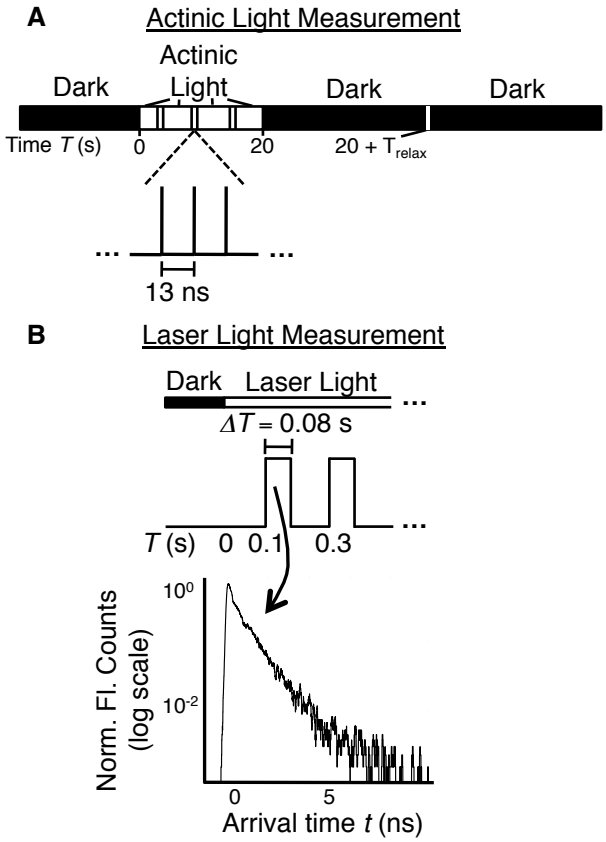

Figure 2.3: Schematic of measurement. (A) In the actinic light measurement, the sample remained in the dark until time $T = 0$ s, when the actinic light treatment was begun. Measurement of the fluorescence lifetime occurred periodically by closing the shutter to the actinic light beam and opening those in front of the pulsed laser and the detector (thin rectangles). The actinic light shutter was closed at $T = 20$ s and a measurement was made a time $\mathrm{T_{relax}}$ later. (B) In the laser light treatment, laser light was applied for 0 s $< T <$ 20 s. Fluorescence acquisition periods were $\Delta T = 0.08$ s long and spaced 0.2 s apart. The first $F(t, T)$ was collected at $T = 0.1$ s to avoid loss of counts for the first measurement due to the opening time for the shutter. A representative fluorescence lifetime trace corresponding to a collection period at the beginning of the 20 s induction time is shown. The data were smoothed with a moving average filter with a span of 25 bins for visual clarity.

measurement, began, at $T = 0$, by opening the shutter in front of the actinic light beam. To make a fluorescence lifetime measurement during qE induction, when 0 s $< T <$ 20 s, the actinic light shutter was closed, shutters in front of a pulsed laser and a detector were opened, and a trigger was sent to the SPC board to initiate collection and binning of fluorescence counts for a time ΔT (Figure 2.1*B*). After ΔT, to resume light adaptation, the laser and detector shutters were closed, and the actinic light shutter was reopened (Figure 2.1*A*). This strategy prevents actinic light from overloading the detector and allows for the collection of fluorescence decays during the qE induction period. To measure fluorescence decays during the qE relaxation period, we closed the actinic light shutter when $T = 20$ s. At a time T_{relax} later the laser and detector shutters were opened, and the SPC board was triggered to collect and bin counts for ΔT, after which the laser and detector shutters were closed. The apparatus measures fluorescence decays $F(t, T)$ at different points along the T axis, where t corresponds to the arrival time of fluorescence photons after excitation of the sample with a laser pulse.

Ideally, the collection time, ΔT, would be set such that $F(t, T + \Delta T) \approx F(t, T)$. As seen in Figure 2.2, inset, the fluorescence yield changes every 0.11 s during the first 3 s of the actinic light treatment, so ΔT should be less than that time. However, enough fluorescence counts ($\sim$1000 counts in the maximum bin) must be obtained during ΔT to allow accurate fitting of the fluorescence decays. A compromise between these two considerations and the electronic limitations of the photon counting board allowed us to collect photons for $\Delta T = 0.08$ s every 0.2 s on the T axis, provided the measurement $F(t, T)$ was repeated on more than 10 different aliquots from an algal culture to increase the number of counts in the maximum bin to $\sim$1000. This ΔT was too small to use the actinic light source as in the strategy described above because the shutters had a open/close time of $\sim$40 ms. Even if faster shutters were used, the sample would be exposed to the laser for 40% of the light adaptation period. For the purposes of measuring light induction of qE in *C. reinhardtii*, we used the laser light as both an actinic light source and as a measuring light.

The repetition rate of the laser (75.7 MHz) and the pulse energy at the sample (5 pJ) were chosen to keep PSII reaction centers closed and maximize fluorescence collection while avoiding singlet-singlet and singlet-triplet annihilation conditions. If singlet-triplet annihilation was a significant factor, the results from the actinic light treatment and the laser light treatment would be different. In fact, measurements on the same sample using the two strategies gave very similar results, which validated the use of the laser as both the actinic light source and the measuring light (Figures 2.5 and 2.6).

At T_{relax}, the time for which the algae are in darkness after the high light treatment, the goal is to measure a fluorescence decay with the PSII reaction centers closed and without any qE induced by the laser during the measurement. However, as seen in the inset of Figure 2.2, it takes $\sim$0.3 s of exposure of dark-acclimated cells to high light before the reaction centers are closed. qE quenching turns on immediately after saturation of the reaction centers. Because these changes may occur at different rates depending on T_{relax}, we averaged the fluorescence curves collected between 0.2 and 1.0 s within ΔT. Selection of this interval resulted in the observation of full reversal of changes in the fluorescence lifetime caused by

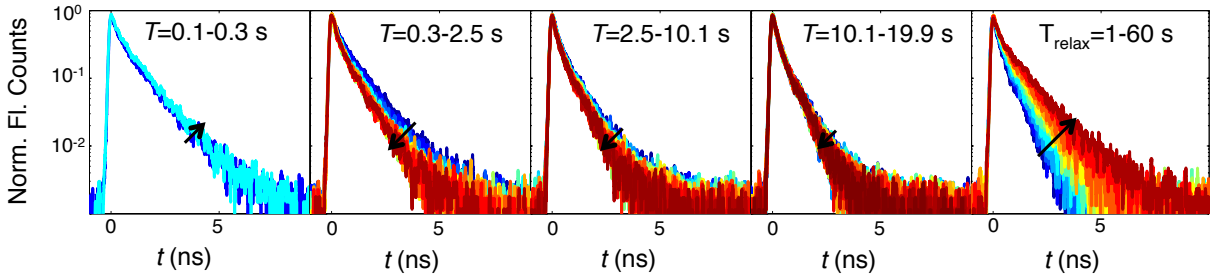

Figure 2.4: Normalized fluorescence decays from emission at 680 nm from the measurement described in Figure 2.3. The data were smoothed with a moving average filter with a span of 20 bins for visual clarity. The direction of the black arrow indicates the T axis. The different colors represent fluorescence decays collected at different times along the T axis.

the 20 s laser light treatment. Only one measurement at $\mathrm{T_{relax}}$ was done per sample to avoid the influence of the laser on any measurements at later $\mathrm{T_{relax}}$ times.

Figure 2.4 shows the results of the experiment described in Figure 2.3*B*. The qualitative dynamics of the fluorescence decays curves match those seen in the PAM fluorescence trace in Figure 2.2. The fluorescence decay time increases in the first 0.3 s due to the closing of all reaction centers in the excitation volume. The fluorescence lifetime decreases substantially in the next 2 s, decreases less from 2.5 to 10.1 s, and barely decreases from 10.1 to 19.5 s. Laser illumination was stopped after 20 s, and the lifetime returned to its initial value 60 s after the light treatment.

2.3.3 Amplitudes and lifetimes from the laser light measurement

To quantify the changes seen in Figure 2.4 over T, fluorescence counts were summed over all collected wavelengths for each $F(t,T)$, and the resulting fluorescence decays were normalized and globally fit using the method of least squares to the equation

$$F(t,T) = \sum_i A_i(T) e^{\frac{-t}{\tau_i}}, \tag{2.2}$$

where the ith component has an amplitude $A_i(T)$, such that $\sum_i A_i(T) = 1$. Three lifetime components were required to give a reasonable fit, as judged by the χ^2 value being between 0.8 and 1.2 and uncorrelated residuals for each $F(t,T)$. Each lifetime and its corresponding amplitude do not necessarily correspond to one physical process and its absorption cross-section in the thylakoid membrane. Rather, each lifetime and its amplitude are possibly the result of a sum of the amplitudes of several processes in the membrane with approximately the same lifetime. To calculate the uncertainty in the fitted parameters, we performed bootstrapping on the fits, which was repeated 500 times to obtain 68% confidence intervals for each of the fitted parameters.

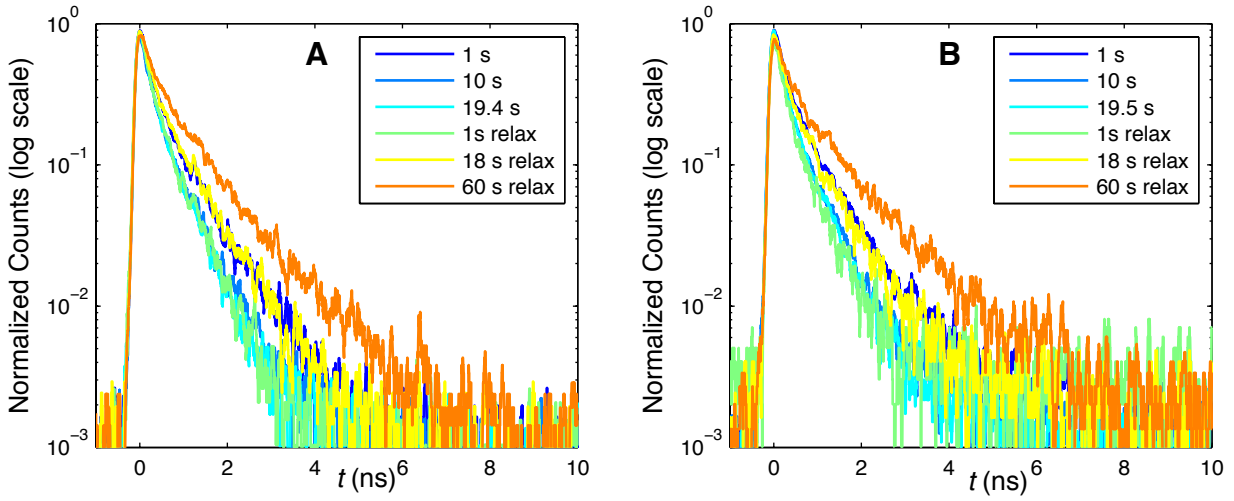

Figure 2.5: Normalized fluorescence decays from emission at 680 nm (A) after 1, 10, and 19.5 s of the actinic light treatment and 1, 18, and 60 s after the actinic light is turned off and (B) after 1, 10, and 19.4 s of the laser light treatment and 1, 18, and 60 s after the laser light is turned off. The data were smoothed with a moving average filter with a span of 20 bins for visual clarity. The measurements were performed as described in Figure 1 of the main text.

The lifetimes from the global fit were 64 (63, 65) ps, 305 ps (304, 320), and 1000 (990, 1074) ps. The 68% confidence intervals indicated in parenthesis were taken as an average over several timepoints. For simplicity, for the remainder of the manuscript, we will call these components the 65 ps, 305 ps, and 1 ns components with amplitudes $A_{65\ \mathrm{ps}}(T)$, $A_{305\ \mathrm{ps}}(T)$, and $A_{1\ \mathrm{ns}}(T)$.

Variable fluorescence is associated only with photosystem II in the thylakoid membrane [20]. Therefore, we associated any changes in the amplitudes of these three components with respect to T with changes in excitation trapping in PSII. $A_{65\ \mathrm{ps}}(T)$ and $A_{305\ \mathrm{ps}}(T)$ are shown in Figure 2.7A and B, respectively. $A_{65\ \mathrm{ps}}(T) + A_{305\ \mathrm{ps}}(T)$ and $A_{1\ \mathrm{ns}}(T)$ are shown in Figure 2.7C. The 68% confidence intervals of the amplitudes at selected points are indicated in these two figures by error bars.

$A_{65\ \mathrm{ps}}(T)$ (Figure 2.7A) decreased slightly for the first 0.3 s of light illumination (inset), then rose from ∼0.61 at $T = 0.3$ s to ∼0.68 when $T = 1$ s and remained constant within error for the remainder of the light adaptation period. Based on this plot, no definite conclusions on the dynamics of this component could be made for 20 s $< T <$ 80 s because of the uncertainty in the amplitude. $A_{305\ \mathrm{ps}}(T)$ (Figure 2.7B) also decreased for the first 0.3 s of illumination (inset) to ∼0.16 but subsequently increased for the remainder of the saturating light treatment, reaching ∼0.25 at $T = 20$ s. Forty-five seconds after the light treatment ended, the amplitude decreased back to the value at $T = 0.3$ s and appeared to decrease to an even lower value by 60 s in darkness. Finally, $A_{1\ \mathrm{ns}}(T)$ increased in the first 0.3 s of light

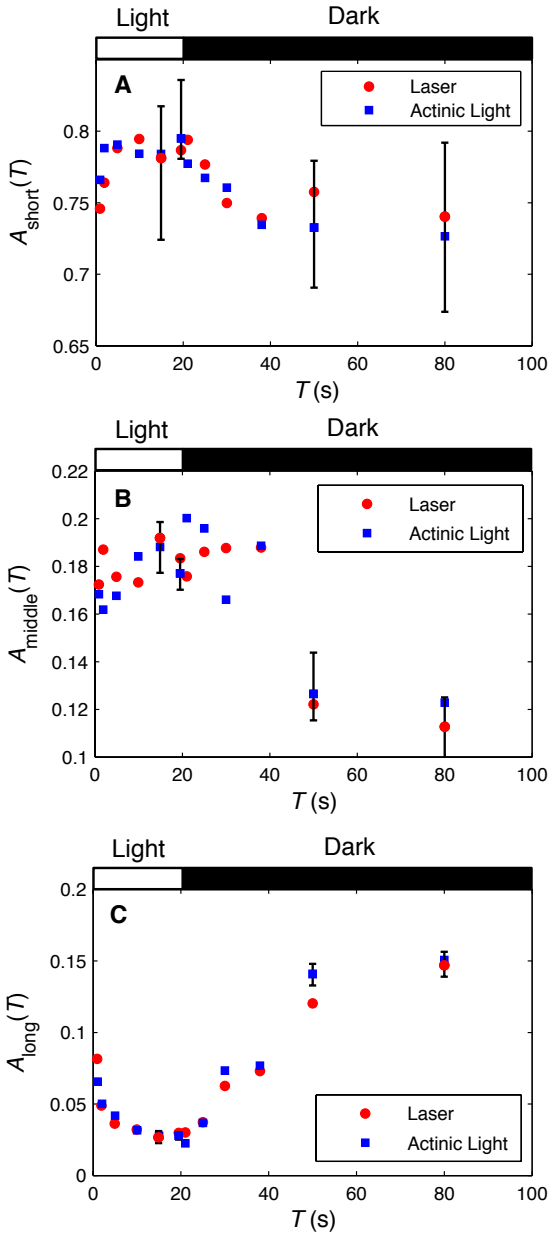

Figure 2.6: Amplitudes as a function of T when comparing the laser light treatment (red circles) with the actinic light treatment (blue squares). The short, middle, and long lifetime components for the actinic light treatment were 60 (57, 61) ps, 330 (320, 340) ps, and 1000 (970, 1030) ps, respectively, where the 68% confidence intervals as calculated by bootstrapping are indicated in parenthesis and are an average over several timepoints. The short, middle, and long lifetime components for the laser light treatment were 50 (47, 51) ps, 300 (287, 316) ps, and 950 (915, 984) ps, respectively. Error bars are shown for the laser light treatment at T = 19.4 s and 80 s and are shown for the actinic light treatment at T =15 s and 50 s.

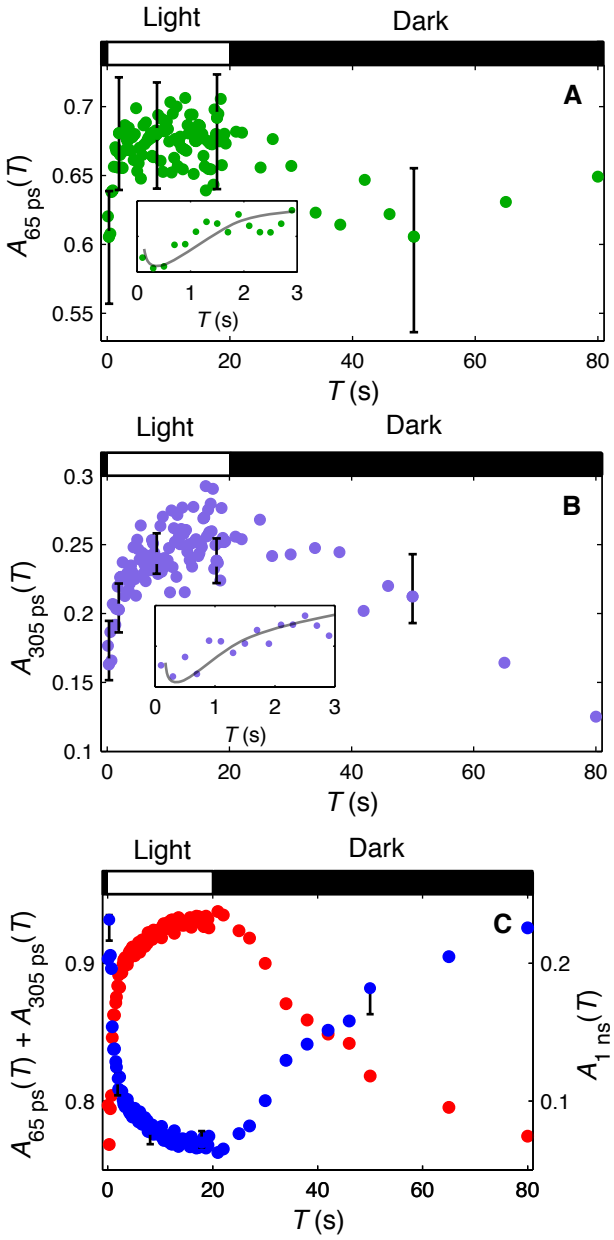

Figure 2.7: Changes in the amplitudes of the fluorescence lifetime components over T. (A) amplitude of the 65 ps component ($A_{65\ \mathrm{ps}}(T)$, red circles), (B) amplitude of the 305 ps component ($A_{305\ \mathrm{ps}}(T)$, violet circles), and (C) Amplitude of the 1 ns component ($A_{1\ \mathrm{ns}}(T)$, blue circles) and the sum of the 65 ps and 305 ps components ($A_{65\ \mathrm{ps}}(T) + A_{305\ \mathrm{ps}}(T)$red circles). The error bars indicate 1 standard deviation in the uncertainty of that parameter and are shown for T =0.3 s, 1.9 s, 7.9 s, 17.7 s, and 50 s. The insets in (A) and (B) show the $A_{65\ \mathrm{ps}}(T)$ and $A_{305\ \mathrm{ps}}(T)$ for 0.3 s $< T <$ 3 s. The lines in the insets are shown to indicate the changes in the amplitude.

illumination, decreased substantially from 0.3 s $< T <$ 3 s, and plateaued by 20 s in actinic light (Figure 2.7*C*). It increased over 60 s in the darkness back to $A_{1\text{ ns}}(T = 0.3\text{ s})$.

We ascribe the changes in amplitudes to changes in the quantities of PSIIs with such lifetimes. Coarse grained models of energy transfer and trapping in PSII [144] as well as measurements of the fluorescence lifetime [49, 58, 65, 85] suggest that PSIIs with a site that can trap excitation energy, such as a qE site and/or an open reaction center, have a lifetime of less than 700 ps. PSIIs with closed reaction centers and no access to an energy trapping site have a lifetime of 1 ns or greater. Therefore, we associate the decrease in $A_{65\text{ ps}}(T)$ and $A_{305\text{ ps}}(T)$ in the first ∼0.3 s of illumination with a decrease in the number of PSIIs with access to an open reaction center as the plastoquinone pool becomes fully reduced. The subsequent increase in $A_{65\text{ ps}}(T)$ and $A_{305\text{ ps}}(T)$ with 0.3 s $< T <$ 20 s is an increase in the number of PSIIs with closed reaction centers and access to a qE quenching site. The decrease in $A_{305\text{ ps}}(T)$ and, to a lesser extent $A_{65\text{ ps}}(T)$, from 20 s $< T <$ 80 s we ascribe to the decrease in the number of PSIIs with closed reaction centers and access to a qE quenching site as qE sites turn off in the darkness. The changes in $A_{1\text{ ns}}(T)$ are changes in the number of PSIIs with access to neither a qE site nor an open reaction center. Because, for $T > 0.3$ s, the changes in $A_{305\text{ ps}}(T)$ are clearly reversible and those for the $A_{65\text{ ps}}(T)$ may be reversible, we are observing one and possibly two lifetimes associated with qE switching on and off in live cells of *C. reinhardtii*.

To test if the increases in both $A_{65\text{ ps}}(T)$ and $A_{305\text{ ps}}(T)$ are linked to a transmembrane pH gradient and thus to qE, we measured time-resolved fluorescence decays after 150 s of an actinic light treatment and after adding 100 μM of the ionophore nigericin to the sample after the light treatment. Nigericin removes the pH gradient across the thylakoid membrane and is typically used to determine whether changes in fluorescence lifetime are due to qE [49]. The fluorescence decays were fit to Eq. 2.2, and the results are shown at the top of Table 2.2. The amplitudes of both short components (in this fit, 70 and 330 ps) decrease upon the addition of nigericin, suggesting that the changes in both $A_{65\text{ ps}}(T)$ and $A_{305\text{ ps}}(T)$ in Figure 2.7 are due to qE. We associate the remaining amplitude of the 70 ps component with PSI quenching [58, 60, 108], and we ascribe the remaining amplitude of the 330 ps component partially to PSI quenching and partly to detached, phosphorylated LHCII trimers [62].

While $A_{65\text{ ps}}(T)$ was not unambiguously reversible (see Figure 2.7*A*), the fact that this component was linked to the pH gradient and that other measurements indicate that this component's amplitude changes are reversible (Figure 2.6) lead us to believe that this component is reversible and attributable to qE.

We fit $A_{65\text{ ps}}(T)$ and $A_{305\text{ ps}}(T)$ from $T = 0.3$ s, when the plastoquinone pool was fully reduced, to the end of the light treatment at $T = 20$ s to a simple rise curve with the form

$$A_i(T) = a\left(1 - \exp\left(-\frac{T - 0.3}{\tau_{rise}}\right)\right) + c. \tag{2.3}$$

The results of the fitting are shown in Table 2.1. The 95% confidence intervals of the rise time, τ_{rise}, for the two components do not overlap. This gives evidence that the changes in

Table 2.1: Fits for the increase in $A_{65\ \mathrm{ps}}(T)$ and $A_{305\ \mathrm{ps}}(T)$ for 0.3 s $< T <$ 20 s (Figure 2.7*A* and *B*). The data were fit to equation Eq. 2.3. The 95% confidence bounds are in shown in parenthesis.

Component	τ_{rise} (s)	a	c
65 ps	0.68 (0.45, 1.47)	0.07 (0.05, 0.10)	0.60 (0.58, 0.62)
310 ps	3.18 (2.27, 5.26)	0.07 (0.06, 0.09)	0.18 (0.16, 0.20)

$A_{65\ \mathrm{ps}}(T)$ and $A_{305\ \mathrm{ps}}(T)$ in Figure 2.7 are due to two different qE triggering processes.

2.3.4 Measurements of qE mutants of *C. reinhardtii*

Fluorescence lifetime measurements on qE mutants of *C. reinhardtii* were performed in addition to those on wild-type. The results from these measurements are shown in Table 2.2. The lifetime was measured on 1) dark-acclimated cells treated with DCMU, which closes the reaction centers (DCMU-treated); 2) cells acclimated to 600 μmol photons m^{-2} s^{-1} light for 150 s (Light-acclimated); and 3) light-acclimated cells treated with nigericin (Nigericin-treated). Differences between the amplitudes of the nigericin-treated cells compared to DCMU-treated cells indicates that NPQ mechanisms besides qE may be occurring during light acclimation. A decrease in the amplitudes of the short components upon the addition of nigericin to light-acclimated cells indicates the presence of qE quenching. The extent of quenching is dictated by the shortness of the lifetimes and the sizes of the changes in amplitude.

In all of the genotypes, the middle component increased in the nigericin-treated cells compared to the DCMU-treated cells. Recently, there were fluorescence lifetime imaging measurements [62] of another NPQ mechanism, state transitions (qT), which involves the detachment of phosphorylated LHCII trimers from the PSII supercomplex and subsequent reattachment of some of the LHCII to PSI [75]. Iwai et al. observed a 250 ps component for detached, phosphorylated, and aggregated LHCIIs in *C. reinhardtii*. Thus, we attribute the increases in the middle components, which range from 300 to 500 ps, to phosphorylated, detached LHCIIs. State transitions, which are highly active in *C. reinhardtii* [42], may have occurred because we did not expose the dark-acclimated cells to red PSI-exciting light to oxidize the plastoquinone pool, as suggested by Peers et al. [115], prior to light acclimation.

The LHCSR3 protein has recently been shown to be required for the qE response in *C. reinhardtii* [115]. In fact, there are three LHCSR isoforms: *LHCSR1*, *LHCSR3.1*, and *LHCSR3.2*. The LHCSR1 protein is 87% identical to LHCSR3. The LHCSR3 protein is in much greater abundance than the LHCSR1 protein. The Niyogi group has isolated mutants without both LHCSR3 isoforms [115], without LHCSR1, and without all three LHCSRs. Our data shows that LHCSR1 does not play a major role in quenching in *C. reinhardtii*. The lifetimes are nearly identical to those from wild-type cells. LHCSR3 is the main protein involved in qE. Without it, neither of the changes observed in the two short lifetimes in wild-type occur. The mutant that lacks all LHCSRs has similar lifetimes to those from the mutant without LHCSR3. Lastly, the mutant lacking the carotenoid lutein had qE, as

Table 2.2: Amplitudes and lifetimes of DCMU-treated and light-acclimated wild-type and qE-mutant *C. reinhardtii* cells before and after addition of nigericin. See Section 2.2.6 for how these measurements were performed. The fluorescence was collected at 680 nm and 68% confidence intervals of the fits as calculated by bootstrapping were within ±0.01 of the amplitudes shown. $\langle\tau\rangle$ is the amplitude-weighted average lifetime.

Genotype	Condition	Amplitudes			$\langle\tau\rangle$ (ps)
wild-type		70 ps	330 ps	1.2 ns	
	DCMU-treated	0.50	0.11	0.39	539
	Light-acclimated	0.51	0.43	0.06	250
	Nigericin-treated	0.35	0.30	0.35	544
no LHCSR1		50 ps	290 ps	1.14 ns	
	DCMU-treated	0.51	0.08	0.41	516
	Light-acclimated	0.50	0.43	0.07	230
	Nigericin-treated	0.36	0.25	0.39	535
no LHCSR3		70 ps	520 ps	1.5 ns	
	DCMU-treated	0.60	0.11	0.29	534
	Light-acclimated	0.56	0.23	0.21	474
	Nigericin-treated	0.55	0.22	0.23	498
no LHCSRs		55 ps	340 ps	1.34 ns	
	DCMU-treated	0.57	0.10	0.33	508
	Light-acclimated	0.52	0.16	0.33	525
	Nigericin-treated	0.53	0.24	0.26	459
no lutein		70 ps	390 ps	1.3 ns	
	DCMU-treated	0.61	0.15	0.24	413
	Light-acclimated	0.59	0.33	0.09	287
	Nigericin-treated	0.61	0.22	0.18	363

seen in the drop in the amplitude of the 390 ps component in light, but the change in the amplitude of the 70 ps component was much smaller than that in wild-type.

2.4 Discussion

To interpret the origin of the two qE components observed, we turn to the current hypotheses for the molecular mechanisms underlying qE, which have been put forth primarily for plants. There is a consensus that the protonation of the PsbS protein as a result of a pH decrease in the thylakoid lumen is thought to be the trigger for the qE process and that the xanthophylls zeaxanthin and lutein are necessary for quenching [38, 126]. However, hypotheses differ on the role of xanthophylls and the location of the qE quenching site. In a series of papers, Avenson et al. and Ahn et al. have proposed that charge transfer quenching of chlorophyll excitations by xanthophylls in the minor complexes of PSII (CP24, CP26, and CP29) is an important contribution to qE in *Arabidopsis thaliana* [2, 7]. In contrast to this

model, Ruban and coworkers propose that low lumen pH leads to the aggregation of LHCII, the major light-harvesting complex of PSII [126]. The aggregated LHCII trimers undergo a conformational change [113] and quench chlorophyll excitations by energy transfer to the S_1 state of lutein and subsequent relaxation [125]. Holzwarth and coworkers have proposed that quenching occurs in both detached LHCII trimers and the minor complexes of PSII [58]. *C. reinhardtii* lacks PsbS but Bonente et al. suggested that a similar triggering role is played by the LHCSR3 protein [22]. In addition, unlike PsbS, LHCSR3 binds pigments, and fluorescence lifetime measurements indicated that the protein could perform pH-dependent quenching [22].

Turning to the data in Figure 2.7, Table 2.1, and Table 2.2, $A_{65\ \mathrm{ps}}(T)$ increases much more rapidly under saturating light than does $A_{305\ \mathrm{ps}}(T)$ after the reduction of the plastoquinone pool, reaching its maximum value at $T \approx 1.3$ s. Kinetic modeling of the transient absorption data showing formation of a cation radical in thylakoids from *A. thaliana* suggested that the time for chlorophyll excitations to be quenched in the minor complexes is ∼30 ps [33]. A possible interpretation of the changes in $A_{65\ \mathrm{ps}}(T)$ for $T > 0.3$ s is that they are due to changes in the number of PSII supercomplexes that can perform the minor complex/charge transfer mechanism. Because of the slower rise time of $A_{305\ \mathrm{ps}}(T)$ following reduction of the plastoquinone pool, we suggest that the changes in $A_{305\ \mathrm{ps}}(T)$ for $T > 0.3$ s correspond to changes in the number of aggregated LHCIIs that are detached from PSII supercomplexes and that this lifetime may be related to the 250 ps lifetime reported by Iwai et al. [62]. The protonation of LHCSR3 may cause it to become a quencher along with the minor complexes as well as a trigger for LHCII aggregation, which would take into account its requirement for both changes in the short lifetimes. The mutant without lutein primarily experienced pH-dependent changes in its 390 ps component. We suggest that lutein is the pigment involved in charge-transfer quenching, while zeaxanthin, without which qE in *C. reinhardtii* is reduced by 30% [98], is involved in quenching in the aggregated LHCIIs.

The assumption that the lifetimes represent separate pools of PSIIs may not be correct. Our interpretation of the lifetimes should be tested by numerical modeling of energy transfer and trapping in PSII and LHCII aggregates, which is described in Chapters 4-6. Recent work has identified the arrangement of proteins in PSII supercomplexes in *C. reinhardtii*, which could be used to develop such models [138]. The rise times of $A_{65\ \mathrm{ps}}(T)$ and $A_{305\ \mathrm{ps}}(T)$ may be representative of the time for the pH to drop in the lumen, the time for a change to happen in the thylakoid membrane [18, 66], or some combination of the two. A recently published systems model of qE in plants [158] could be amended for analyzing this aspect of the data.

More generally, the technique described here can easily be applied to studying other photosynthetic organisms and components of NPQ. In the next chapter, we adapt this technique to plant leaves.

Chapter 3

Development of the fluorescence lifetime 'snapshots' technique for measuring leaves

3.1 Introduction

Much of the research on light harvesting and qE has been done on the proteins, membranes, chloroplasts, and leaves of plants. Also, plant qE represents the second of the two mechanisms of qE that occur in eukaryotic oxygenic photosynthetic organisms (Section 1.5.1). The fluorescence lifetimes of thylakoids [49, 50], chloroplasts [65], and leaves [58, 77, 78] have been measured only on dark-acclimated or light-acclimated samples. For these reasons, we altered the fluorescence lifetime snapshot technique to also be able to measure the fluorescence lifetimes of leaves during light acclimation.

For leaves, we can apply the actinic light measurement described in Figure 2.3, in which the pulsed laser is periodically applied to the sample and serves as both a measuring and saturating light. The induction and relaxation of qE in plants occurs on the tens of seconds to minutes timescales (Figure 1.6), which is much slower than the seconds timescale for algae (Figure 2.2). Therefore, the timescale for data collection, ΔT, for leaves can be much longer than that for algae and still accurately capture the changes in fluorescence lifetime over T.

There are two main differences with measuring leaves as compared to algae. First, the leaf is flat and thus the sample holder and the geometry of laser incidence must be altered. Second, closing the reaction centers in leaves requires white light with intensities of ~20,000 μmol photons m^{-2} s^{-1}. This requirement is significantly different from algae, where light at 1000 μmol photons m^{-2} s^{-1} is nearly saturating. If high intensity pulses were applied to the sample in Figure 2.2, the resulting F'_m spikes would barely rise above the trace shown. Therefore, the primary difficulty in measuring the fluorescence lifetime snapshots of leaves is in collecting only the fluorescence emitted when the reaction centers are closed.

3.2 Alterations to sample geometry and holder

We used front-face detection on the abaxial, or front, side of the leaf (Figure 3.1). The angle of incidence was chosen to maximize fluorescence collection. A monochromator was added to be able to select specific wavelengths of fluorescence because the PMT detector used was different from the one used in Chapter 2 and did not have a spectroscope attached. A leaf holder was built so that the leaf stem could be immersed in water and remain hydrated during the measurement. Performing the measurement without water altered the qE relaxation kinetics of the leaf. Otherwise, the setup was identical to that shown in Figure 2.1.

3.3 Results

3.3.1 Scanning the saturation time

In the algae actinic light experiment (Section 2.3.2), the collection time ΔT and the time that the laser spent on the sample were equal to measure the fluorescence lifetime with the PSII reaction centers closed. In leaves, however, PSII RCs do not immediately saturate upon application of the laser. Instead, the laser must be applied for a saturation time to close all the reaction centers (Figure 3.2). Only after the RCs are saturated can the fluorescence lifetime with all RCs closed be measured for a collection time. The saturation time for a snapshot at a particular T time is dependent on the redox state of the plastoquinone pool, which changes in different light conditions. Too long of a saturation time and the laser will induce qE during a measurement. Therefore, we needed to measure the saturation time for every T time. The saturation time was scanned between 0 and 0.8 s by 0.2 s, and the collection time was 0.2 s. The fluorescence decay was measured during the collection time after each saturation time and the amplitude-weighted lifetime $\langle\tau\rangle$ (Equation 2.1) measured. The saturation time at which $\langle\tau\rangle$ is largest is the one in which the RCs are closed without turning on qE. The sum of the saturation time and the collection time was never >1 s because qE will turn on after exposure to high light for that long [93]. An example of determining the saturation time for a T time is shown in Figure 3.3 for a dark-acclimated leaf before an actinic light was applied.

To determine whether the saturation times derived for the different points along the T axis were correct, we compared the results from a fluorescence lifetime snapshot measurement to those from an NPQ trace performed with the same actinic light treatment (bars on top of Figure 3.4). An NPQ trace is generated by calculating the NPQ parameter (Eq. 1.4) for each F'_{m}. The result of measuring an NPQ trace from several leaves from a wild-type plant is shown in blue in Figure 3.4. To make a direct comparison with the PAM trace, we had to collect fluorescence lifetimes at the same wavelength as that from PAM fluorimeters ($\sim$715 nm). The fluorescence decay was measured after the saturation time determined by the scanning method shown in Figure 3.3. In the measurement, the actinic light turns on at $T = 0$, and one measurement was taken before the actinic light was turned on. The NPQ

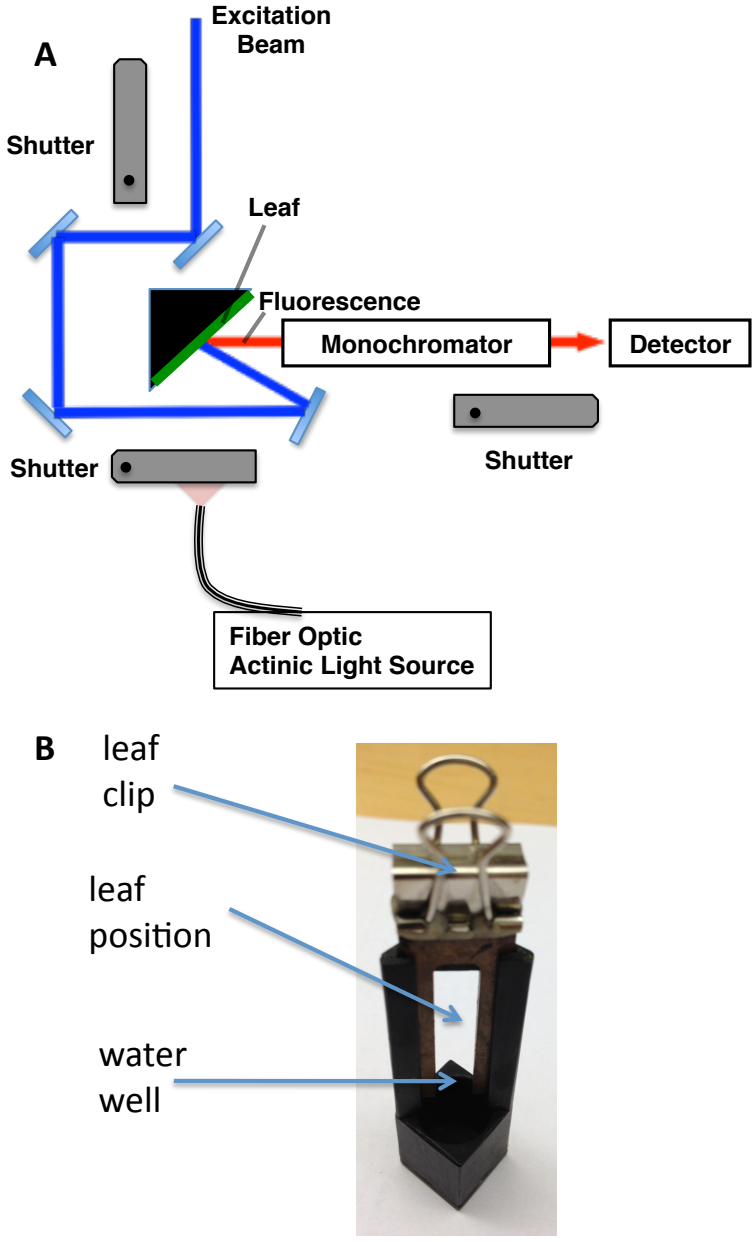

Figure 3.1: *A*, Schematic of the laser and sample geometry for taking fluorescence lifetime snapshots of leaves. The leaf is positioned such that the laser hits the abaxial side of the leaf at an angle that maximized fluorescence collection. The fluorescence goes through a monochromator to select a small range of wavelengths. *B*, Picture of leaf holder for fluorescence lifetime snapshot measurements. A leaf clip slides in and out of the black sample holder. The black sample holder has a well at bottom that can hold ∼1 mL of water. A leaf is removed from the plant and slipped into the leaf clip. The stem of the leaf penetrates the surface of the water in the well when the clip is slid into the black sample holder.

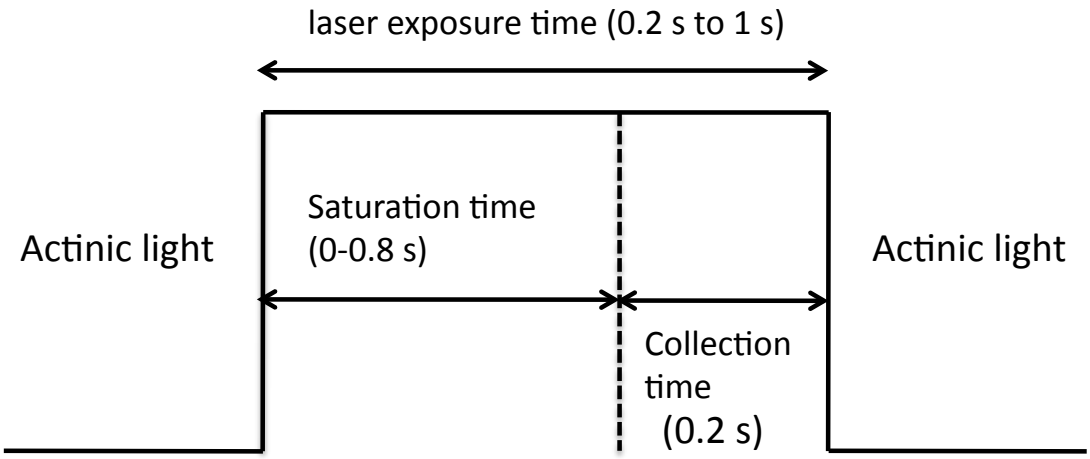

Figure 3.2: Schematic of saturation and collection times. Most the time during the measurement, the sample is exposed to steady state actinic light (Figure 2.3). The sample is briefly exposed (laser exposure time) to a pulsed laser. Fluorescence lifetime data is collected only for the last 0.2 s of the laser exposure time, after the PSII RCs close.

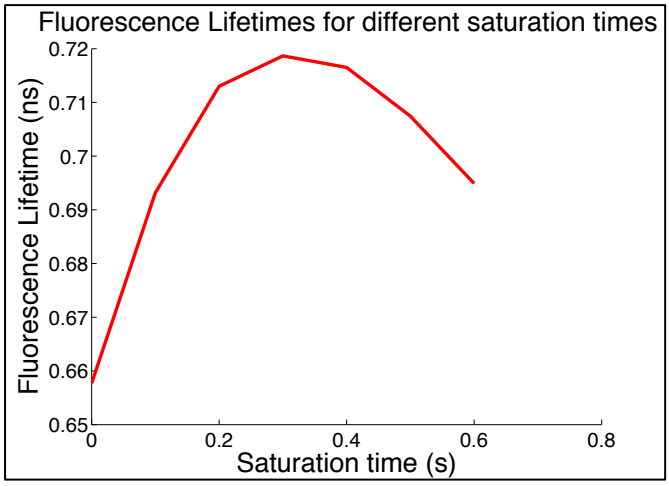

Figure 3.3: Determination of the saturation and collection times for measuring the fluorescence lifetime of a dark-acclimated wild-type leaf. The laser intensity was 5 mW at 410 nm and the wavelength of fluorescence was 715 nm.

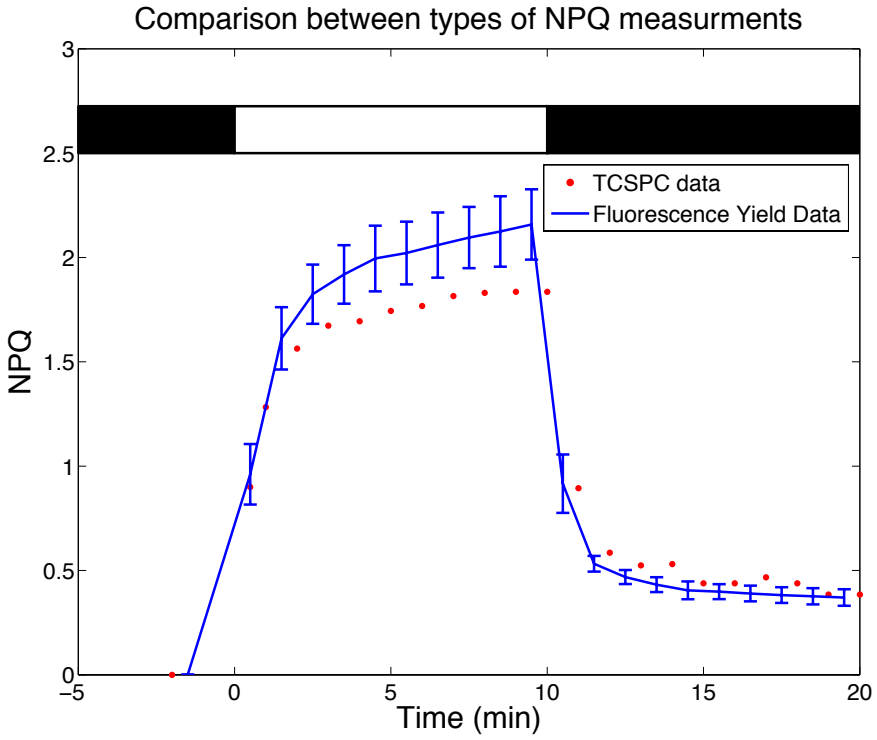

Figure 3.4: Comparison between NPQ traces generated by PAM fluorimetry and fluorescence lifetime snapshots. The curves are very similar, suggesting that the saturation times used for the fluorescence lifetime snapshot measurement are correct.

parameter using fluorescence lifetimes is

$$\mathrm{NPQ} = \frac{\langle \tau_{T<0} \rangle - \langle \tau_{T\geq 0} \rangle}{\langle \tau_{T<0} \rangle} \tag{3.1}$$

Figure 3.4 shows the comparison between the two measurements, both of which were done with an actinic light intensity of 700 μmol photons m^{-2} s^{-1}. The dynamics are quite similar, suggesting that the fluorescence lifetime snapshot measurement is physiologically accurate. The amplitude of quenching in the PAM measurement may be higher because the instrument has a cutoff filter that allows fluorescence at wavelengths higher 710 nm to be detected. The cutoff filter may not be sharp at 710 nm. If so, more of the fluorescence in the PAM measurement is due to PSII than in the fluorescence lifetime snapshot measurement here. Because the PSII contributes to nearly all of the variable fluorescence in plants, this would result in more NPQ in the PAM measurement.

Table 3.1: Amplitude-weighted average lifetimes ($\langle\tau\rangle$) of wild-type *A. thaliana* leaves before, during, and after 10 min of acclimation to 1200 μmol photons m^{-2} s^{-1} [29]. The fluorescence was collected at 684 nm and 68% confidence intervals of the fits as calculated by bootstrapping are shown.

Condition	$\langle\tau\rangle$ (ns)
dark-acclimated	1.61 ± 0.05
light acclimated for 10 min	0.46 ± 0.01
re-dark acclimated for 10 min	1.01 ± 0.04

3.3.2 Fluorescence lifetimes of wild-type *A. thaliana* leaves during light acclimation

To obtain the fluorescence lifetimes of the grana membrane during light acclimation, we performed the snapshot measurement with the saturation times used for generating Figure 3.4 but acquired the fluorescence at 680 nm. At this wavelength, nearly all of the fluorescence is due to PSII [147]. The fluorescence decays could *not* be globally fit to a sum of three exponentials. Instead, both the amplitudes and lifetimes had to vary in order to fit the data. As a result, the lifetimes could not be given a specific physical interpretation. For this reason, we report the average fluorescence lifetimes of a) dark-acclimated, b) after 10 min of 1200 μmol photons m^{-2} s^{-1} actinic light, and c) after 10 min of darkness after the 10 min of high light treatment. The average lifetime decreases by 75% after 10 min of high light. After 10 min in the dark, $\langle\tau\rangle$ recovers to 60% of the dark-acclimated lifetime.

3.4 Discussion

The average fluorescence lifetimes of dark-acclimated and light-acclimated chloroplasts and leaves have been reported previously (Table 3.2). We include previous measurements on chloroplasts because they have been shown to induce levels of qE seen in leaves [65]. A comparison with the previous measurements of dark-acclimated chloroplasts/leaves with closed PSII RCs shows that our measurement of 1.61 ns is in between those done previously. Holzwarth et al. closed the PSII RCs by shining a 100 μmol photons m^{-2} s^{-1} blue light on the sample right before the measurement was taken [85]. It was not shown by either experiment or calculation that this light intensity would close all PSII RCs, and the reason why the reported lifetime for dark-acclimated leaves is so low could be because not all RCs were closed. Johnson and Ruban showed that isolated dark-acclimated chloroplasts treated with 3 % v/v glutaraldehyde to partially cross-link the proteins in the grana membrane and exposed to 100 μmol photons m^{-2} s^{-1} light have the fluorescence yield of dark-acclimated chloroplasts under the presence of a saturating light pulse [65]. Glutaraldehyde is added to prevent the membrane from being able to change and turn on quenching. The disadvantage with this method is that the membrane is in a poorly characterized state following addition of glutaraldehyde. In our measurement, the lifetime is significantly faster than that of Johnson

Table 3.2: Previously measured lifetimes of dark-acclimated and light-acclimated chloroplasts of spinach [65] and leaves of *A. thaliana* [58, 77]. The light condition, the paper from which the results were taken, the sample preparation used, and the average fluorescence lifetime are shown. Whether or not the authors indicate that the PSII RCs are closed (clos.) or partially open (part.) is shown in the sample preparation column. Fluorescence was detected at 685 nm [65], 686 nm [58], and between 645 nm and 689 nm [77].

Light Condition	Paper	Sample Preparation	$\langle\tau\rangle$ (ns)
Dark acclimated (qE off)	Johnson and Ruban [65]	chloroplasts x-linked with 3 % (v/v) glutaraldehyde and exposed to 100 μmol photons m^{-2} s^{-1} (clos.)	2.1
	Holzwarth et al. [58]	leaves incubated in 45 μM DCMU for 12 h (clos.)	1.25
Light acclimated (qE on)	Li et al. [77]	leaf discs exposed to 1250 μmol photons m^{-2} s^{-1} for 15 min, followed by 5 min of 140 μmol photons m^{-2} s^{-1} (part.)	0.57
	Johnson and Ruban [65]	chloroplasts exposed to 5 min of 300 μmol photons m^{-2} s^{-1}, followed by x-linking with 3 % (v/v) glutaraldehyde (part.)	0.58
	Holzwarth et al. [58]	leaves exposed to 45 min of 600 μmol photons m^{-2} s^{-1} (clos.)	0.41

and Ruban. It may be that some sort of quenching is turning on during the snapshot before the RCs are saturated. That is, the peak of the curve in Figure 3.3 may not represent the fluorescence lifetime when all the RCs are closed and no qE is on. This reason might explain why the NPQ curve measured using the fluorescence lifetime snapshot does not reach the same NPQ amplitude as that from the PAM measurement.

The fluorescence lifetime of the light-acclimated leaves that we report is in the range of the previously reported data. Interestingly, both of the measurements done with the RCs partially open have significantly longer lifetimes that ours. Under those conditions, there are both qE and RC sites available for quenching excitation compared to our case, where there are only qE sites. We would suggest that the difference is due to the fact that the previous two results were obtained on samples where there was less qE, but Johnson and Ruban reported similar amounts of qE to that reported here using PAM fluorescence. The lower lifetime reported by Holzwarth et al. might be attributable to the reason described above.

Besides the potential problem that we are not measuring the dark-acclimated lifetime accurately, it has been suggested that measuring the fluorescence lifetime of leaves is problematic due to reabsorption and emission by chlorophylls [65]. It has been shown that the lifetimes of leaves and chloroplasts are quite similar [130], so this seems to be a small problem, as long as fluorescence is detected at 680 nm. Most of the reabsorption fluorescence is emitted at much redder wavelengths. Overall, the fluorescence lifetime snapshot technique described here gives us, currently, the best view into how light harvesting is changing in the presence of high light in leaves.

While the measurement is reasonable, we could not give the lifetimes a physical interpretation as with algae because the fluorescence decays could not be globally fit. How can we leverage the fluorescence lifetime snapshot data from leaves and algae to answer mechanistic (Figure 1.7) questions about light harvesting in variable light conditions?

Chapter 4

The need for accurate energy transfer models for interpreting the fluorescence lifetime snapshot data

4.1 Physical origin of chlorophyll fluorescence from grana membranes

Thus far we have been able to make new measurements of light harvesting as it acclimates to changing light intensities. However, we have not been able to get the details of light harvesting when quenching is on (Figure 1.7, right) from the data itself. Instead, as discussed in Chapter 2, we were forced to lean on the literature to make hypotheses about the sites and mechanisms of quenching. To understand how we can mine that information from the snapshot data, we should reconsider the physical origin of chlorophyll fluorescence and the models that have been used to interpret it.

The lack of the structural information about the membrane that is necessary for constructing a quantitative picture of energy transfer has necessitated simplified models for interpreting fluorescence data. One such model is the "container" model, shown in Figure 4.1. There are two key assumptions to this model. First, excitation transfer is assumed to be fast compared to any of the decay processes. Second, excitation energy absorbed at any chlorophyll is assumed to be able to access any other chlorophyll in the membrane. In this case, we can imagine Chl excitation as a liquid in a container that can be drained by any of the intrinsic pathways (fluorescence, intersystem crossing, internal conversion) as well as a photochemistry pathway that results in charge separation and NPQ. The yield of any of the pathways is simply proportional to the areas of the drains at the bottom of the container of excitation, since the area is proportional to the flux of excitation through that pathway.

The container model has been used extensively to interpret PAM fluorescence measure-

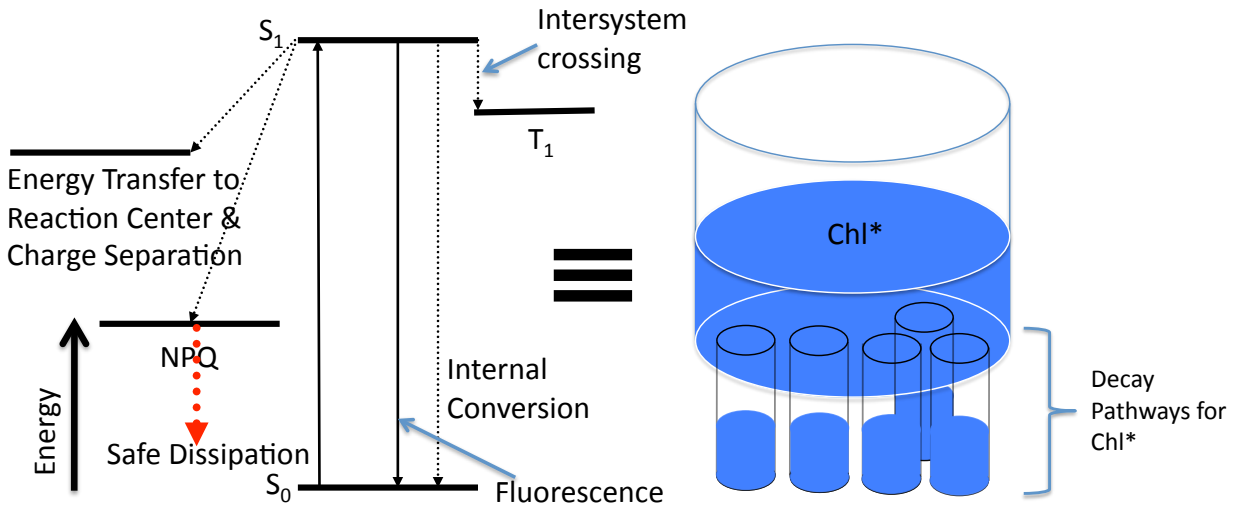

Figure 4.1: A schematic of the "container" model for chlorophyll excitation energy dissipation in PSII. A Jablonski diagram equivalent of the model is shown on the left. The excitation is shown in blue, with drains at the bottom of the container for the different decay pathways.

ments [3, 8]. In this case, the fluorescence yield in a PAM trace is

$$\Phi_F = G\frac{k_F}{k_F + k_{ISC} + k_{IC} + k_{PC} + k_{NPQ}}, \tag{4.1}$$

where G is a gain constant, k_F is the rate constant for fluorescence, k_{ISC} is the rate constant for intersystem crossing, k_{PC} is the rate constant for photochemistry in the reaction center, and k_{NPQ} is the rate constant for NPQ. Both k_{PC} and k_{NPQ} can be considered to be proportional to the concentration of open reaction centers and quenchers, respectively. Thus, they change as the actinic light incident on the sample changes. The saturating flashes close the reaction centers, and, under these conditions, $k_{PC} = 0$. The yield of the different decay pathways can be calculated by algebraic operations on the fluorescence yield at different points along the trace. For example,

$$\Phi_{NPQ} = \frac{k_{NPQ}}{k_F + k_{ISC} + k_{IC} + k_{PC} + k_{NPQ}} = \frac{F_\mathrm{m} - F'_\mathrm{m}}{F_\mathrm{m}} \times \frac{F_\mathrm{s}}{F'_\mathrm{m}}, \tag{4.2}$$

where F_m and F'_m are defined as in Figure 1.6 and F_s is the fluorescence yield right before the saturating flash at F'_m is applied. This model is also easy to incorporate into systems models of the thylakoid membrane [14, 158, 160].

The assumptions of the container model break down when the model is used to analyze fluorescence lifetime data. If the container model was valid, the fluorescence lifetime of grana membranes would be describable by one fluorescence lifetime that would be equal to $\frac{1}{\sum_i k_i}$, where the denominator is a sum over all of the rate constants of the decay pathways. However, as seen in the results from Chapters 2 and 3, the fluorescence decays from photosynthetic

organisms must be fit to multiple exponentials. This disagreement suggests that the many assumptions of energy transfer in the "container" model and its predictions (for example, that the yield of quenching is proportional to the concentration of quenchers) are incorrect.

A slightly more complex description of energy transfer that takes into account the multiple exponentials in the fluorescence decay simply assumes that each lifetime is a pool of PSIIs that satisfies the assumptions of the "container" model. The pools of PSIIs, however, can not transfer energy between each other, which results in multiple fluorescence lifetimes. This view was used to interpret the lifetimes in Chapter 2 and seemed reasonable because the same three lifetimes could fit the different snapshots. This model was useful for showing the benefit of the fluorescence lifetime snapshot technique - that it is a measurement that can simultaneously measure the slow biochemical timescales of feedback and the fast timescales of light harvesting - but could not reveal much specific information about the site and rates of quenching.

Neither of the above models explicitly includes any timescale for energy transfer in the membrane, when, in fact, such rates may play an important role in determining the yields of the different photophysical decay pathways and the fluorescence lifetime. The general physical picture of energy transfer describes excitation moving through a kinetic network, depicted schematically in Figure 1.7. The excitation populations of the nodes in the network $P(t)$ can then be described using the master-equation formalism,

$$\dot{P}(t) = KP(t), \tag{4.3}$$

where K is the rate matrix containing the first order rate constants of energy transfer, dumping, and trapping for all of the nodes. Equation 4.3 is solved to give

$$P(t) = Ce^{t\Lambda}C^{-1}P(0), \tag{4.4}$$

where C is the matrix defining the eigenvectors of K and Λ is a diagonal matrix containing the eigenvalues of K. If we assume that the rate of fluorescence for each node is the same, then the sum of $P(t)$ over all states gives the fluorescence decay and the integral of that decay gives the fluorescence yield.

What are the nodes and what is the rate matrix that properly describes the energy transfer network in the grana membrane? Previous work has assumed some network structure and then fitted the resulting K to fluorescence lifetime data [57, 149]. The electron radical pair equilibrium (ERPE) model assumes that all of the antenna can be described by one node and that the remaining nodes are radical pair states in the reaction center [58]. In this case, the dynamics in the fluorescence decay are due entirely to electron transfer kinetics. Another group has used models that assume that the membrane can be approximated by a PSII supercomplex in which the nodes are the proteins [26]. The fluorescence decay in this case was partially influenced by energy transfer dynamics. The fluorescence decay is both ensemble-averaged and averaged over all sites. Therefore, generating a model (a rate matrix K) and fitting the rate constants in that matrix to fluorescence lifetime measurements *does not guarantee* that the model is accurate or unique for describing energy transfer through the system.

There is a great need for a detailed, structure-based model of energy transfer in grana membranes. The rates in such a model would be derived from the relevant physical processes. Such a model could be used to map the energy transfer dynamics seen in the fluorescence lifetime onto the chlorophylls of PSII and LHCII. Given an accurate description of the energy transfer network, one can then begin to gain an intuition for how the positioning of antenna proteins relative to reaction centers make PSII efficient at light harvesting in low light and what changes to the antenna can protect reaction centers in high light.

4.2 A strategy for obtaining a detailed model of the grana membrane

The changes in the energy transfer network shown in Figure 1.7 are, at root, changes in the rate matrix K. However, K is complicated. It contains information about the connectivity and rates of energy transfer and the rates of NPQ, fluorescence, intersystem crossing, and charge separation. Typically, the appropriate K for a pigment-protein complex is calculated using a combination of x-ray crystallography data and ultrafast spectroscopy characterization of the type described in Section 1.4.1. However, the grana membrane cannot be characterized using those ultrafast techniques. It is very heterogeneous and scatters light and also the various electronic states are not easily spectrally separated. Fluorescence lifetimes and the fluorescence yields are the only available data.

If we knew the underlying structure of energy transfer in dark-acclimated membranes, we could simply alter K to find what changes in it best fit the available fluorescence data. The idea is that the crystal structures of pigment-protein complexes are of proteins that are not undergoing quenching. We can use these structures to make an energy transfer model for the dark-acclimated membrane (Figure 1.7, left). This model will serve as a good model of how energy flows in the grana membrane and explain the principles behind the high quantum efficiency of light to chemical energy conversion in dim sunlight. To understand how light harvesting changes in high light conditions, we can fit the fluorescence lifetime snapshot data using the energy transfer model by putting qE quenching sites into the model and finding out, for example, what number, location, and rates of quenching give a good fit to the data. If we have a accurate description of energy transfer in grana membranes without quenching, we will have a basis by which we can extract the mechanistic information from the fluorescence lifetime snapshots.

The assumption that crystal structures of photosynthetic proteins are of dark-acclimated proteins is somewhat controversial. The crystals of LHCII have been found to have a shorter fluorescence lifetime than LHCII in solution [113, 148]. Still, detailed energy transfer models are built by using the structure to fit the Hamiltonian of the electronic excited states of the pigments to data on isolated proteins in solution [104, 118]. The approach outlined above is currently the most feasible way to understand the changes in light harvesting in variable light conditions.

Still, the fluorescence decay of grana membranes is that of the sum of populations over

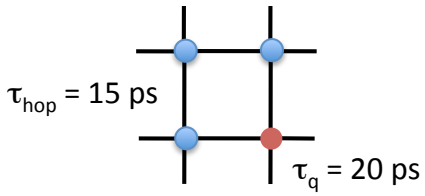

Figure 4.2: A schematic of a simple lattice model for describing energy transfer in grana membranes. The nodes indicate chlorophyll clusters. Energy is transferred to any node with which there is a connection with a timescale of 15 ps. Purple nodes can only transfer excitation to any or dump excitation with a 2 ns timescale. The red node indicates a quenching site, that can also dump excitation with a timescale of 20 ps.

all sites. Is the fluorescence lifetime too coarse-grained of a measurement to reveal detailed information about energy transfer? We simulated population decay on a simple lattice to show how differences in the rate matrix K will indeed affect the fluorescence lifetime. The lattice model is shown in Figure 4.2. It is a square, 70 $\times$ 70 lattice. Excitation can transfer from a node to any nodes with which it is connected with a time constant of 15 ps. Excitation is dumped (by intersystem crossing or fluorescence) with a 2 ns timescale. If a node is a quenching site, it can quench excitation with a timescale of 20 ps. 4% of the sites in the lattice were quenchers. Excitation was initiated uniformly over all sites. The decay when the quenchers were all put in the top left corner is shown in blue in Figure 4.3. The decay when the quenchers were randomly distributed throughout the lattice is shown in red in Figure 4.3. When the quenchers are all in the corner, the fluorescence decays much more slowly than when they are randomly distributed because most of the excitation has to travel long distances before it reaches a quenching site. A different K gives a substantially different decay. The strategy we are proposing should at least significantly constrain the range of possible energy transfer networks for the grana membrane.

4.3 The energy transfer model for the grana membrane must be coarse-grained

The grana membrane contains ~10,000 chlorophylls. All-chlorophyll energy transfer models typically are very computationally expensive and do not scale well with the number of chlorophylls. Therefore, we need to build a coarse-grained model of energy transfer in the membrane that still accurately describes the energy transfer dynamics. Such a model *must* originate from a calculation of the energy transfer rates using the specific locations, orientations, and environments of the pigments within the component pigment-protein complexes,. From detailed models of individual pigment-protein complexes, a proper assessment of the rate-limiting steps [157] and the correct coarse-graining can be applied to the membrane for computational simplification and mechanistic clarification.

The grana membrane is densely packed with PSIIs and LHCIIs [41]. PSII reversibly binds

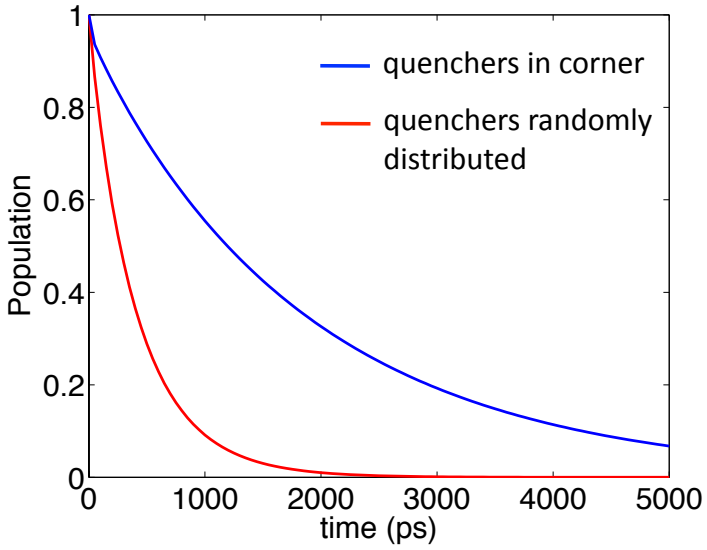

Figure 4.3: Population decay in the lattice model with two different distribution of quenchers. In the case of the blue line, the quenchers were all put in the top left corner of the lattice.

with LHCII to form PSII supercomplexes. PSII supercomplexes and LHCIIs form a large, variably fluid array of pigment-protein complexes [69]. To understand the energy transfer network in the grana membrane requires models for energy transfer 1) within LHCII, 2) within PSII supercomplexes, and 3) between LHCII and PSII. Recently, a detailed model of LHCII was published [104]. No detailed model of PSII supercomplexes exists to date. In the following chapter, we construct such a detailed model to understand the principles of light harvesting in PSII and determine the most coarse-grained model of energy transfer that still accurately describes transfer through the system.

Chapter 5

A structure-based model of energy transfer and trapping in Photosystem II supercomplexes

5.1 Introduction

A complete model of light harvesting in PSII supercomplexes requires both characterizing the kinetics of light harvesting and understanding how the spatial organization of chlorophylls generates these kinetics. When considering complicated kinetics, isolating the rate-limiting step or steps is a convenient simplification for understanding the overall process. Two rate-limiting steps have been hypothesized for light harvesting in the smallest supercomplex, called the core complex, which has a dimer structure and contains the core antenna proteins (CP43 and CP47) and the reaction center. The excitation radical-pair equilibrium (ERPE) model suggests that excitation will equilibrate throughout the collection of antenna pigments on a timescale much faster than excitation is converted into chemical energy [86]. The ERPE model is, therefore, also known as a trap-limited model since trapping at the RC (via charge separation) is the rate-limiting step. The second hypothesis, supported by a computational model of energy transfer in the core complex [118], assumes a slow rate of transfer between the core antenna proteins and the RC. This hypothesis is known as the transfer-to-trap limited model, where transfer into the RC is the rate-limiting step. Fluorescence decay curves measured on the core complex, however, can be fit with either a trap-limited or transfer-to-trap limited kinetic model [146]. One experimental study has measured a series of fluorescence decay curves of various PSII supercomplexes [31]. These measurements, when fit to a slightly more detailed kinetic model that incorporated spatial structure, suggested that light harvesting is trap-limited. Taken together, the experimental measurements and models of PSII form a conflicted picture of energy transfer and trapping.

Even without knowledge of the detailed kinetics, there have been suggestions about the organizational principle that governs the structure of PSII supercomplexes and results in efficient light harvesting. One possibility is the so-called "energy funnel," in which higher

energy chlorophylls are further from the RC [20]. Energy transfer down the gradient would result in unidirectional transport of excitation towards the RC. Previous computational work on PSII core complexes and LHCII trimers, however, suggests that no energy gradient exists in a supercomplex [104, 118]. In the absence of an energy gradient, efficient light harvesting in PSII supercomplexes has been attributed to a small collection of fast energy transfer steps forming efficient pathways of energy transfer that extend from the periphery of the supercomplex to the reaction center [27, 35, 129]. We call this hypothesis the pathways model of energy transfer since it corresponds to assuming that light harvesting in a PSII supercomplex is reducible to a series of energy transfer steps that make-up a minimal time pathway from an excited chlorophyll to the RC [112]. Fine-grain population dynamics are not readily accessible to experimental probes, so addressing the question of organizational principles in PSII supercomplexes requires a structure-based model of energy transfer.

With the recent experimental work that resolved the orientations and approximate distances between proteins in the largest PSII supercomplex [32] ($C_2S_2M_2$) it has become feasible to build a structure-based model of energy transport for PSII supercomplexes. The number of chlorophylls in a supercomplex (>300 in $C_2S_2M_2$) still makes constructing such a model a daunting computational challenge. We can decrease the computational cost of calculating the rate matrices for a supercomplex and simplify the kinetics of energy transfer by coarse graining over groups of chlorophyll. Such a coarse graining is complicated by the large variations in electronic couplings between pigments. In the presence of small electronic couplings, excitations are localized to single pigments and energy transfer between pigments is caused by electronic coupling. In the presence of strong electronic coupling, excitations are delocalized over multiple pigments and energy transfer between delocalized states is driven by the phonon modes of the bath. While modified Redfield theory interpolates energy transfer rates between both limits of electronic coupling, it does not account for the dynamic localization caused by phonon modes that are strongly coupled to the chlorophyll excited states. Previous work on two components of PSII supercomplexes, LHCII trimers [89, 91, 104, 105, 121] and the core complex [118], have used a combined generalized Förster/modified Redfield approach to incorporate an ad hoc correction for the influence of dynamic localization. In the combined approach, chlorophylls are grouped into clusters (called domains) based on the strength of their electronic coupling. In the work of Raszewski and Renger [118] on the core complex, chlorophyll pairs with electronic coupling greater than a threshold value of 34 cm^{-1} were included in the same domain. The treatment of LHCII by Novoderezhkin and coworkers [104] used a threshold value of 15 cm^{-1}. No single threshold value will correctly balance electronic delocalization against dynamic localization for all the intermediate couplings in PSII supercomplexes. We, therefore, introduce a method for domain assignment where in cases of moderate-to-strong coupling the inclusion of a chlorophyll into a domain (or not) is selected on the basis of whether it increases (decreases) the separation of timescales between intra- and inter-domain transfer rates. The resulting domains can be used to coarse-grain the energy transfer dynamics by assuming infinitely fast intra-domain thermalization.

Using the combined generalized Förster and modified Redfield approach with our separa-

tion of timescales metric for domain assignments, we constructed a rate matrix that describes population transport through the chlorophylls bound by PSII supercomplexes. In order to answer questions about the overall kinetics of PSII supercomplexes, we used an effective linearization technique, first introduced by Yang and Fleming [157], that decomposed the average timescale of light harvesting into contributions from possible rate-limiting steps. Next, we used calculations of photochemical yields in the presence or absence of different domains to assess the appropriateness of the pathways model for explaining the origin of efficient light harvesting by PSII supercomplexes. In both of these discussions, looking forward to Chapter 6, we extrapolate our results to comment on energy transfer and trapping in the membrane. Finally, we show that fluorescence lifetime measurements are not a good proxy for accuracy of energy transfer model and that the domain level model is the most coarse-grained model that accurately describes energy transfer in PSII supercomplexes.

5.2 Detailed description of structure-based energy transfer model of PSII

This section is divided into three portions. The first explains our approach to treating excitation energy transfer within the pigments of the PSII supercomplex. In this work, we exclude carotenoid molecules from our treatment, and our usage of the term pigment applies only to the chlorophyll *a* (Chl-a), chlorophyll *b* (Chl-b), and pheophytin molecules contained in PSII. Our approach follows previous treatments [104, 118, 121] in which energy transfer within strongly bound pigment clusters is treated by modified Redfield theory and transfer between clusters is described by generalized Förster theory. The second portion describes the physical parameters we use to model the system including the spatial structure, the inter-pigment coupling, and site energies. The final portion outlines how we use the calculated rates to construct fluorescence decay spectra and a linearized kinetics model for PSII supercomplexes.

5.2.1 Excitation energy transfer theory

System and Hamiltonian

To describe pigment-protein complexes (PPC) containing N pigments, we account for only two electronic states of each pigment the singlet ground-state ($S_0 = |\phi_g\rangle$) and the lowest-lying singlet-excited state ($S_1 = |\phi_e\rangle$). We describe the N-pigment complex with product states shown in Equations (5.1), (5.2), (5.3) which span the zero-, single-, and double-excitation space, respectively. The higher-order excitation spaces can be constructed analogously. These states are collectively called the site-basis, since they correspond to excitations localized on individual pigments. In the following discussion, μ and γ index the site basis.

$$|0\rangle = \prod_{i=1}^{N} |\phi_{i,g}\rangle \tag{5.1}$$

$$|\mu\rangle = |\phi_{\mu,e}\rangle \prod_{\substack{i=1 \\ i\neq\mu}}^{N} |\phi_{i,g}\rangle \tag{5.2}$$

$$|\mu,\gamma\rangle = |\phi_{\mu,e}\rangle|\phi_{\gamma,e}\rangle \prod_{\substack{i=1 \\ i\neq\mu,\gamma}}^{N} |\phi_{i,g}\rangle \tag{5.3}$$

In light intensities appropriate for the physiological conditions of photosynthetic PPCs, the excitation energy dynamics sample only the single-excitation space [61]. The single-excitation dynamics are driven by the Hamiltonian (shown here in the site-basis) given in Equation (5.4), where H^{el} contains the electronic vertical-excitation of individual pigments ($\hbar\Omega_\mu$, called the site energy) and the coupling between transitions of pigment pairs ($\hbar J_{\mu,\gamma}$, called the excitonic coupling), $H^{\text{el-ph}}$ describes the coupling of the electronic and phonon degrees of freedom, and H^{ph} is the phonon Hamiltonian (within a Harmonic-oscillator approximation) indexed by ξ.

$$H = H^{\text{el}} + H^{\text{el-ph}} + H^{\text{ph}} \tag{5.4}$$

$$H^{\text{el}} = \sum_{\mu=1}^{N} |\mu\rangle(\hbar\Omega_\mu + \Delta_\mu)\langle\mu| + \sum_{\mu,\gamma} |\mu\rangle\hbar J_{\mu,\gamma}\langle\gamma| \tag{5.5}$$

$$H^{\text{el-ph}} = \sum_{i=1}^{N} |\mu\rangle\hat{u}_\mu\langle\mu| \tag{5.6}$$

$$H^{\text{ph}} = \sum_{\xi} \hbar\omega_\xi(p_\xi^2 + q_\xi^2)/2 \tag{5.7}$$

The site energy of each pigment is sensitive to changes in the protein configuration that occur on timescales much longer than the timescales of excitation and fluorescence. These long timescale fluctuations are incorporated into the Hamiltonian by adding a random variable Δ_μ that samples a Gaussian distribution with zero mean and a standard deviation of σ_μ. Different values of Δ_μ represent inhomogeneous realizations of the pigments. The electron-phonon coupling is written in terms of the energy gap fluctuation operator ($\hat{u}_\mu$), defined in Equation 5.8, that describes the time-evolution of the energy gap between the ground state and excited state harmonic oscillators [61]. We assume that the excited state harmonic oscillator has the same frequency but a displaced equilibrium position ($R^{(0)}_{\mu,e/g}$) with respect to the ground-state.

$$\hat{u}_\mu = -\sum_{\xi} \hbar\omega_\xi(R^{(0)}_{\mu,e} - R^{(0)}_{\mu,g})q_\xi \tag{5.8}$$

Weak inter-pigment coupling

In the limit that the coupling between pigments is much weaker than the electron-phonon coupling, the absorption line shape is a sum of the absorptions of individual pigments in a protein bath. The absorption and fluorescence line shapes of an individual pigment, given by Equations (5.9) and (5.10), are written in terms of the vertical transition frequency (Ω_μ), line-broadening function ($g_\mu(t)$), and reorganization energy (λ_μ) [61, 107]. The real-value components of the Fourier transform of Equation (5.9) and (5.10) are the frequency domain line shapes of the absorption and fluorescence spectrum, respectively.

$$A_\mu(t) = e^{-i\Omega_\mu t - g_\mu(t)} \tag{5.9}$$

$$F_\mu(t) = e^{-i(\Omega_\mu - 2\lambda_\mu)t - g_\mu^*(t)} \tag{5.10}$$

$$g_\mu(t) = \int_0^\infty \frac{\mathrm{d}\omega}{\pi\omega^2}\chi''_\mu(\omega)\left[(1-\cos(\omega t))\coth\left(\frac{\omega}{2k_bT}\right) + i(\sin(\omega t) - \omega t)\right] \tag{5.11}$$

$$\lambda_\mu = \int_0^\infty \frac{\mathrm{d}\omega}{\pi\omega}\chi''_\mu(\omega) \tag{5.12}$$

The absorption and fluorescence spectra of each pigment are broadened by fluctuations of the phonon environment coupling to the electronic state of the pigments ($H^{\text{el-ph}}$). This influence is incorporated into the line-broadening function ($g_\mu(t)$) through the spectral density ($\chi''_\mu(\omega)$) that describes the distribution of phonon modes as a function of frequency, weighted by their coupling to the electronic structure of the pigment.

Energy transfer, in this limit, results from coupling between the transition dipole moments of pigments (the off-diagonal terms in H^{el}) and can be described by Förster theory [61, 107]. The rate of transfer is proportional to the square of the coupling between the pigments multiplied by the overlap of the fluorescence spectrum of the donor with the absorption spectrum of the acceptor, as given in Equation (5.13).

$$k_{\gamma\leftarrow\mu} = \frac{|H^{\text{el}}_{\mu,\gamma}|^2}{\hbar^2\pi}\int_0^\infty \mathrm{d}t A_\gamma(t)F^*_\mu(t) \tag{5.13}$$

Strong inter-pigment coupling

When the Coulombic coupling between pigments ($\hbar J_{\mu,\gamma}$) is much stronger than the electron-phonon coupling, the excited states of strongly coupled pigments will occur in coherent superpositions called excitons. Excitonic states $|m\rangle$ are the eigenvectors of the electronic Hamiltonian (H^{el}).

$$|m\rangle = \sum_{\mu=1}^{N} U_{\mu,m}|\mu\rangle \tag{5.14}$$

In this limit, the absorption and fluorescence line shapes are determined by both the electron-phonon coupling and the excitonic structure. The absorption and fluorescence lineshapes, described in the time-domain, are shown in Equations (5.15) and (5.16). Excitonic lineshapes and reorganization energies are linear combinations of pigment functions, see Equations (5.17) and (5.18) [107].

$$A_m(t) = e^{-i\Omega_m t - G_{mmmm}(t)} \tag{5.15}$$

$$F_m(t) = e^{-i(\Omega_m - 2\Lambda_{mmmm})t - G^*_{mmmm}(t)} \tag{5.16}$$

$$G_{mnpq}(t) = \sum_\mu U_{\mu,m}U_{\mu,n}U_{\mu,p}U_{\mu,q}g_\mu(t) \tag{5.17}$$

$$\Lambda_{mnpq} = \sum_\mu U_{\mu,m}U_{\mu,n}U_{\mu,p}U_{\mu,q}\lambda_\mu(t) \tag{5.18}$$

Energy transfer between excitons occurs because the electron-phonon coupling drives fluctuations in the site energies of pigments (the diagonal term of H^{el} in the site basis), which results in an off-diagonal coupling between excitonic states. Phonon driven energy transfer can be described by modified Redfield theory [156, 107], given in Equations (5.19)-(5.20), where the electron-phonon coupling is transformed into the exciton basis and the off-diagonal terms are treated as a perturbation to second-order.

$$k_{n\leftarrow m} = 2\Re \int_0^\infty \mathrm{d}t A_n(t) F^*_m(t) V_{n,m}(t) \tag{5.19}$$

$$V_{n,m}(t) = e^{2G_{mmnn}(t) + 2i\Lambda_{mmnn}(t)} \times \left[\ddot{G}_{mmnn}(t) - \{\dot{G}_{mmmn}(t) - \dot{G}_{mnnn}(t) + 2i\Lambda_{mmmn}\}^2\right] \tag{5.20}$$

The derivation of Equations (5.19) and (5.20) have been presented previously.[156] [19] A concern with using modified Redfield theory is the appearance of negative rates of transfer as the result of numerical instabilities for some inhomogeneous realizations [156]. In the following, if either the up-hill transfer rate or down-hill transfer rate between any pair of excitons was negative, it was replaced with a rate reconstructed from the other rate of the pair using the detailed-balance criterion. If both rates were negative, the calculation was dropped and a new inhomogeneous realization was selected.

Constructing domains

Photosystem II contains 326 pigments with a large range of inter-pigment couplings, so neither the strong- nor weak-interpigment coupling limit is applicable to all the pigment-pigment transfers within the supercomplex. One approach is to divide PSII into groups of pigments that are strongly coupled (called domains) and approximate energy transfer within these groups by the strong coupling limit and between these groups by the weak coupling limit. Photosystem II, however, has many intermediate couplings, thus the separation between strong and weak is ambiguous and the precise grouping of chlorophylls is subjective

[121, 104]. We chose to group pigments to improve the separation of timescales between inter- and intra-domain transfer.

In this treatment, pigments must have coupling above a threshold value [104] ($V_{\text{cutoff}} = 15\ \text{cm}^{-1}$) and give rise to excitons that rapidly exchange energy to be included in the same domain. Since energy transfer between excitons is driven by site fluctuations, two excitons that have substantial overlap in the site-basis will be rapidly mixed by fluctuations in site energy. This allows excitonic overlap to act as a proxy for energy transfer rates. To calculate this overlap, we removed all coupling in H^{el} less than 15 cm^{-1} and then calculated the transformation matrix ($\tilde{\mathbf{U}}$) associated with this new Hamiltonian. Using the transformation matrix we calculated the excitonic overlap that two sites experience using Equation (5.21). If the overlap is larger than the threshold value ($S_{\mu,\gamma} > 0.1$, selected to reproduce separation of timescales in LHCII), the two pigments contribute to excitons that exchange energy rapidly. This overlap, however, is also sensitive to the inhomogenous realization, so the two pigments are only in the same domain if $S_{\mu,\gamma} > 0.1$ in at least 50% of all inhomogeneous realizations.

$$S_{\mu,\gamma} = \sum_m \frac{\tilde{U}^2_{\mu,m}\tilde{U}^2_{\gamma,m}}{\Upsilon_m} \tag{5.21}$$

$$\Upsilon_m = \sum_\mu \tilde{U}^4_{\mu,m} \tag{5.22}$$

The new hybrid basis ($|M\rangle$) was constructed by forming blocks within H^{el} of the pigments belonging to the same domain and then solving for the eigenvectors of each block ($U_{\mu,M}$). These block-eigenvectors form an orthonormal basis with the property that $\langle M|H^{\text{el}}|N\rangle = 0$ if M and N belong to the same domain and M is not equal to N. These vectors do not form an eigenbasis of H^{el}, but they are an eigenbasis within each domain. We then calculated energy transfer within a domain using modified Redfield theory and energy transfer between domains using generalized Förster theory. Generalized Förster theory (Equations (5.23) and (5.24)) uses coupling matrix elements calculated between the new basis vectors ($|M\rangle$) and overlap integrals between excitonic line shape functions analogous to those given in Equation (5.15) and (5.16), since the basis is composed of states delocalized within each domain [61, 107].

$$k_{M\leftarrow N} = \frac{|V_{M,N}|^2}{\hbar^2\pi}\int_0^\infty \mathrm{d}t A_M(t)F^*_N(t) \tag{5.23}$$

$$|V_{M,N}|^2 = |\sum_{\mu,\gamma} U_{\mu,M}H^{\text{el}}_{\mu,\gamma}U_{\gamma,N}|^2 \tag{5.24}$$

Boltzmann-averaged rates between domains

The excitation energy transfer rates within a domain are, by construction, much faster than the rate of transfer between domains. This separation of timescales allows for excitation within a domain to thermalize rapidly with respect to transfer out of the domain. The rate

of transfer from domain d to domain a is described by Equation 5.25, which performs a sum over the rate of transfer from all the excitons M in d to all the excitons N in a weighted by the Boltzmann population of exciton M ($P_M^{(d)}$) [118].

$$k_{a\leftarrow d}^{\mathrm{dom}} = \sum_{\substack{|M\rangle\in d \\ |N\rangle\in a}} k_{N\leftarrow M} P_M^{(d)} \tag{5.25}$$

$$P_M^{(d)} = \frac{e^{-E_M/k_BT}}{\sum_{|M\rangle\in d} e^{-E_M/k_BT}} \tag{5.26}$$

Excitation within the supercomplex can then be simplified into a collection of domain populations connected by Boltzmann-averaged rates of transfer. The domain model was found to closely reproduce the full model, as shown in the Results and Discussion Section, and will be used extensively in this paper because of the computational simplification that it allows.

Constructing coarse-grained models of energy transfer

To construct coarse-grained models of energy transfer between compartments composed of many domains, we assumed rapid thermalization within a compartment. These compartments range in size from several domains that incorporate all the chlorophyll in a single protein to 116 domains that incorporate all the chlorophyll in the largest supercomplex ($C_2S_2M_2$). The rates between compartments were calculated using Equations (5.25) and (5.26), except the acceptor and donor sites were compartments consisting of several domains. If a domain was shared between two compartments, the domain was put into the compartment containing more chlorophylls assigned to that domain. The low energy domain shared by CP29 and CP24 consists of three chlorophylls from each protein. For the model with protein compartments, this domain was put in the CP29 protein compartment. In the model in which all chlorophylls in PSII form a single compartment, the rate k_{CS} (see next Section) was modified by the Boltzmann population of excitons in the RC domain.

5.2.2 Photosystem II: parameters

Structures

The $C_2S_2M_2$ PSII supercomplex is a two-fold symmetric dimer (Figure 5.1a). The supercomplex contains four LHCII trimers and two copies of each of the minor complexes, CP26, CP24, and CP29 as well as two copies of the reaction center core. The structure of the $C_2S_2M_2$ PSII supercomplex was recently obtained at 12 Å resolution [32]. This resolution determined the relative orientations and approximate distances between proteins in the supercomplex. The structure of the reaction center core dimer from cyanobacteria [141] and the structure of the LHCII trimer from spinach [79] have both been solved by x-ray crystallography. We have used a monomer from the LHCII structure for each of the minor complexes. The CP29 crystal structure was recently published [110], but because there

is as yet no Hamiltonian for this protein, we did not use it in our calculations. Still, the CP29 structure showed high homology with an LHCII monomer, except that Chl 605 in the LHCII monomer has no equivalent in CP29. For this reason, that chlorophyll is deleted in our $C_2S_2M_2$ structure in the LHCII monomer representing CP29. The vertical position of the proteins in the membrane was determined using the Orientations of Proteins in Membranes Database [80]. The lateral orientation was determined using the results of Caffarri and coworkers [32]. The protein structures presented in the paper were generated using the VMD software package [59]. The different supercomplex structures needed to model the fluorescence lifetime data from Caffarri and coworkers [31] were constructed by deleting proteins from the $C_2S_2M_2$ supercomplex. The LHCII trimers within a supercomplex (up to 2 LHCII-s and 2 LHCII-m) are all identical structures with different nomenclature only to identify their positions within the complex.

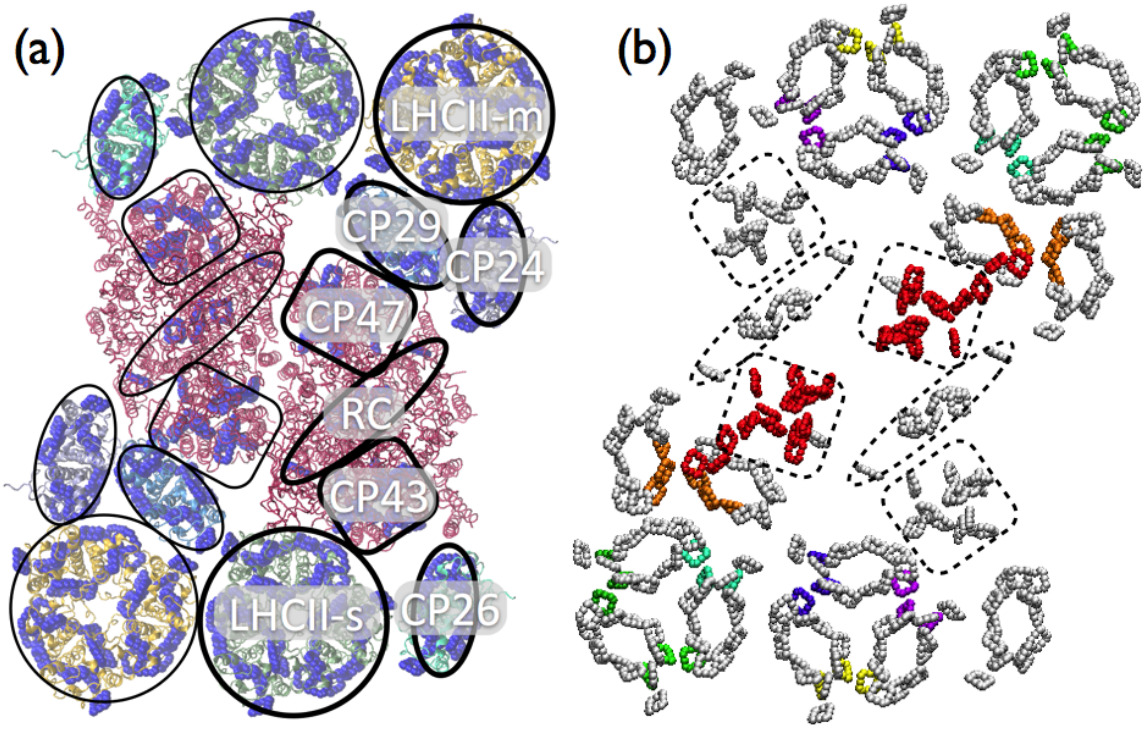

Figure 5.1: The $C_2S_2M_2$ protein structure and pigment arrangement are shown based on the structure determined by Caffarri and coworkers [32]. (a) The protein and pigment arrangement are shown. Chlorophylls are represented as blue spheres outlining the chlorin ring. Thick (thin) black outlines surround proteins associated with the right (left) monomer unit of the $C_2S_2M_2$. (b) The protein scaffold has been removed to expose the pigments bound by each protein unit. Pigments belonging to domains contained within a single protein unit are shown in grey. Pigments assigned to a domain delocalized between more than one protein are colored according to their domain assignment.

Hamiltonian

H^{el} is divided into three types of terms: (1) site energies, (2) intra-protein couplings (the interactions of pigments contained within the same protein scaffold), and (3) inter-protein couplings (the interactions of pigments contained in different proteins scaffolds). The site energies, inhomogeneous distributions, and intra-protein couplings were set to literature values [90, 104, 117, 118, 119]. The inter-protein couplings were constructed using the dipole-dipole approximation (Equation (5.27)), where $\vec{R}_{\mu,\gamma}$ is a vector describing the center-to-center difference in position of the pigments μ and γ. The transition dipole moments are taken from the literature [104, 118, 90, 117, 119]. The spectral density, describing the electron-phonon coupling, for each chlorophyll is the same as that used in the literature when originally extracting the site energy for the chlorophyll.

$$J_{\mu,\gamma} = \frac{\vec{v}_\mu \cdot \vec{v}_\gamma}{|R_{\mu,\gamma}|^3} - 3\frac{(\vec{v}_\mu \cdot \vec{R}_{\mu,\gamma})(\vec{v}_\gamma \cdot \vec{R}_{\mu,\gamma})}{|R_{\mu,\gamma}|^5} \tag{5.27}$$

5.2.3 Electron transfer scheme

A detailed model of excitation and electron transport within the reaction center presented by Novoderezhkin and coworkers [106] proposed that charge separation can be initiated through either the excited states of special pair ($P^*_{D2}/P^*_{D1} \rightarrow P^+_{D2}P^-_{D1}$) or the associated D1 chlorophyll ($Chl^*_{D1} \rightarrow Chl^+_{D1}Phe^-_{D1}$). The electron transport scheme contains five different charge separated populations with eleven rate constants. Novoderzhkin and coworkers used pump-probe data to parameterize their electron transfer model. In this work, we will be simulating fluorescence decay curves which are only sensitive to the very coarse features of energy transfer. As such, we will decrease the number of fit parameters associated with our model. We chose to describe the electron transport scheme phenomenologically by including only two radical pair states. The two states (RP1 and RP2) and three kinetic rates that define the electron transfer process in our model are shown in Figure 5.2. The radical pair states RP1 and RP2 do not have direct physical interpretation in terms of molecular charge separated states. Instead, the kinetic rates and populations describe the overall behavior of charge separation without assuming any particular molecular identity for the electron transport through the reaction center. The three kinetic rates (k_{CS}, k_{RC}, and k_{irr}) describing electron transfer were determined by fitting the experimental fluorescence decay spectra with simulated curves.

5.2.4 Simulating fluorescence decays

The master-equation formalism introduced in Section 4.1 and shown again in Equation (5.28) defines energy transfer in terms of the rate matrix (K) which contains the transfer rates between excitons or domains and the transfer rates from the RC to the charge separated states and the population vector ($P(t)$) describing the distribution of excitation at a given time. Additional loss pathways in the form of radiative (k_{fl}) and non-radiative (k_{nr}) are

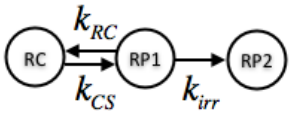

Figure 5.2: Charge separation scheme. RC represents the reaction center domain, which contains four chlorophyll (two special pair and two associated chlorophyll) and two pheophytin. Each reaction center in a PSII supercomplex performs electron transfer using the same rate constants.

also present in the system and are treated explicitly as additional compartments within the kinetic model. The fluorescence rate of each exciton was scaled by its transition dipole moment squared with the average fluorescence timescale across all states of the system set to 16 ns [15, 109]. The non-radiative rate was assumed to be equal for all excitons with a timescale of 2 ns [15, 159].

$$\dot{P}(t) = KP(t) \tag{5.28}$$

The fluorescence decay spectra were calculated as a function of the initial excitation by projecting into the basis of the eigenvectors of the rate matrix ($|u\rangle$), as shown in Equations 5.29-5.31 [155]. The decay timescales (τ_u) are the inverse of the u^{th} eigenvalue of the rate matrix, the fluorescence weight factor ($0 \leq \tilde{k}_m^{fl} \leq 1$) is the relative fluorescence rate of each exciton, and the similarity transform matrix (Θ^{-1}) projects from excitons ($|M\rangle$) to the eigenvectors of the rate matrix ($|u\rangle$).

$$F(t) = \sum_M \tilde{k}_M^{fl} \langle M|e^{Kt}|P(0)\rangle \tag{5.29}$$

$$F(t) = \sum_u a_u e^{-t/\tau_u} \tag{5.30}$$

$$a_u = \sum_M \tilde{k}_M^{fl} \langle M|\Theta|u\rangle\langle u|\Theta^{-1}|P(0)\rangle \tag{5.31}$$

Since experimental measurements of fluorescence lifetimes using time-correlated single photon counting have finite resolution we have implemented resolution loss by setting a lower limit to lifetime components (τ_u) of 8 ps. Any amplitude a_u associated with a lifetime less than the lower limit is shifted up to 8 ps.

5.2.5 Calculating linearized kinetics

To analyze the rate-limiting steps for trapping within PSII, we have chosen to calculate a decomposition of the average trapping time in terms of a hierarchical linearization of the overall kinetic rate matrix. Following the work of Yang and Fleming [157], the average trapping time can be described using a sequence of rate matrices ($\mathbf{K}_i$) and kinetic compartments

(σ_i) constructed to satisfy the condition that the i^{th} compartment is a perfect trap within the $\mathbf{K}_{i+1}$ rate matrix. RP2 is a trap for the entire rate matrix, so we begin by defining $\sigma_0 =$ RP2 and $\mathbf{K}_1$ is the domain rate matrix, composed of thermal transfer rates between domains. Subsequent kinetic compartments and rate matrices are defined in terms of Equation (5.32) and (5.33).

$$\mathbf{K}_i = \mathbf{K}_{i-1} - \mathbf{K}_{i-1}|\sigma_{i-1}\rangle\langle\sigma_{i-1}| \quad \text{for } i \geq 2 \tag{5.32}$$

$$\langle\sigma_i| = \langle\sigma_{i-1}|\frac{\mathbf{K}_i}{\sqrt{\langle\sigma_{i-1}|\mathbf{K}_i\mathbf{K}_i^T|\sigma_{i-1}\rangle}} \tag{5.33}$$

The effective forward transfer time ($\tau^{\text{eff}}_{i\leftarrow i+1}$) is the average time for transfer from compartment $i+1$ to compartment i in the presence of the back-transfer away from the final charge separation state (RP2). The effective forward transfer time described in Equation (5.34) contains two contributions. The first ($k^{-1}_{i\leftarrow i+1}$) can be considered the inverse of the rate of transfer between the $i+1$ and i compartments. The second term, $(1+r_{i+2})$ corrects the forward transfer rate for trajectories that first back-transfer to compartments greater than $i+1$.

$$\tau^{\text{eff}}_{i\leftarrow i+1} = k^{-1}_{i\leftarrow i+1}(1+r_{i+2}) \tag{5.34}$$

$$k^{-1}_{i\leftarrow i+1} = \sqrt{\langle\sigma_{i-1}|\mathbf{K}_i\mathbf{K}_i^T|\sigma_{i-1}\rangle} \times \frac{\sum_{n\in\text{Domain}}\langle n|\sigma_{i-1}\rangle}{\sum_{n\in\text{Domain}}\langle n|\sigma_i\rangle} \tag{5.35}$$

$$r_i = -\frac{\sum^{N_{max}}_{n\in\text{Domain}}\langle n|\mathbf{Q}_{i+1}(\mathbf{Q}_{i+1}\mathbf{K}_1\mathbf{Q}_{i+1})^{-1}\mathbf{Q}_{i+1}\mathbf{K}_i|\sigma_i\rangle}{\sum^{N_{max}}_{n=1}\langle n|\sigma_i\rangle} \tag{5.36}$$

$$\mathbf{Q}_i = \mathbf{I} - \sum_{n=1}^{i-1}|\sigma_n\rangle\langle\sigma_n| \tag{5.37}$$

The average trapping time is determined by both the effective rates of transfer along the chain of compartments and the initial population of excitation within the system. The contribution of $\tau^{\text{eff}}_{(i-1)\leftarrow(i)}$ to the average trapping time is weighted by ρ_i, the fraction of population initiated in compartments $j \geq i$.

$$\tau_{\text{trap}} = \sum_{i=0}^{N_{max}} t_{i-1\leftarrow i} \tag{5.38}$$

$$t_{i-1\leftarrow i} = \tau^{\text{eff}}_{i\leftarrow i+1}\rho_{i+1} \tag{5.39}$$

$$\rho_i = \sum_{j=i}^{N_{max}} P_j(t=0) \tag{5.40}$$

5.3 Model of photosystem II

5.3.1 Pigment Domain Assignments Reveal Inter-Protein Domains

Photosystem II pigments (Chl-a, Chl-b, and pheophytin) were grouped into strongly interacting clusters called domains. While it is often assumed that pigments will interact most strongly with other pigments bound within the same protein [26, 143], we have used the supercomplex structure to assign domains with an unbiased approach that depends only on the couplings and energy gaps of the relevant chlorophylls. This method has revealed a small set of pigments that form domains delocalized across multiple proteins. Figure 5.1b shows the $C_2S_2M_2$ supercomplex with the protein scaffold removed to display only the pigments. Chlorophylls belonging to a domain delocalized over more than one protein unit are shown in colors according to their domain assignment. Within LHCII trimers we see delocalization between high energy pigments belonging to different monomers (e.g. the yellow, blue, and purple chlorophylls bound by LHCII-s). CP24 and CP29 share a domain that contains the lowest energy exciton of both proteins (the orange chlorophyll). Additionally, CP29 has two pigments that belong in the same domain as 15 of the 16 CP47 chlorophylls (the red chlorophylls). The remainder of the chlorophyll (shown in grey) have the same domain assignments within a $C_2S_2M_2$ supercomplex as they would in an isolated protein.

5.3.2 Testing infinitely fast intra-domain equilibration

The domain assignments used in this work were selected to increase the separation of timescales between inter- and intra-domain transfer rates. In the limit that a complete separation of timescales is achieved, the much faster intra-domain rates will result in excitation energy thermalizing prior to transfer out of the domain. We constructed a new rate matrix (domain model) that coarse-grains the system at the domain level by assuming infinitely fast intra-domain thermalization. To assess the error associated with this domain model, we calculated the domain populations as a function of time both with and without assuming infinitely fast equilibration within domains. For these calculations, electron transfer in the RC is treated as infinitely fast and irreversible. To assess the similarity of the dynamics in both cases, we calculate two error metrics $\Delta^{(d)}_{\text{max}}$ (Equation 5.41) and $\Delta^{(d)}_{\text{Integral}}$ (Equation 5.42). $\Delta^{(d)}_{\text{max}}$ measures the maximum absolute deviation of the two population traces as a percentage of the maximum population of the domain calculated with the full rate matrix. The second metric, $\Delta^{(d)}_{\text{Integral}}$, reports the integral of the absolute deviation over all time as a fraction of the integral of the population calculated using the full rate matrix over all time.

$$\Delta^{(d)}_{\text{max}} = \frac{\max|P^{(d)}_{\text{exc}}(t) - P^{(d)}_{\text{dom}}(t)|}{\max\ P^{(d)}_{\text{exc}}(t)} \tag{5.41}$$

$$\Delta^{(d)}_{\text{Integral}} = \frac{\int_0^\infty |P^{(d)}_{\text{exc}}(t) - P^{(d)}_{\text{dom}}(t)|\mathrm{d}t}{\int_0^\infty P^{(d)}_{\text{exc}}(t)\mathrm{d}t} \tag{5.42}$$

No matter what domain is initially excited, we found that $\Delta^{(d)}_{\text{max}} < 2\%$ and $\Delta^{(d)}_{\text{integral}} < 7\%$ for all domains of $C_2S_2M_2$. The population curve with the largest error in both of these measures is shown in Figure 5.3. The difference between the dynamics calculated with the full rate matrix versus the domain rate matrix in this plot is barely differentiable by eye. The excellent agreement between the domain model and the full calculation supports our method for assigning chlorophylls to domains using a separation of timescales metric. We have used the domain model as the reference calculation for the remainder of the paper.

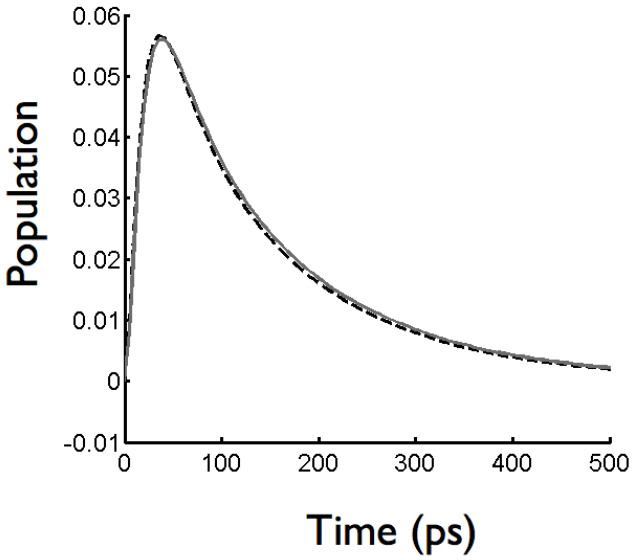

Figure 5.3: A comparison between the domain population curves with the largest value $\Delta^{(d)}_{\text{max}}$ and $\Delta^{(d)}_{\text{Integral}}$. Population trace calculated with the generalized Förster/modified Redfield (Domain) model is shown with a dashed black (sold grey) line.

5.3.3 Extracting charge separation rates

The fluorescence lifetime of a PSII supercomplex is determined by both the rates of energy transfer in the antenna and electron transfer kinetics in the reaction center. We incorporated the electron transfer rates (shown in Figure 5.2) into the domain model and extracted their values by fitting fluorescence decay spectra. In previous work, Caffarri and coworkers [31] measured fluorescence decay spectra collected from 5 bands separated using sucrose density gradient centrifugation on thylakoid membranes. These bands were labeled, in order of increasing size, as B7 to B11. The protein composition of each band is shown by the cartoon

	B8-B11	B7 (Core Complex)
τ_{CS} (ps)	0.64	4.4
τ_{RC} (ps)	160	130
τ_{irr} (ps)	520	250

Table 5.1: Best fit electron transfer timescales for the Domain Model.

in the top-right corners of Figure 5.4b-f. No single set of electron transfer rates reasonably fit both the core complex (B7) and any of the larger supercomplexes simultaneously. As a result, two different sets of electron transfer timescales ($\tau = k^{-1}$) are shown in Table 5.1, one for the fit to the core complex data (B7) and the other for the fit to the data from the larger supercomplexes (B8-B11). The core complex data is described by a much slower initial charge separation and faster irreversible electron/hole separation. The difference between the core and supercomplex electron transfer kinetics has been observed previously [31]. The origin, however, remains unclear: it could be an artifact of the modeling or the result of a physical difference in the samples not accounted for in the current structure/parameter data. In the following we use the B8-B11 electron transfer rates to explore the dynamics of light harvesting in the largest supercomplex, $C_2S_2M_2$ (B11).

5.4 Timescales of light harvesting in $C_2S_2M_2$

The rate matrix provides a complete description of the kinetics of excitation energy and electron transfer, but a simplified picture would decompose the average timescale for trapping into contributions from a small set of effective forward transfer rates. For the process of energy capture (τ_{capture}) in $C_2S_2M_2$, from initial excitation in the antenna to irreversible electron hole separation, we define four kinds of contributions: 1) the diffusion time (τ_{diff}) that characterizes the transfer of excitation energy within the antenna to pigments kinetically connected to the reaction center, 2) the transfer-to-the-trap time (τ_{TtT}) that characterizes excitation energy transferring from these pigments in the antenna to the RC, 3) the initial charge separation time (τ_{iCS}) that characterizes excitation energy driving electron hole separation, and 4) the irreversible charge separation time (τ_{irrCS}) that characterizes the final separation of the electron and hole [35, 145] (Equation (5.43)).

$$\tau_{\mathrm{capture}} = \tau_{\mathrm{diff}} + \tau_{\mathrm{TtT}} + \tau_{\mathrm{iCS}} + \tau_{\mathrm{irrCS}} \tag{5.43}$$

It is generally agreed that energy capture in PSII is limited by the rate of irreversible electron hole separation, which is one to two orders of magnitude slower that the other timescales involved [26, 52, 86, 146]. We define light harvesting as the conversion of excitation energy to the RP1 state. As such, light harvesting is described by only the first three timescales associated with energy capture ($\tau_{\mathrm{LH}} = \tau_{\mathrm{diff}} + \tau_{\mathrm{TtT}} + \tau_{\mathrm{iCS}}$). Previous work [86, 146, 147] has suggested that the kinetics of light harvesting in PSII are either trap limited ($\tau_{\mathrm{iCS}} \gg$

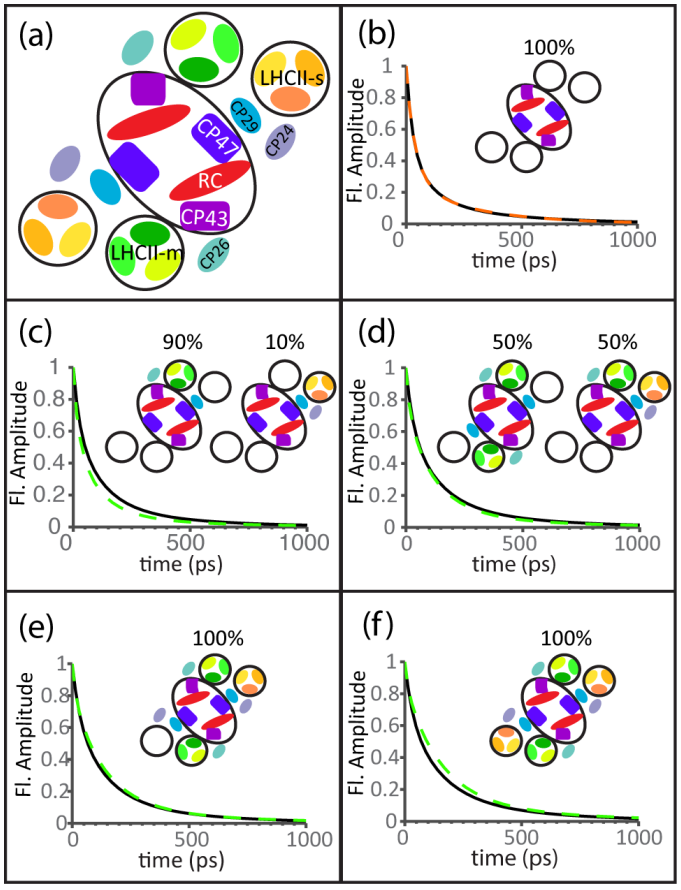

Figure 5.4: (a) A cartoon structure of PSII supercomplex proteins is shown to assist with the interpretation of the cartoons in the top-right corner of each box, representing the contributions of different supercomplexes to each band. A comparison between experimental (black line, taken from Caffari and coworkers [31]) and simulated (orange and green dashed-lines for B7 and B8-B11, respectively, calculated with the domain model) fluorescence decay spectra for (b) B7, (c) B8, (d) B9, (e) B10, and (f) B11. The simulated spectra are calculated using the best fit electron transfer timescales given in Table 5.1.

$\tau_{\mathrm{TtT}} + \tau_{\mathrm{diff}}$) or transfer-to-trap limited ($\tau_{\mathrm{TtT}} \gg \tau_{\mathrm{iCS}} + \tau_{\mathrm{diff}}$). Knowledge of the rate-limiting step would inform our interpretation of fluorescence lifetime data from both supercomplexes and intact membranes [35, 122].

One challenge in determining the relative contributions of τ_{diff}, τ_{TtT}, τ_{iCS}, and τ_{irrCS} is that they are not directly related to the rates of transfer in the rate matrix. These timescales describe the overall behavior of energy transport, which involves forward and reverse rates of transfer mixed with entropic effects (the connectivity of the different domains within the rate matrix). Yang and Fleming [157] have demonstrated a method that decomposes the average trapping time into contributions from different physical processes. In this treatment, a linear chain of compartments (σ_i), as shown in Figure 5.5, is constructed to reproduce the

average timescale of capture. The compartments are linear combinations of domains that form an orthonormal set. Excitation energy flows down the chain from the periphery of the supercomplex ($\sigma_{N_{max}}$) to the final charge separation state RP2 (σ_0). The effective forward transition time ($\tau^{\text{eff}}_{i-1\leftarrow i}$, given in Equation (5.34)) describes the timescale of transfer from σ_i to σ_{i-1} corrected for trajectories where excitation initially performs back transfer to higher compartments in the chain prior to transferring from σ_i to σ_{i-1}. The effective transition times describe the kinetic structure of the rate matrix in a form that allows for determining the four timescales for energy capture. These timescales, however, do not account for the initial distribution of excitation. A population-weighted effective transfer time ($t_{i-1\leftarrow i}$) weights $\tau^{\text{eff}}_{i-1\leftarrow i}$ for the population of excitation that will flow through compartment i, which takes into account the initial excitation distribution (Equations (5.38) - (5.40)). For PSII with the electron transfer scheme shown in Figure 5.2, τ_{TtT}, τ_{iCS}, and τ_{irrCS} are described by timescales of transfer ($t_{i-1\leftarrow i}$) between the first 4 compartments along the chain. τ_{diff} is described by a sum over the remaining timescales of transfer along the chain.

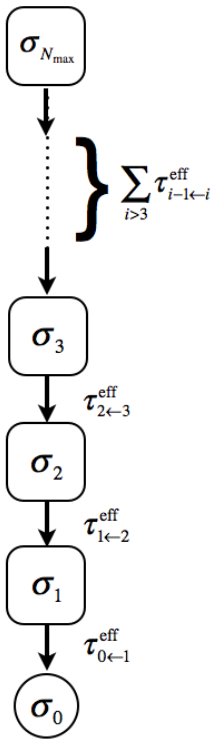

Figure 5.5: A diagram of the linear excitation energy cascade is shown where σ_0 represents RP2 in $C_2S_2M_2$. The effective timescales of transfer between compartments ($\tau^{\text{eff}}_{i-1\leftarrow i}$) is the average time of transfer from compartment i to $i-1$ averaging over all pathways starting at compartment i.

The experimental fluorescence decay curves plotted in Figure 5.4 (black lines) have initial excitation evenly distributed among Chl-a molecules in the PSII supercomplexes. This is

Compartments	$t^{\text{chlA}}_{i-1\leftarrow i}$ (ps)	$t^{periphery}_{i-1\leftarrow i}$ (ps)	Description
$0 \leftarrow 1$	560	560	RP2 $\leftarrow$ RP1 (τ_{irrCS})
$1 \leftarrow 2$	11	11	RP1 $\leftarrow$ RC (τ_{iCS})
$2 \leftarrow 3$	94	100	RC $\leftarrow$ Antenna (τ_{TtT})
$\sum_{i=3}^{Nmax}[(i+1) \leftarrow (i)]$	50	110	Diffusion in Antenna (τ_{diff})

Table 5.2: The timescales of transfer for the effective linearization scheme of $C_2S_2M_2$ supercomplex.

an important initial condition to consider since spectroscopic probes of supercomplexes will excite a wide spatial distribution of chlorophylls. We have calculated the population-weighted effective transfer times for evenly distributed Chl-a excitation ($t^{chlA}_{i-1\leftarrow i}$), shown in Table 5.2. The contributions of different components to τ_{LH} breaksdown as follows: 30% from τ_{diff}, 60% from τ_{TtT}, and 10% from τ_{iCS}. Given the balance between the diffusion and transfer-to-trap contributions, when Chl-a molecules are evenly excited, light harvesting in $C_2S_2M_2$ should not be considered to occur in any of the previously suggested limits, though it is closer to the transfer-to-trap limit than any other.

When a supercomplex resides within a membrane, a larger fraction of excitations will be initialized in the periphery of the supercomplex as a result of energy transfer from adjacent LHCII trimers or supercomplexes. This initial condition is quite different from those expected for measurements on isolated supercomplexes. Using our linearized kinetic model of PSII supercomplexes, however, we can explore the timescales of trapping associated with excitations entering from the edge of the supercomplex ($t^{periphery}_{i-1\leftarrow i}$). For peripheral excitations, τ_{diff} and τ_{TtT} each contribute approximately 50% of τ_{LH}. Incorporating additional energy transfer into and out of the domains contained in $C_2S_2M_2$, as a result of the additional pigments bound in the membrane, will increase both τ_{diff} and τ_{TtT}. It is likely, however, that τ_{diff} will increase more as the effective antenna size increases, and the average timescale for light harvesting will shift towards the diffusion limit.

5.5 Spatial aspects of light harvesting in $C_2S_2M_2$

The overall efficiency of photoconversion depends on the energy transfer rates that arise from the combined energetic and spatial organization of chlorophyll in PSII supercomplexes. Our model shows no evidence of an energy funnel, in agreement with previous work on PSII antenna and core complex [118, 104]. Studies of LHCII trimers have suggested that a low energy cluster of Chl-a act as a favored exit site [129]. Using the structure of PSII supercomplexes and considering the distances between chlorophyll, Caffarri and coworkers [32] have extended this thought by proposing that the exit site of LHCII-s should experience fast transport to a nearby pigment of CP43. A series of such rapid energy transfer steps could form a favored pathway from the peripheral LHCII trimers to the RC. Such a pathway

would increase the photochemical yield by allowing excitation energy to reach a reaction center prior to loss by fluorescence or intersystem crossing. Using the domain model we explore the appropriate description of the spatial distribution of energy flow through PSII supercomplexes.

We tested for the presence of favored energy transfer pathways in each quadrant of PSII. If a small number of such pathways exist, the photochemical yield should substantially decrease when one of these energy pathways is disrupted by removing an essential domain. We selected the two unique quadrants of $C_2S_2M_2$ as the subsystems of interest: the bottom right quadrant (RC, CP43, CP26, LHCII-s) and the top right quadrant (RC, CP47, CP29, CP24, LHCII-m), as shown in Figure 5.1a. We first calculated the photochemical yield of both subsystems. Subsequently, we performed a series of calculations of the photochemical yield for each subsystem in which one of the domains of the subsystem was removed. In all calculations Chl-a's were evenly excited on the LHCII monomer farthest from the RC. There was only one case where removing a domain reduced the photochemical yield to less than 85% of the photochemical yield of the intact subsystem. The one case corresponded to removing the 17 chlorophyll domain shared between CP47 and CP29, which removes all but one of the chlorophylls bound by CP47. This results in greatly suppressed photochemical yield since, as can be seen in Figure 5.1b, the deletion of the large CP47 domain removes all chlorophyll in the vicinity of the reaction center. The general robustness to domain removal demonstrates that no single domain (excluding the 17 chlorophyll CP47 domain) is essential for efficient energy transfer to the reaction center. Instead, there are many energy transfer rates substantially faster than the timescale of loss (fluorescence and intersystem crossing) and this results in a collection of pathways that are fast enough to maintain high photochemical yield.

Next, we characterized how the timescale of light harvesting depends on a single spatial dimension, the average distance of the chlorophyll composing a domain to the nearest RC (d_{RC}). Figure 5.6 plots the average timescale for light harvesting (τ_{LH}) for excitation initiated in each domain against d_{RC}. The calculation of τ_{LH} for excitation initiated in a particular domain is equivalent to calculating the mean first passage time from that domain to the first radical pair state (RP1) [112]. The dots represent the results of one calculation. The colored contours (with increasing density from blue to red) show the underlying distribution extracted from calculations with 500 realizations of the site energies. The overall process of light harvesting in PSII supercomplexes is insensitive to inhomogeneous realizations, as demonstrated by the similar width of the distributions for a single realization and for 500 realizations. Further, τ_{LH} for an excitation is linearly dependent on its distance to the nearest RC, with a slope of approximately ten picoseconds per nanometer.

When a supercomplex is embedded in the grana membrane, it is surrounded by a dense array of pigment-protein complexes. A reaction center embedded in this array might be capable of efficiently capturing excitation energy initially absorbed far outside of the supercomplex it belongs to. Light harvesting is efficient anywhere that τ_{LH} is substantially smaller than the $\sim$2 ns timescale of excitation loss to unproductive pathways (fluorescence and intersystem crossing). The linear dependence shown in Figure 5.6 cannot be directly

extended to a membrane since the slope of the line will vary with the increased number of pigments and the unassociated LHCII may experience slower transport into the supercomplex than proteins bound by the supercomplex experience within it. However, the large disparity between the timescale of excitation loss (∼2 ns) and the ∼200 ps timescale of light harvesting found at the periphery of $C_2S_2M_2$ suggests that photosystem II reaction centers can efficiently harvest light from antenna assemblies much larger than that of $C_2S_2M_2$.

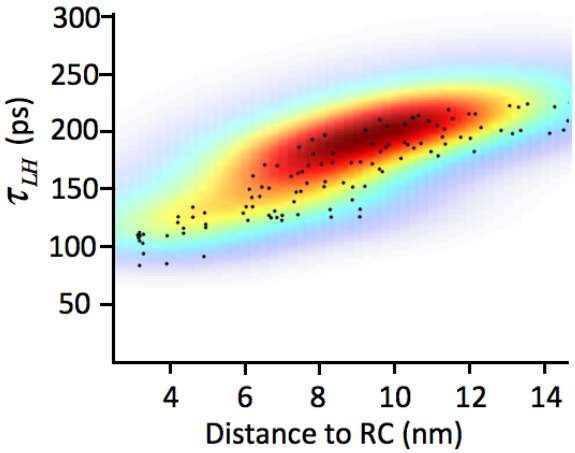

Figure 5.6: The timescale of light harvesting (τ_{LH}) for excitation initiated in each domain is plotted against the average distance from that domain to the nearest reaction center. The black dots denote the results from one inhomogeneous realization of the site energies. The colored contours (red indicating more points, blue indicating less) show the underlying distribution extracted from compartments calculated from 500 inhomogeneous realizations of the site energies. The underlying distribution was calculated with 2D Gaussian smoothing.

5.6 Coarse-grained models of energy transfer in $C_2S_2M_2$

5.6.1 The domain model is the most coarse-grained model that reproduces the energy transfer dynamics in $C_2S_2M_2$

One goal for this model was to determine the most coarse-grained treatment of energy transfer that reproduced the exact dynamics as calculated by the modified Redfield/generalized Förster treatment. We already showed that the domain model accurately describes the dynamics of energy transfer. We sought to determine whether any of the previously proposed coarse-grained models could also reproduce accurate energy transfer dynamics. There are three different coarse-grained treatments of the domain model of $C_2S_2M_2$ (Figure 5.7a-c) that correspond to kinetic limits that have been considered previously in the literature: 1) the ERPE model [86] assumes fast equilibration within all pigments of PSII,

2) the transfer-to-trap limited (TTL) model [146] assumes fast equilibration within the antenna pigments but slow transfer from the antenna to the RC (and vice-versa), and 3) the protein model [26, 31] assumes excitation equilibrates rapidly within a protein followed by slower transfer between proteins. Each of these models was constructed by coarse graining the domain model into compartments defined by regions of fast equilibration. The rates between compartments were calculated using Equations (5.25) and (5.26). The electron transfer rates used were those calculated using the domain model. As seen in Figure 5.7d, none of these coarse-grained treatments quantitatively reproduced the population dynamics of the initial charge separated state (RP1) for $C_2S_2M_2$ calculated with the domain model. This result is not surprising, given the breakdown of timescales for τ_{trap} described in Section 5.4. The most computationally feasible and most accurate model of energy transfer for PSII supercomplexes is one in which excitation energy transfers between domains.

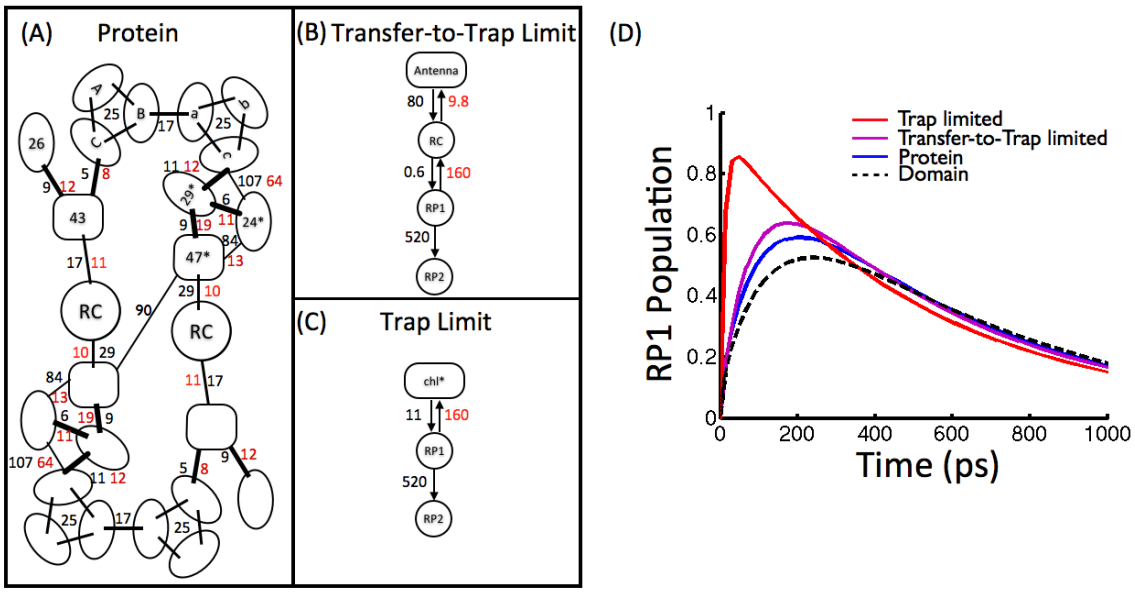

Figure 5.7: A comparison between different coarse grain models of $C_2S_2M_2$ is shown both as kinetic schemes and simulated RP1 population trace. (A)-(C) The timescales of transfer (k^{-1}) for the various coarse-grain models are shown in units of ps. Numbers in black (red) represent transfers that move excitation closer to (farther away from) the charge separated states. (A)-(C) represent the protein model, transfer-to-trap limited model, and the trap limited model, respectively. (D) The simulated curves for the RP1 population calculated with ($\tau_{\text{cs}} = 0.61$ ps, $\tau_{\text{rc}} = 160$ ps, and $\tau_{\text{irr}} = 520$ ps) are shown in black (Domain), blue (Protein), purple (transfer-to-trap limited), and red (trap limited). The initial excitation was distributed evenly among Chl-a molecules.

B8-B11	Domain	Protein	TTL	ERPE
τ_{CS} (ps)	0.64	2.1	2.2	0.28
τ_{RC} (ps)	160	140	91	1.0
τ_{irr} (ps)	520	260	190	33
RMSE ($\times 10^{-2}$)	1.7	1.6	1.4	1.9

Table 5.3: The best fit electron transfer timescales for the Domain, Protein, Transfer-to-Trap Limited, and ERPE models.

5.6.2 Quality of fit to fluorescence decays is not a proxy for accuracy of energy transfer models

Energy transfer models of PSII have typically been constructed by fitting kinetic models to fluorescence decay curves. The quality of fit has been used as an indicator of how well these kinetic models describe the underlying dynamics [57, 149]. However, it may be that the fluorescence lifetime data is too coarse-grained to be able to distinguish between models with many fitting parameters because it is the sum over the excitation populations of all domains (Equation 5.29). Indeed, it has recently been shown that different kinetic models K can fit the same fluorescence lifetime data [136, 146]. We fit the electron transfer parameters for each of the coarse-grained models described in the previous section to the data in Figure 5.4. Each of the three models is capable of simultaneously reproducing all four experimental fluorescence decay curves. The time-constants that describe electron transfer for the best simultaneous fit to bands B8-B11 for each model are shown in Table 5.3, and the root-mean square error (RMSE) is reproduced in the last row. The electron transfer rates extracted for each model vary significantly from the domain model results, simply because the energy transfer rates describe substantially different dynamics. The quality of the fits (as reported by the RMSE), however, is very similar to that produced by the domain model. Therefore, a model with a good fit to fluorescence lifetime data does not necessarily describe the energy transfer dynamics correctly. The electron transfer rates extracted from such a fit will not accurately describe the kinetics of electron hole separation in reaction centers. More generally, caution should be taken when making mechanistic claims based on fitting kinetic models to fluorescence decay data.

Chapter 6

Outlook: a structure-based energy transfer model for the grana membrane

6.1 How to extend domain model to grana membrane

In the previous Chapter, we showed that the domain model was the most coarse-grained model that accurately describes energy transfer in PSII supercomplexes. Such a model has already been developed for LHCII [104]. We would like to extend the domain models to the grana membrane, which is composed of PSII supercomplexes and LHCIIs. The rates between domains is given by generalized Förster theory (Equations 5.23 and 5.24). We assume that the absorption and fluorescence lineshapes of the excitons in LHCII and PSII and the exciton and domain definitions do not change when the proteins are in the membrane. The latter assumes that it is unlikely for there to be couplings between pigments in different LHCIIs and PSIIs that exceed those within an exciton within an LHCII or PSII. To calculate the rates of energy transfer between domains, the only additional information needed is the site basis electronic couplings (H^{el} in Equation 5.24), which are dependent on the relative orientations and the distances between chlorophylls (Equation 5.27).

The spatial organization of LHCIIs and PSIIs in grana membranes is necessary for calculating the energy transfer rates. The organization has been imaged using atomic force microscopy and electron microscopy [69]. The locations of PSIIs can be identified through the oxygen evolving complex, which protrudes from the plane of the membrane into the lumen. PSIIs have been shown to sometimes form arrays that contain tens of PSII supercomplexes in well-defined lattices. LHCII lacks a protrusion, and the locations of LHCIIs are much harder to determine, unless they are in a PSII array. Recently, two groups have provided visual evidence that a rearrangement of LHCIIs and PSIIs is occurring during qE [18, 64]. Obtaining the specific locations of chlorophylls in both PSIIs and LHCIIs both in dark-acclimated and light-acclimated membranes requires a simulation of the energetic interactions between LHCIIs and PSIIs in the grana membrane that can recapitulate the

previously obtained imaging data.

Recently, Schneider and Geissler developed a Monte Carlo simulation of grana membranes that could reproduce the previous imaging results and showed that the reason for the occasional formation of arrays was due to the fact that the system is poised near phase coexistence [131]. The model uses simple shapes for the PSII C_2S_2 supercomplex (rods) and LHCII trimers (circles) and includes two coupled layers of a grana stack (i.e., the bottom membrane of one grana disc with the top membrane of the grana disc below it). The two input parameters for the model are the free LHCII to PSII supercomplex ratio and the number density of PSII. Within this framework, energetic interactions between PSIIs and LHCIIs within one membrane and between the two layers of the membrane can be varied to give different membrane configurations. Figure 6.1 shows two results of the simulation with different parameters and after equilibration (20,000,000 Monte Carlo steps). CP24 is not included in the simulation, but energetic interactions are included to simulate the reversible binding of LHCII-M to the PSII supercomplex (orange dots in Figure 6.1).

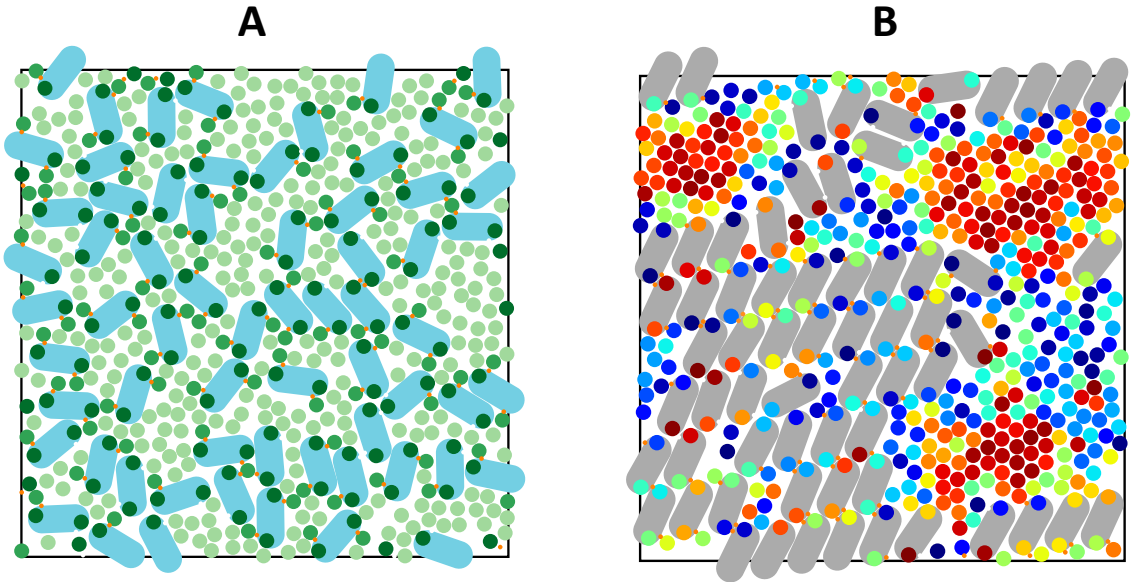

Figure 6.1: Two examples of grana membrane simulations generated using the Monte Carlo model of Schneider and Geissler [131]. PSII supercomplexes (C_2S_2) are shown as rods and LHCII trimers as circles. Both simulations were done assuming the same interactions between two layers of the grana membrane (only the top layer is shown). Both images are taken after 20 million steps in the simulation. A) Membrane configuration when protein density is 70%, the lateral energy of interaction of LHCIIs is 0, and the LHCII:PSII ratio is 6. B) Membrane configuration when protein density is 75%, the lateral energy of interaction of LHCIIs is 1 k_BT, and the LHCII:PSII ratio is 6.

We plan to use the membrane simulation to generate a model for energy transfer in grana membranes. For the dark-acclimated case, the membrane configuration is dependent on the

protein density and the LHCII:PSII ratio, as there are thought to be no intramembrane LHCII to LHCII energetic interactions. The protein density and LHCII:PSII ratio have been measured in recent fluorescence lifetime measurements on dark-acclimated BBY and thylakoid membrane preparations [27, 147]. The membrane energy transfer model will then be a free parameter-less model, assuming that the electron transfer rates determined in Section 5.3.3 also apply to the membrane. Assuming this model gives a good fit to the fluorescence lifetime data, we can then increase the energetic interaction between LHCIIs to generate membrane configurations that might occur during qE.

The calculation of the domain rate matrix for the membrane is computationally feasible because the calculations that are most intensive can be used for any membrane configuration. The generalized Förster energy transfer rates between domains in different LHCIIs and PSIIs can be calculated using the locations of chlorophylls in the membrane simulations, assuming that the free LHCII trimers are randomly oriented. The overlap integrals in equation 5.23 and the transformation matrices U in equation 5.24 can be calculated, tabulated, and used for determining the domain rate matrix of any membrane configuration to decrease considerable computational time. The site-basis electronic coupling H^{el}, however, must be calculated for every unique membrane configuration.

6.2 Questions to be addressed using membrane model

As was mentioned at the beginning of this thesis in Section 1.1, we set out to understand the principles of light harvesting in variable light conditions. In low light, this amounts to understanding how the organization of proteins in the grana membrane gives rise to the high quantum yield of charge separation. In high light, we are trying to figure out how the energy transfer network in the membrane changes to safely dissipate excess excitation. The grana membrane model is a detailed model that can be used to answer these questions.

6.2.1 Light harvesting

The membrane model will show how the physical picture of energy transfer in PSII changes when the PSII supercomplex is surrounded by other PSIIs and LHCIIs. In PSII supercomplexes excited at the periphery, a majority of the timescale for light harvesting was in diffusion to sites that could transfer to the trap. In the membrane, the diffusion time will likely increase, as there are then additional LHCIIs that can transfer into a PSII. In addition, the distance dependence of the timescale for light harvesting, which was linear within a PSII supercomplex, will plateau at some distance.

Knowledge of the diffusion timescale and the distance at which the timescale of light harvesting plateaus will be useful in generating a reduced picture of light harvesting. Such a reduced picture will be useful for interpreting the many types of fluorescence measurements that are used to study photosynthesis [111]. Physical pictures that were put forth many years ago include the ‘lake’ and ‘puddle’ models [17]. In these pictures, whether or not excitation can transfer to another location in the membrane is the most important factor in accurately

describing energy transfer in the membrane. In the 'lake' model, all of chlorophylls can transfer to any other chlorophyll in the membrane. In the 'puddle' model, energy can be transferred anywhere within a puddle of antenna and RCs but not between puddles. Based on the work on the PSII supercomplex in the previous Chapter, the assumption that the location of pigments relative to RCs is unimportant to describing energy transfer in membranes is likely incorrect. Moreover, these models do not distinguish between kinetic connectivity and excitation diffusion length. It is quite possible that a domain has a kinetic path to any other domain in the membrane. However, before the excitation can get there, it might be dissipated by fluorescence, intersystem crossing, or charge separation by a neighboring reaction center. This elaboration suggests that it is unlikely that the 'lake' model is correct. However, a modified 'puddle' model in which the dynamics of energy transfer within one PSII supercomplex and a few neighboring LHCIIs is enough to effectively describe energy transfer in the membrane would be a useful simplification. Recently, van Amerongen and coworkers have put forth a couple of such models based on fitting to fluorescence lifetime data [26, 147]. Our structure-based model of energy transfer in membranes can systematically determine whether simplified models are useful and which ones would be the best to use.

Lastly, as mentioned in the previous Section, PSII supercomplexes have been shown to form ordered arrays in grana membranes. The role of such arrays in light harvesting remains unclear. We can calculate the quantum yield of charge separation in the reaction center in membrane configurations that have different amounts of array formation.

6.2.2 Mechanism of qE in plants and algae

Understanding the mechanism of qE requires us to understand how Figure 1.7 occurs in the actual grana membrane. The membrane energy transfer model will allow us to describe the energetic connectivity of the membrane before qE turns on (left side of Figure 1.7). What remains unknown is what the energetic connectivity of the membrane is as and when qE turns on (right side of Figure 1.7). In addition, we do not know how the different components of qE in either algae or plants work in concert to produce this change in the membrane.

The membrane model can be fit to fluorescence lifetime snapshots from algae and leaves. The values of the parameters that give a good fit to the data will constrain the space of possible membrane configurations when qE is on. Such an analysis could be applied to snapshot data not only from wild-type algae and leaves but also from qE mutants. The properties of the membrane that we can fit are

1. LHCII aggregation size. It has been suggested that there is a reorganization of the membrane during qE [64]. The LHCII aggregation size can be varied based on the energy of intra-membrane interactions between LHCIIs (Figure 6.1*B*). This parameter is equivalent to the change in connectivity in Figure 1.7.

2. the location and number of quenchers, or quencher density.

3. quenching rate.

As seen in Chapter 3, the average fluorescence lifetime of leaves with closed reaction centers goes from 1.6 ns in the dark to 450 ps with qE on. What changes in the membrane are needed to cause that change in lifetime? The quenching rate and quencher density are tightly coupled parameters that will decrease the fluorescence lifetime. We would predict that a higher quenching rate would mean that fewer quenchers are needed to get a particular drop in fluorescence lifetime. But if the membrane is not energetically well connected, it may be that density of quenchers is the primary way that the membrane can tune the amount of excitation that results in qE.

It may be difficult to extend the membrane model to snapshot data from qE mutants, because the organization of the membrane may be quite different than that in wild-type. For example, the *lut2* mutant of plants has been shown to have less qE than wild-type, but the lack of lutein prevents LHCII from properly folding [37]. In this case, the membrane model can be used to model more coarse-grained data such as fluorescence yield. The membrane model can determine how the chlorophyll fluorescence yield depends on the number/rates of quenchers and the amount of LHCII aggregation. Until now, the wealth of fluorescence yield data on qE mutants was difficult to interpret quantitatively. For instance, increasing the expression level of the PsbS protein in plants can increase the extent of qE until it reaches 2x the level found in wild-type [100]. At that point qE plateaus with increasing PsbS. Is this effect more likely to be due to an increase in the number or rates of quenchers? The answer may be more accessible with the membrane model. More generally, we can characterize the effect that the components required for qE (Section 1.5.1) have on the structure of the energy transfer network.

Lastly, the membrane model can be used to test the physical plausibility of the proposed mechanisms of qE quenching in plants and algae. The proposed mechanism for algae is described in Chapter 2 and is based on the hypotheses put forth for the plant mechanism. In plants, there are two main mechanistic hypotheses, which have been derived mainly from in vitro measurements. The membrane model can be used to determine the feasibility of the proposed mechanisms in vivo.

The first mechanism is founded on the fact that LHCII has the intrinsic ability to perform quenching has been primarily supported by the Ruban and van Grondelle groups [126]. In this hypothesis, the roles of PsbS and zeaxanthin are to induce the aggregation of LHCII. Once aggregated, some LHCIIs will increase the proportion of time spent in a "dark" quenching state [71]. In that state, it will dissipate excitations by transferring primarily by energy transfer from a chlorophyll singlet state to a now-accessible lutein S_1 state, followed by relaxation by internal conversion [125]. On the basis of the modeling of fluorescence and pump-probe data of LHCII aggregates, Valkunas et al. suggested that there is one activated quenching site with a timescale of quenching of 5.8 ps per 100 LHCII monomers in an LHCII aggregate [143]. Krüger et al., showed that LHCII remains in the "dark" state 30% of the time under qE conditions [71]. The membrane model can be used to determine whether either of these numbers can reproduce fluorescence measurements on intact leaves.

The second mechanism has been primarily supported by our group and the Walla group. In this model, PsbS, zeaxanthin/lutein, and antenna proteins are required for the formation

of a minimal qE complex [151, 158]. Once this complex forms in the membrane, chlorophyll/carotenoid interactions [21] allow the quenching of excitation by a charge-transfer mechanism [55] in the minor light-harvesting complexes [2, 7] in which zeaxanthin or lutein [6] is directly involved. A coarse-grained kinetic model that fit this data suggested that the timescale for transfer from surrounding chlorophyll to the quenching site occurred on 20 ps timescale [33]. The membrane model can determine whether this timescale is reasonable, given the rates of transfer calculated.

Bibliography

[1] J. Adolphs and T. Renger. How proteins trigger excitation energy transfer in the FMO complex of green sulfur bacteria. *Biophys. J.*, 91(8):2778–2797, 2006.

[2] T. K. Ahn, T. J. Avenson, M. Ballottari, Y.-C. Cheng, K. K.. Niyogi, R. Bassi, and G. R. Fleming. Architecture of a charge-transfer state regulating light harvesting in a plant antenna protein. *Science*, 320(5877):794–797, 2008.

[3] T. K. Ahn, T. J. Avenson, G. Peers, Z. Li, L. Dall'Osto, R. Bassi, K. K. Niyogi, and G. R. Fleming. Investigating energy partitioning during photosynthesis using an expanded quantum yield convention. *Chem. Phys.*, 357(1-3):151–158, 2009.

[4] A. Alboresi, C. Gerotto, G. M. Giacometti, R. Bassi, and T. Morosinotto. *Physcomitrella patens* mutants affected on heat dissipation clarify the evolution of photoprotection mechanisms upon land colonization. *Proc. Natl. Acad. Sci. U. S. A.*, 107(24):11128–33, 2010.

[5] K. Amarnath, J. Zaks, S. D. Park, K. K. Niyogi, and G. R. Fleming. Fluorescence lifetime snapshots reveal two rapidly reversible mechanisms of photoprotection in live cells of *Chlamydomonas reinhardtii*. *Proc. Natl. Acad. Sci. U. S. A.*, 109(22):8405–10, 2012.

[6] T. J. Avenson, T. K. Ahn, K. K. Niyogi, M. Ballottari, R. Bassi, and G. R. Fleming. Lutein can act as a switchable charge transfer quencher in the CP26 light-harvesting complex. *J. Biol. Chem.*, 284(5):2830–2835, 2009.

[7] T. J. Avenson, T. K. Ahn, D. Zigmantas, K. K.. Niyogi, Z. Li, M. Ballottari, R. Bassi, and G. R. Fleming. Zeaxanthin radical cation formation in minor light-harvesting complexes of higher plant antenna. *J. Biol. Chem.*, 283(6):3550–8, 2008.

[8] N. R. Baker. Chlorophyll fluorescence: A probe of photosynthesis in vivo. *Annu. Rev. Plant Biol.*, 59:89–113, 2008.

[9] M. Ballottari, L. Dall'Osto, T. Morosinotto, and R. Bassi. Contrasting behavior of higher plant photosystem I and II antenna systems during acclimation. *J. Biol. Chem.*, 282(12):8947–8958, 2007.

[10] J. Barber. Molecular basis of the vulnerability of photosystem II to damage by light. *Aust. J. Plant Physiol.*, 22:201–208, 1994.

[11] L. M. C. Barter, M. Bianchietti, C. Jeans, M. J. Schilstra, B. Hankamer, B. A. Diner, J. Barber, J. R. Durrant, and D. R. Klug. Relationship between excitation energy transfer, trapping, and antenna size in photosystem II. *Biochemistry*, 40(13):4026–34, 2001.

[12] W. Becker. *The bh TCSPC Handbook*. Self-published, Berlin, 4th edition, 2010.

[13] G. S. Beddard and G. Porter. Concentration quenching in chlorophyll. *Nature*, 260(5549):366–367, 1976.

[14] N. E. Belyaeva, F. J. Schmitt, V. Z. Paschenko, G. Yu Riznichenko, A. B. Rubin, and G Renger. PSII model based analysis of transient fluorescence yield measured on whole leaves of *Arabidopsis thaliana* after excitation with light flashes of different energies. *BioSystems*, 103(2):188–195, 2011.

[15] N. E. Belyaeva, F. J. Schmitt, R. Steffen, V. Z. Paschenko, G. Yu. Riznichenko, Yu. K. Chemeris, G. Renger, and A. B. Rubin. PSII model-based simulations of single turnover flash-induced transients of fluorescence yield monitored within the time domain of 100 ns-10 s on dark-adapted *Chlorella pyrenoidosa* cells. *Photosynth. Res.*, 98(1-3):105–119, 2008.

[16] R. Berera, R. van Grondelle, and J. T. M. Kennis. Ultrafast transient absorption spectroscopy: principles and application to photosynthetic systems. *Photosynth. Res.*, 101(2-3):105–118, 2009.

[17] K. Bernhardt and H. Trissl. Theories for kinetics and yields of fluorescence and photochemistry: how, if at all, can different models of antenna organization be distinguished experimentally? *Biochim. Biophys. Acta, Bioenerg.*, 1409(3):125–42, 1999.

[18] N. Betterle, M. Ballottari, S. Zorzan, S. de Bianchi, S. Cazzaniga, L. Dall'Osto, T. Morosinotto, and R. Bassi. Light-induced dissociation of an antenna hetero-oligomer is needed for non-photochemical quenching induction. *J. Biol. Chem.*, 284(22):15255–15266, 2009.

[19] The equation for $V_{n,m}(t)$ shown in this paper has a different form from that given by Yang and Fleming because we have made use of the additional simplification provided by real valued eigenvectors.

[20] R. E. Blankenship. *Molecular Mechanisms of Photosynthesis*. Blackwell Science, 2002.

[21] S. Bode, C. C. Quentmeier, P.-N. Liao, N. Hafi, T. Barros, L. Wilk, F. Bittner, and P. J. Walla. On the regulation of photosynthesis by excitonic interactions between carotenoids and chlorophylls. *Proc. Natl. Acad. Sci. U. S. A.*, 106(30):12311–12316, 2009.

[22] G. Bonente, M. Ballottari, T. B. Truong, T. Morosinotto, T. K. Ahn, G. R. Fleming, K. K. Niyogi, and R. Bassi. Analysis of LhcSR3, a protein essential for feedback de-excitation in the green alga *Chlamydomonas reinhardtii*. *PLoS Biol.*, 9(1):e1000577, 2011.

[23] G. Bonente, S. Pippa, S. Castellano, R. Bassi, and M. Ballottari. Acclimation of *Chlamydomonas reinhardtii* to different growth irradiances. *J. Biol. Chem.*, 287(8):5833–47, 2012.

[24] P. G. Bowers and G. Porter. Quantum yields of triplet formation in solutions of chlorophyll. *Proc. R. Soc. A.*, 296(1447):435–441, 1967.

[25] J. M. Briantais, C. Vernotte, M. Picaud, and G. H. Krause. A quantitative study of the slow decline of chlorophyll a fluorescence in isolated chloroplasts. *Biochim. Biophys. Acta*, 548(1):128–38, 1979.

[26] K. Broess, G. Trinkunas, C. D. van der Weij-de Wit, J. P. Dekker, A. van Hoek, and H. van Amerongen. Excitation energy transfer and charge separation in photosystem II membranes revisited. *Biophys. J.*, 91(10):3776–3786, 2006.

[27] K. Broess, G. Trinkunas, A. van Hoek, R. Croce, and H. van Amerongen. Determination of the excitation migration time in photosystem II - consequences for the membrane organization and charge separation parameters. *Biochim. Biophys. Acta, Bioenerg.*, 1777(5):404–409, 2008.

[28] M. D. Brooks and K. K. Niyogi. Use of a pulse-amplitude modulated chlorophyll fluorometer to study the efficiency of photosynthesis in *Arabidopsis* plants. *Methods Mol. Biol.*, 775:299–310, 2011.

[29] M. D. Brooks, E. J. Sylak-Glassman, G. R. Fleming, and K. K. Niyogi. A thioredoxin-like/beta-propeller protein maintains the efficiency of photosynthetic light harvesting in *Arabidopsis*. *Manuscript in review*, 2013.

[30] C. Büchel and W Kühlbrandt. Structural differences in the inner part of photosystem II between higher plants and cyanobacteria. *Photosynth. Res.*, 85:3–13, 2005.

[31] S. Caffarri, K. Broess, R. Croce, and H. van Amerongen. Excitation energy transfer and trapping in higher plant photosystem II complexes with different antenna sizes. *Biophys. J.*, 100(9):2094–2103, 2011.

[32] S. Caffarri, R. Kouřil, S. Kereiche, E. J. Boekema, and R. Croce. Functional architecture of higher plant photosystem II supercomplexes. *EMBO J.*, 28(19):3052–3063, 2009.

[33] Y.-C. Cheng, T. K. Ahn, T. J. Avenson, D. Zigmantas, K. K.. Niyogi, M. Ballottari, R. Bassi, and G. R. Fleming. Kinetic modeling of charge-transfer quenching in the CP29 minor complex. *J. Phys. Chem. B*, 112(42):13418–13423, 2008.

[34] R. Croce, M. G. Müller, S. Caffarri, R. Bassi, and A. R. Holzwarth. Energy transfer pathways in the minor antenna complex CP29 of photosystem II: a femtosecond study of carotenoid to chlorophyll transfer on mutant and wt complexes. *Biophys. J.*, 84(4):2517–2532, 2003.

[35] R. Croce and H. van Amerongen. Light-harvesting and structural organization of photosystem II: from individual complexes to thylakoid membrane. *J. Photochem. Photobiol. B*, 104(1-2):142–153, 2011.

[36] J. A. Cruz, C. A. Sacksteder, A. Kanazawa, and D. M. Kramer. Contribution of electric field ($\Delta\psi$) to steady-state transthylakoid proton motive force (pmf) in vitro and in vivo. Control of pmf parsing into $\Delta\psi$ and ΔpH by ionic strength. *Biochemistry*, 40(5):1226–1237, 2001.

[37] L. Dall'Osto, C. Lico, J. Alric, G. Giuliano, M. Havaux, and R. Bassi. Lutein is needed for efficient chlorophyll triplet quenching in the major LHCII antenna complex of higher plants and effective photoprotection in vivo under strong light. *BMC Plant Biol.*, 6(1):32, 2006.

[38] S. de Bianchi, M. Ballottari, L. Dall'Osto, and R. Bassi. Regulation of plant light harvesting by thermal dissipation of excess energy. *Biochem. Soc. Trans.*, 38:651–660, 2010.

[39] S. de Bianchi, N. Betterle, R. Kouřil, S. Cazzaniga, E. Boekema, R. Bassi, and L. Dall'Osto. *Arabidopsis* mutants deleted in the light-harvesting protein Lhcb4 have a disrupted photosystem II macrostructure and are defective in photoprotection. *Plant Cell*, 23(7):2659–79, 2011.

[40] S. de Bianchi, L. Dall'Osto, G. Tognon, T. Morosinotto, and R. Bassi. Minor antenna proteins CP24 and CP26 affect the interactions between photosystem II subunits and the electron transport rate in grana membranes of *Arabidopsis*. *Plant Cell*, 20(4):1012–28, 2008.

[41] J. P. Dekker and E. J. Boekema. Supramolecular organization of thylakoid membrane proteins in green plants. *Biochim. Biophys. Acta, Bioenerg.*, 1706(1-2):12–39, 2005.

[42] R. Delosme, J. Olive, and F. A. Wollman. Changes in light energy distribution upon state transitions: an in vivo photoacoustic study of the wild type and photosynthesis mutants from *Chlamydomonas reinhardtii*. *Biochim. Biophys. Acta, Bioenerg.*, 1273(2):150–158, 1996.

[43] B. Demmig-Adams and K. Winter. Characterisation of three components of non-photochemical fluorescence quenching and their response to photoinhibition. *Aust. J. Plant Physiol.*, 15:163–177, 1988.

[44] A. Dreuw, G. R. Fleming, and M. Head-Gordon. Chlorophyll fluorescence quenching by xanthophylls. *Phys. Chem. Chem. Phys.*, 5(15):3247, 2003.

[45] C. D. P. Duffy, M. P. Johnson, M. Macernis, L. Valkunas, W. Barford, and A. V. Ruban. A theoretical investigation of the photophysical consequences of major plant light-harvesting complex aggregation within the photosynthetic membrane. *J. Phys. Chem. B*, 114(46):15244–15253, 2010.

[46] S. Eberhard, G. Finazzi, and F.-A. Wollman. The dynamics of photosynthesis. *Annu. Rev. Genet.*, 42:463–515, 2008.

[47] G. R. Fleming, G. S. Schlau-Cohen, K. Amarnath, and J. Zaks. Design principles of photosynthetic light-harvesting. *Faraday Discuss.*, 155:27–41, 2012.

[48] F. Fungo, L. Otero, E. Durantini, W. J. Thompson, J. J. Silber, T. A. Moore, A. L. Moore, D. Gust, and L. Sereno. Correlation of fluorescence quenching in carotenoporphyrin dyads with the energy of intramolecular charge transfer states. Effect of the number of conjugated double bonds of the carotenoid moiety. *Phys. Chem. Chem. Phys.*, 5(3):469–475, 2003.

[49] A. M. Gilmore, T. L. Hazlett, and Govindjee. Xanthophyll cycle-dependent quenching of photosystem II chlorophyll a fluorescence: Formation of a quenching complex with a short fluorescence lifetime. *Proc. Natl. Acad. Sci. U. S. A.*, 92(6):2273–2277, 1995.

[50] A. M. Gilmore, V. P. Shinkarev, T. L. Hazlett, and Govindjee. Quantitative analysis of the effects of intrathylakoid pH and xanthophyll cycle pigments on chlorophyll a fluorescence lifetime distributions and intensity in thylakoids. *Biochemistry*, 37(39):13582–13593, 1998.

[51] N. S. Ginsberg, Y.-C. Cheng, and G. R. Fleming. Two-dimensional electronic spectroscopy of molecular aggregates. *Acc. Chem. Res.*, 42(9):1352–63, 2009.

[52] M. L. Groot, N. P. Pawlowicz, L. J. G. W. van Wilderen, J. Breton, I. H. M. van Stokkum, and R. van Grondelle. Initial electron donor and acceptor in isolated photosystem II reaction centers identified with femtosecond mid-ir spectroscopy. *Proc. Natl. Acad. Sci. U. S. A.*, 102(37):13087–92, 2005.

[53] M. Havaux, L. Dall'Osto, and R. Bassi. Zeaxanthin has enhanced antioxidant capacity with respect to all other xanthophylls in Arabidopsis leaves and functions independent of binding to PSII antennae. *Plant Physiol.*, 145(4):1506–20, 2007.

[54] L. Hendrickson, R. T. Furbank, and W. S. Chow. A simple alternative approach to assessing the fate of absorbed light energy using chlorophyll fluorescence. *Photosynth. Res.*, 82(1):73–81, 2004.

[55] N. E. Holt, D. Zigmantas, L. Valkunas, X.-P. Li, K. K. Niyogi, and G. R. Fleming. Carotenoid cation formation and the regulation of photosynthetic light harvesting. *Science*, 307(5708):433–6, 2005.

[56] O. Holub, M. J. Seufferheld, C. Gohlke, Govindjee, G. J. Heiss, and R. M. Clegg. Fluorescence lifetime imaging microscopy of *Chlamydomonas reinhardtii*: non-photochemical quenching mutants and the effect of photosynthetic inhibitors on the slow chlorophyll fluorescence transient. *J. Microsc.-Oxford*, 226(2):90–120, 2007.

[57] A. R. Holzwarth. Data analysis of time-resolved measurements. In J. Amesz and A. J. Hoff, editors, *Biophysical Techniques in Photosynthesis*, volume 26 of *Advances in Photosynthesis and Respiration*. Kluwer Academic Publishers, Dordrecht, 1996.

[58] A. R. Holzwarth, Y. Miloslavina, M. Nilkens, and P. Jahns. Identification of two quenching sites active in the regulation of photosynthetic light-harvesting studied by time-resolved fluorescence. *Chem. Phys. Lett.*, 483(4-6):262–267, 2009.

[59] W. Humphrey, A. Dalke, and K. Schulten. VMD – Visual Molecular Dynamics. *J. Mol. Graphics*, 14:33–38, 1996.

[60] J. A. Ihalainen, I. H. M. van Stokkum, K. Gibasiewicz, M. Germano, R. van Grondelle, and J. P. Dekker. Kinetics of excitation trapping in intact photosystem i of chlamydomonas reinhardtii and *Arabidopsis thaliana*. *Biochim. Biophys. Acta, Bioenerg.*, 1706(3):267–275, 2005.

[61] A. Ishizaki, T. R. Calhoun, G. S. Schlau-Cohen, and G. R. Fleming. Quantum coherence and its interplay with protein environments in photosynthetic electronic energy transfer. *Phys. Chem. Chem. Phys.*, 12(27):7319, 2010.

[62] M. Iwai, M. Yokono, N. Inada, and J. Minagawa. Live-cell imaging of photosystem II antenna dissociation during state transitions. *Proc. Natl. Acad. Sci. U. S. A.*, 107(5):2337–2342, 2010.

[63] P. Jahns and A. R. Holzwarth. The role of the xanthophyll cycle and of lutein in photoprotection of photosystem II. *Biochim. Biophys. Acta, Bioenerg.*, 1817(1):182–193, 2012.

[64] M. P. Johnson, T. K. Goral, C. D. P. Duffy, A. P. R. Brain, C. W. Mullineaux, and A. V. Ruban. Photoprotective energy dissipation involves the reorganization of photosystem II light-harvesting complexes in the grana membranes of spinach chloroplasts. *Plant Cell*, 23(4):1468–1479, 2011.

[65] M. P. Johnson and A. V. Ruban. Photoprotective energy dissipation in higher plants involves alteration of the excited state energy of the emitting chlorophyll(s) in the light harvesting antenna II (LHCII). *J. Biol. Chem.*, 284(35):23592–23601, 2009.

[66] M. P. Johnson and A. V. Ruban. Restoration of rapidly reversible photoprotective energy dissipation in the absence of PsbS protein by enhanced ΔpH. *J. Biol. Chem.*, 286(22):19973–19981, 2011.

[67] M. P. Johnson, A. Zia, and A. V. Ruban. Elevated ΔpH restores rapidly reversible photoprotective energy dissipation in Arabidopsis chloroplasts deficient in lutein and xanthophyll cycle activity. *Planta*, 235(1):193–204, 2012.

[68] A. Z. Kiss, A. V. Ruban, and P. Horton. The PsbS protein controls the organization of the photosystem II antenna in higher plant thylakoid membranes. *J. Biol. Chem.*, 283(7):3972–8, 2008.

[69] R. Kouřil, J. P. Dekker, and E. J. Boekema. Supramolecular organization of photosystem II in green plants. *Biochim. Biophys. Acta, Bioenerg.*, 1817(1):2–12, 2012.

[70] G. H. Krause and E. Weis. Chlorophyll fluorescence and photosynthesis: the basics. *Annu. Rev. Plant Biol.*, 42(1):313–349, 1991.

[71] T. P. J. Krüger, C. Ilioaia, M. P. Johnson, A. V. Ruban, E. Papagiannakis, P. Horton, and R. van Grondelle. Controlled disorder in plant light-harvesting complex II explains its photoprotective role. *Biophys. J.*, 102(11):2669–76, 2012.

[72] C. Külheim, J. Ågren, and S. Jansson. Rapid regulation of light harvesting and plant fitness in the field. *Science*, 297(5578):91–93, 2002.

[73] J. R. Lakowicz. *Principles of Fluorescence Spectroscopy*. Springer, 3rd edition, 2006.

[74] H. K. Ledford and K. K. Niyogi. Singlet oxygen and photo-oxidative stress management in plants and algae. *Plant Cell Environ.*, 28(8):1037–1045, 2005.

[75] S. Lemeille and J.-D. Rochaix. State transitions at the crossroad of thylakoid signalling pathways. *Photosynth. Res.*, 106(1-2):33–46, 2010.

[76] X. P. Li, O. Björkman, C. Shih, A. R. Grossman, M. Rosenquist, S. Jansson, and K. K. Niyogi. A pigment-binding protein essential for regulation of photosynthetic light harvesting. *Nature*, 403(6768):391–395, 2000.

[77] X. P. Li, A. M. Gilmore, S. Caffarri, R. Bassi, T. Golan, D. Kramer, and K. K.. Niyogi. Regulation of photosynthetic light harvesting involves intrathylakoid lumen pH sensing by the PsbS protein. *J. Biol. Chem.*, 279(22):22866–22874, 2004.

[78] X. P. Li, P Müller-Moulé, A. M. Gilmore, and K. K. Niyogi. PsbS-dependent enhancement of feedback de-excitation protects photosystem II from photoinhibition. *Proc. Natl. Acad. Sci. U. S. A.*, 99(23):15222–15227, 2002.

[79] Z. F. Liu, H. C. Yan, K. B. Wang, T. Y. Kuang, J. P. Zhang, L. L. Gui, X. M. An, and W. R. Chang. Crystal structure of spinach major light-harvesting complex at 2.72 Å resolution. *Nature*, 428(6980):287–292, 2004.

[80] M. A. Lomize, A. L. Lomize, I. D. Pogozheva, and H. I. Mosberg. OPM: orientations of proteins in membranes database. *Bioinformatics*, 22(5):623–5, 2006.

[81] Y.-Z. Ma, N. E. Holt, X.-P. Li, K. K.. Niyogi, and G. R. Fleming. Evidence for direct carotenoid involvement in the regulation of photosynthetic light harvesting. *Proc. Natl. Acad. Sci, U. S. A.*, 100(8):4377–82, 2003.

[82] A. Marin, F. Passarini, R. Croce, and R. van Grondelle. Energy transfer pathways in the CP24 and CP26 antenna complexes of higher plant photosystem II: a comparative study. *Biophys. J.*, 99(12):4056–4065, 2010.

[83] S. Matsubara and W. S. Chow. Populations of photo inactivated photosystem II reaction centers characterized by chlorophyll a fluorescence lifetime *in vivo*. *Proc. Natl. Acad. Sci. U. S. A.*, 101(52):18234–18239, 2004.

[84] A. Melis. Photosystem-II damage and repair cycle in chloroplasts: what modulates the rate of photodamage *in vivo*? *Trends Plant Sci.*, 4(4):130–135, 1999.

[85] Y. Miloslavina, I. Grouneva, P. H. Lambrev, B. Lepetit, R. Goss, C. Wilhelm, and A. R. Holzwarth. Ultrafast fluorescence study on the location and mechanism of non-photochemical quenching in diatoms. *Biochim. Biophys. Acta, Bioenerg.*, 1787(10):1189–1197, 2009.

[86] Y. Miloslavina, M. Szczepaniak, M. G. Müller, J. Sander, M. Nowaczyk, M. Rögner, and A. R. Holzwarth. Charge separation kinetics in intact photosystem II core particles is trap-limited. A picosecond fluorescence study. *Biochemistry*, 45(7):2436–42, 2006.

[87] J. Minagawa. State transitions–the molecular remodeling of photosynthetic supercomplexes that controls energy flow in the chloroplast. *Biochim. Biophys. Acta, Bioenerg.*, 1807(8):897–905, 2011.

[88] P. Mohanty, B. Z. Braun, and Govindjee. Light-induced slow changes in chlorophyll a fluorescence in isolated chloroplasts: effects of magnesium and phenazine methosulfate. *Biochim. Biophys. Acta*, 292(2):459–76, 1973.

[89] F. Müh, M. E.-A. Madjet, and T. Renger. Structure-based identification of energy sinks in plant light-harvesting complex II. *J. Phys. Chem. B*, 114(42):13517–13535, 2010.

[90] F. Müh, M. E.-A. Madjet, and T. Renger. Structure-based simulation of linear optical spectra of the CP43 core antenna of photosystem II. *Photosynth. Res.*, 111(1-2):87–101, 2012.

[91] F. Müh and T. Renger. Refined structure-based simulation of plant light-harvesting complex II: linear optical spectra of trimers and aggregates. *Biochim. Biophys. Acta, Bioenerg.*, 1817(8):1446–1460, 2012.

[92] M. G. Müller, P. Lambrev, M. Reus, E. Wientjes, R. Croce, and A. R. Holzwarth. Singlet energy dissipation in the photosystem II light-harvesting complex does not involve energy transfer to carotenoids. *ChemPhysChem*, 11(6):1289–1296, 2010.

[93] P. Müller, X. P. Li, and K. K. Niyogi. Non-photochemical quenching. A response to excess light energy. *Plant Physiol.*, 125(4):1558, 2001.

[94] N. Murata and K. Sugahara. Control of excitation transfer in photosynthesis. 3. Light-induced decrease of chlorophyll a fluorescence related to photophosphorylation system in spinach chloroplasts. *Biochim. Biophys. Acta*, 189(2):182–92, 1969.

[95] R. Nevo, D. Charuvi, O. Tsabari, and Z. Reich. Composition, architecture and dynamics of the photosynthetic apparatus in higher plants. *Plant J.*, 70(1):157–176, 2012.

[96] M. Nilkens, E. Kress, P. Lambrev, Y. Miloslavina, M. Müller, A. R. Holzwarth, and P. Jahns. Identification of a slowly inducible zeaxanthin-dependent component of non-photochemical quenching of chlorophyll fluorescence generated under steady-state conditions in *Arabidopsis*. *Biochim. Biophys. Acta, Bioenerg.*, 1797(4):466–475, 2010.

[97] K. K. Niyogi, O. Björkman, and A. R. Grossman. Chlamydomonas xanthophyll cycle mutants identified by video imaging of chlorophyll fluorescence quenching. *Plant Cell*, 9(8):1369–1380, 1997.

[98] K. K. Niyogi, O. Björkman, and A. R. Grossman. The roles of specific xanthophylls in photoprotection. *Proc. Natl. Acad. Sci. U. S. A.*, 94(25):14162–14167, 1997.

[99] K. K. Niyogi, A. R. Grossman, and O. Björkman. *Arabidopsis* mutants define a central role for the xanthophyll cycle in the regulation of photosynthetic energy conversion. *Plant Cell*, 10(7):1121–34, 1998.

[100] K. K. Niyogi, X. P. Li, V. Rosenberg, and H. S. Jung. Is PsbS the site of non-photochemical quenching in photosynthesis? *J. Exp. Bot.*, 56(411):375–382, 2005.

[101] K. K. Niyogi, C. Shih, W. S. Chow, B. J. Pogson, D. DellaPenna, and O. Björkman. Photoprotection in a zeaxanthin- and lutein-deficient double mutant of Arabidopsis. *Photosynth. Res.*, 67(1-2):139–145, 2001.

[102] K. K. Niyogi and T. B. Truong. Evolution of flexible non-photochemical quenching mechanisms that regulate light harvesting in oxygenic photosynthesis. *Curr. Opin. Plant Biol.*, 2013. http://dx.doi.org/10.1016/j.pbi.2013.03.011.

[103] U. Noomnarm and R. M. Clegg. Fluorescence lifetimes: fundamentals and interpretations. *Photosynth. Res.*, 101(2-3):181–94, 2009.

[104] V. Novoderezhkin, A. Marin, and R. van Grondelle. Intra- and inter-monomeric transfers in the light harvesting LHCII complex: the Redfield–Förster picture. *Phys. Chem. Chem. Phys.*, 13(38):17093, 2011.

[105] V. I. Novoderezhkin, M. A. Palacios, H. van Amerongen, and R. van Grondelle. Excitation dynamics in the LHCII complex of higher plants: modeling based on the 2.72 Å crystal structure. *J. Phys. Chem. B*, 109(20):10493–10504, 2005.

[106] V. I. Novoderezhkin, E. Romero, J. P. Dekker, and R. van Grondelle. Multiple charge-separation pathways in photosystem II: Modeling of transient absorption kinetics. *ChemPhysChem*, 12(3):681–688, 2011.

[107] V. I. Novoderezhkin and R. van Grondelle. Physical origins and models of energy transfer in photosynthetic light-harvesting. *Phys. Chem. Chem. Phys.*, 12(27):7352–7365, 2010.

[108] T. G. Owens, S. P. Webb, L. Mets, R. S. Alberte, and G. R. Fleming. Antenna structure and excitation dynamics in photosystem I. II. Studies with mutants of *Chlamydomonas reinhardtii* lacking photosystem II. *Biophys. J.*, 56(1):95–106, 1989.

[109] M. A. Palacios, F. L. de Weerd, J. A. Ihalainen, R. van Grondelle, and H. van Amerongen. Superradiance and exciton (de)localization in light-harvesting complex II from green plants. *J. Phys. Chem. B*, 106(22):5782–5787, 2002.

[110] X. Pan, M. Li, T. Wan, L. Wang, C. Jia, Z. Hou, X. Zhao, J. Zhang, and W. Chang. Structural insights into energy regulation of light-harvesting complex CP29 from spinach. *Nat. Struct. Mol. Biol.*, 18(3):309–U94, 2011.

[111] G. C. Papageorgiu and Govindjee, editors. *Chlorophyll a Fluorescence: A Signature of Photosynthesis*, volume 19 of *Advances in Photosynthesis and Respiration*. Springer, Dordrecht, The Netherlands, 2004.

[112] S. Park, M. K. Sener, D. Y. Lu, and K. Schulten. Reaction paths based on mean first-passage times. *J. Chem. Phys.*, 119(3):1313–1319, 2003.

[113] A. A. Pascal, Z. F. Liu, K. Broess, B. van Oort, H. van Amerongen, C. Wang, P. Horton, B. Robert, W. Chang, and A. Ruban. Molecular basis of photoprotection and control of photosynthetic light-harvesting. *Nature*, 436(7047):134–137, 2005.

[114] F. Passarini, E. Wientjes, R. Hienerwadel, and R. Croce. Molecular basis of light harvesting and photoprotection in CP24: unique features of the most recent antenna complex. *J. Biol. Chem.*, 284(43):29536–46, 2009.

[115] G. Peers, T. B. Truong, E. Ostendorf, A. Busch, D. Elrad, A. R. Grossman, M. Hippler, and K. K. Niyogi. An ancient light-harvesting protein is critical for the regulation of algal photosynthesis. *Nature*, 462(7272):518–521, 2009.

[116] B. J. Pogson, K. K. Niyogi, O. Björkman, and D. DellaPenna. Altered xanthophyll compositions adversely affect chlorophyll accumulation and nonphotochemical quenching in *Arabidopsis* mutants. *Proc. Natl. Acad. Sci. U. S. A.*, 95(22):13324–9, 1998.

[117] G. Raszewski, B. A. Diner, E. Schlodder, and T. Renger. Spectroscopic properties of reaction center pigments in photosystem II core complexes: revision of the multimer model. *Biophys. J.*, 95(1):105–19, 2008.

[118] G. Raszewski and T. Renger. Light harvesting in photosystem II core complexes is limited by the transfer to the trap: can the core complex turn into a photoprotective mode? *J. Am. Chem. Soc.*, 130(13):4431–4446, 2008.

[119] G. Raszewski, W. Saenger, and T. Renger. Theory of optical spectra of photosystem II reaction centers: location of the triplet state and the identity of the primary electron donor. *Biophys. J.*, 88(2):986–98, 2005.

[120] J. A. Raven. The cost of photoinhibition. *Physiol. Plant*, 142(1):87–104, 2011.

[121] T. Renger, M. E. Madjet, A. Knorr, and F. Müh. How the molecular structure determines the flow of excitation energy in plant light-harvesting complex II. *J. Plant Physiol.*, 168(12):1497–1509, 2011.

[122] T. Renger and E. Schlodder. Primary photophysical processes in photosystem II: Bridging the gap between crystal structure and optical spectra. *ChemPhysChem*, 11(6):1141–1153, 2010.

[123] K. H. Rhee, E. P. Morris, J. Barber, and W. Kühlbrandt. Three-dimensional structure of the plant photosystem II reaction centre at 8 Å resolution. *Nature*, 396(6708):283–286, 1998.

[124] B. Robert. Resonance Raman spectroscopy. *Photosynth. Res.*, 101(2-3):147–155, 2009.

[125] A. V. Ruban, R. Berera, C. Ilioaia, I. H. M. van Stokkum, J. T. M. Kennis, A. A. Pascal, H. van Amerongen, B. Robert, P. Horton, and R. van Grondelle. Identification of a mechanism of photoprotective energy dissipation in higher plants. *Nature*, 450(7169):575–578, 2007.

[126] A. V. Ruban, M. P. Johnson, and Christopher D. P Duffy. The photoprotective molecular switch in the photosystem II antenna. *Biochim. Biophys. Acta, Bioenerg.*, 1817(1):167–181, 2012.

[127] G. Schansker, S. Z. Toth, L. Kovacs, A. R. Holzwarth, and G. Garab. Evidence for a fluorescence yield change driven by a light-induced conformational change within photosystem II during the fast chlorophyll a fluorescence rise. *Biochim. Biophys. Acta, Bioenerg.*, 1807(9):1032–1043, 2011.

[128] G. H. Schatz, H. Brock, and A. R. Holzwarth. Kinetic and energetic model for the primary processes in photosystem II. *Biophys. J.*, 54(3):397–405, 1988.

[129] G. S. Schlau-Cohen, T. R. Calhoun, N. S Ginsberg, E. L. Read, M. Ballottari, R. Bassi, R. van Grondelle, and G. R. Fleming. Pathways of energy flow in LHCII from two-dimensional electronic spectroscopy. *J. Phys. Chem. B*, 113(46):15352–15363, 2009.

[130] G. Schmuck and I. Moya. Time-resolved chlorophyll fluorescence spectra of intact leaves. *Remote Sens. Environ.*, 47:72–76, 1994.

[131] A. R. Schneider and P. L. Geissler. Coexistence between fluid and crystalline phases of proteins in photosynthetic membranes. *Preprint*, arXiv/1302.6323v1 [cond-mat.soft], 2013.

[132] U. Schreiber. Pulse-amplitude-modulation (PAM) fluorometry and saturation pulse method: an overview. *Chlorophyll a fluorescence: a signature of photosynthesis*, pages 279–319, 2004.

[133] U. Schreiber, U. Schliwa, and W. Bilger. Continuous recording of photochemical and non-photochemical chlorophyll fluorescence quenching with a new type of modulation fluorometer. *Photosynth. Res.*, 10(1):51–62, 1986.

[134] A. Stirbet and Govindjee. On the relation between the Kautsky effect (chlorophyll a fluorescence induction) and photosystem II: basics and applications of the OJIP fluorescence transient. *J. Photochem. Photobiol. B, Biol.*, 104(1-2):236–57, 2011.

[135] K. Takizawa, J. A. Cruz, A. Kanazawa, and D. M. Kramer. The thylakoid proton motive force *in vivo*. Quantitative, non-invasive probes, energetics, and regulatory consequences of light-induced *pmf*. *Biochim. Biophys. Acta, Bioenerg.*, 1767(10):1233–1244, 2007.

[136] L. Tian, S. Farooq, and H. van Amerongen. Probing the picosecond kinetics of the photosystem II core complex *in vivo*. *Phys. Chem. Chem. Phys.*, 15(9):3146, 2013.

[137] A. Tokmakoff. 5.74 Introductory Quantum Mechanics II, spring 2011. (Massachusetts Institute of Technology: MIT OpenCourseWare), `http://ocw.mit.edu` (Accessed April 16, 2013. License: Creative Commons BY-NC-SA.

[138] R. Tokutsu, N. Kato, K. H. Bui, T. Ishikawa, and J. Minagawa. Revisiting the supramolecular organization of photosystem II in *Chlamydomonas reinhardtii*. *J. Biol. Chem.*, 287(37):31574–81, 2012.

[139] C. Tommos and G.T. Babcock. Oxygen production in nature: a light-driven metalloradical enzyme process. *Acc. Chem. Res.*, 31(1):18–25, 1998.

[140] N. J. Turro, V. Ramamurthy, and J. C. Scaiano. *Modern Molecular Photochemistry of Organic Molecules*. University Science Books, 2010.

[141] Y. Umena, K. Kawakami, J.-R. Shen, and N. Kamiya. Crystal structure of oxygen-evolving photosystem II at a resolution of 1.9 Å. *Nature*, 473(7345):55–60, 2011.

[142] L. Valkunas, J. Chmeliov, T. P. J. Krüger, C. Ilioaia, and R. van Grondelle. How photosynthetic proteins switch. *J. Phys. Chem. Lett.*, 3:2779–2784, 2012.

[143] L. Valkunas, J. Chmeliov, G. Trinkunas, C. D. P. Duffy, R. van Grondelle, and A. V. Ruban. Excitation migration, quenching, and regulation of photosynthetic light harvesting in photosystem II. *J. Phys. Chem. B*, 115(29):9252–9260, 2011.

[144] L. Valkunas, G. Trinkunas, J. Chmeliov, and A. V. Ruban. Modeling of exciton quenching in photosystem II. *Phys. Chem. Chem. Phys.*, 11(35):7576–7584, 2009.

[145] H. van Amerongen, L. Valkunas, and R. van Grondelle. *Photosynthetic Excitons*. World Scientific Publishing Company Incorporated, 2000.

[146] C. D. van der Weij-de Wit, J. P. Dekker, R. van Grondelle, and I. H. M. van Stokkum. Charge separation is virtually irreversible in photosystem II core complexes with oxidized primary quinone acceptor. *J. Phys. Chem. A*, 115(16):3947–3956, 2011.

[147] B. van Oort, M. Alberts, S. de Bianchi, L. Dall'Osto, R. Bassi, G. Trinkunas, R. Croce, and H. van Amerongen. Effect of antenna-depletion in photosystern II on excitation energy transfer in *Arabidopsis thaliana*. *Biophys. J.*, 98(5):922–931, 2010.

[148] B. van Oort, A. Maréchal, A. V. Ruban, B. Robert, A. A. Pascal, N. C. A. de Ruijter, R. van Grondelle, and H. van Amerongen. Different crystal morphologies lead to slightly different conformations of light-harvesting complex II as monitored by variations of the intrinsic fluorescence lifetime. *Phys. Chem. Chem. Phys.*, 13(27):12614, 2011.

[149] I. H. M. van Stokkum, D. S. Larsen, and R. van Grondelle. Global and target analysis of time-resolved spectra. *Biochim. Biophys. Acta, Bioenerg.*, 1657(2-3):82–104, 2004.

[150] I. H. M. van Stokkum, B. van Oort, F. van Mourik, B. Gobets, and H. van Amerongen. (sub)-picosecond spectral evolution of fluorescence studied with a synchroscan streak-camera system and target analysis. In T. Aartsma and J. Matysik, editors, *Biophysical Techniques in Photosynthesis, Vol. 2*, volume 26 of *Advances in Photosynthesis and Respiration*, pages 223–240. Kluwer Academic Publishers, 2008.

[151] L. Wilk, M. Grunwald, P.-N. Liao, P. J. Walla, and W. Kuhlbrandt. Direct interaction of the major light-harvesting complex II and PsbS in nonphotochemical quenching. *Proc. Natl. Acad. Sci. U. S. A.*, 110:5452—5456, 2013.

[152] C. A. Wraight and A. R. Crofts. Energy-dependent quenching of chlorophyll alpha fluorescence in isolated chloroplasts. *Eur. J. Biochem.*, 17(2):319–27, 1970.

[153] A. E. Yakushevska, P. E. Jensen, W. Keegstra, H. van Roon, H. V. Scheller, E. J. Boekema, and J. P. Dekker. Supermolecular organization of photosystem II and its associated light-harvesting antenna in *Arabidopsis thaliana*. *Eur. J. Biochem.*, 268(23):6020–8, 2001.

[154] A. E. Yakushevska, W. Keegstra, E. J. Boekema, J. P. Dekker, J. Andersson, S. J.sson, A. V. Ruban, and P. Horton. The structure of photosystem II in *Arabidopsis*: localization of the CP26 and CP29 antenna complexes. *Biochemistry*, 42(3):608–13, 2003.

[155] M. Yang, A. Damjanovic, H. M. Vaswani, and G. R. Fleming. Energy transfer in photosystem I of cyanobacteria *Synechococcus elongatus*: Model study with structure-based semi-empirical Hamiltonian and experimental spectral density. *Biophys. J.*, 85(1):140–158, 2003.

[156] M. Yang and G. R. Fleming. Influence of phonons on exciton transfer dynamics: comparison of the Redfield, Förster, and modified Redfield equations. *Chem. Phys.*, 282:161–180, 2002.

[157] M. Yang and G. R. Fleming. Construction of kinetic domains in energy trapping processes and application to a photosynthetic light harvesting complex. *J. Chem. Phys.*, 119(11):5614–5622, 2003.

[158] J. Zaks, K. Amarnath, D. M. Kramer, K. K. Niyogi, and G. R. Fleming. A kinetic model of rapidly reversible nonphotochemical quenching. *Proc. Natl. Acad. Sci. U. S. A.*, 109(39):15757–62, 2012.

[159] X.-G. Zhu, Govindjee, N. R. Baker, E. deSturler, D. R. Ort, and S. P. Long. Chlorophyll a fluorescence induction kinetics in leaves predicted from a model describing each discrete step of excitation energy and electron transfer associated with photosystem II. *Planta*, 223(1):114–133, 2005.

[160] X.-G. Zhu, Y. Wang, D. R. Ort, and S. P. Long. e-photosynthesis: a comprehensive dynamic mechanistic model of c3 photosynthesis: from light capture to sucrose synthesis. *Plant Cell Environ.*, 2012. doi: 10.1111/pce.12025.